UNIVERSITY OF THESSALY
SCHOOL OF ENGINEERING
DEPARTMENT OF MECHANICAL ENGINEERING

DESIGN OF A DRONE FOR LAST-MILE PARCEL DELIVERY IN HARSH ENVIRONMENTS

by

FERDINAND DUKA

Supervisor: Dr Emmanouil Bouzakis

Associate Professor

Submitted in partial fulfillment of the requirements for the degree of Diploma in Mechanical Engineering at the University of Thessaly

Volos, 2024

Institutional Repository - Library & Information Centre - University of Thessaly
03/09/2026 06:00:57 EEST - 216.73.216.156

UNIVERSITY OF THESSALY
SCHOOL OF ENGINEERING
DEPARTMENT OF MECHANICAL ENGINEERING

DESIGN OF A DRONE FOR LAST-MILE PARCEL DELIVERY IN HARSH ENVIRONMENTS

by

FERDINAND DUKA

Supervisor: Dr Emmanouil Bouzakis

Associate Professor

Submitted in partial fulfillment of the requirements for the degree of Diploma in Mechanical Engineering at the University of Thessaly

Volos, 2024

Institutional Repository - Library & Information Centre - University of Thessaly
03/09/2026 06:00:57 EEST - 216.73.216.156

© 2024 Ferdinand Duka

All rights reserved. The approval of the present Diploma Thesis by the Department of Mechanical Engineering, School of Engineering, University of Thessaly, does not imply acceptance of the views of the author (Law 5343/32 art. 202).

Institutional Repository - Library & Information Centre - University of Thessaly
03/09/2026 06:00:57 EEST - 216.73.216.156

Approved by the Committee on Final Examination:

Advisor Dr. Emmanouil Bouzakis,
Associate Professor, Department of Mechanical Engineering, University of Thessaly

Member Dr. Alexis Kermanidis,
Associate Professor, Department of Mechanical Engineering, University of Thessaly

Member Dr. Helen Kamoutsi,
Department of Mechanical Engineering, University of Thessaly

Date Approved: [October 2024]

Institutional Repository - Library & Information Centre - University of Thessaly
03/09/2026 06:00:57 EEST - 216.73.216.156

Acknowledgements

First of all I would like to express my gratitude to my supervisor, Dr. Emmanouil Bouzakis for his guidance and support through this journey. The excellence of our cooperation due to his willingness to help and to provide valuable insights had a great impact on my thesis. Moreover I would like to thank Dr. Alexis Kermanidis and Dr. Helen Kamoutsi for sparing their valuable time to read and assess my thesis. Also, I have to thank my parents for their unconditional love and support all these years, helping me evolve to be a better person in every aspect. Last but not least, a thank you to my brother, my friends and my girlfriend for always being there for me when I needed them.

Institutional Repository - Library & Information Centre - University of Thessaly
03/09/2026 06:00:57 EEST - 216.73.216.156

DESIGN OF A DRONE FOR LAST-MILE PARCEL DELIVERY IN HARSH ENVIRONMENTS

FERDINAND DUKA

Department of Mechanical Engineering, University of Thessaly

Supervisor: Dr Emmanouil Bouzakis

Associate Professor

Abstract

In this diploma thesis, a payload-carrying UAV that should be able to operate in harsh environments of high altitudes and extreme temperatures is conceptually designed and manufacturing methods were proposed. In order to achieve the optimal design, scientific literature, software analysis and modelling are combined. Firstly, in the introductory chapter the problem/goal of the thesis is determined and some basic elements about UAVs are mentioned. In the second chapter, the components that will provide power to the UAV are selected through literature research. The rest of the propulsion system components are determined both through literature research and modelling. The third paragraph contains the design process of every part of the UAV's airframe which is realized through the CAD software Autodesk Fusion 360. The design is followed by FEA analysis conducted in the same software while the materials selection process is completed with the aid of the CES Edupack software. Methods of fabrication and machining for the drone's parts are analyzed in the fourth chapter. The most appropriate methods are determined through research on scientific literature while considering the material, geometry and special features of each part. In the final chapter the optimal decisions that were concluded through the whole project are summarized.

Institutional Repository - Library & Information Centre - University of Thessaly
03/09/2026 06:00:57 EEST - 216.73.216.156

ΣΧΕΔΙΑΣΜΟΣ ΜΗ ΕΠΑΝΔΡΩΜΕΝΟΥ ΑΕΡΙΟΥ ΟΧΗΜΑΤΟΣ ΓΙΑ ΔΙΑΝΟΜΗ ΤΕΛΕΥΤΑΙΟΥ-ΜΙΛΙΟΥ ΣΕ ΔΥΣΚΟΛΑ ΠΕΡΙΒΑΛΛΟΝΤΑ

ΦΕΡΝΤΙΝΑΝΤ ΝΤΟΥΚΑ

Τμήμα Μηχανολόγων Μηχανικών, Πανεπιστήμιο Θεσσαλίας, 2024

Επιβλέπων Καθηγητής: Δρ. Εμμανουήλ Μπουζάκης,

Αναπληρωτής Καθηγητής

Περίληψη

Σε αυτή τη διπλωματική εργασία, ενα μη επανδρωμένο αεροσκάφος (Μ.Ε.Α.) που δύναται να κουβαλήσει βάρος και να λειτουργήσει σε δύσκολα περιβάλλοντα υψηλών υψομέτρων και ακραίων θερμοκρασιών, σχεδιάζεται και μεθόδοι για την κατασκευή του προτείνονται. Για την επίτευξη του βέλτιστου σχεδίου, επιστημονική βιβλιογραφία, ανάλυση μέσω λογισμικού και μοντελοποίηση συνδυάζονται. Αρχικά, στο εισαγωγικό κεφάλαιο, το πρόβλημα/σκοπός της εργασίας προσδιορίζονται και βασικά στοιχεία σχετικά με τα Μ.Ε.Α. αναφέρονται. Στο δεύτερο κεφάλαιο τα εξαρτήματα που παρέχουν ισχύ στο αεροσκάφος επιλέγονται μέσω βιβλιογραφικής έρευνας. Τα υπόλοιπα εξαρτήματα του συστήματος προώθησης επιλέγονται μέσω βιβλιογραφικής έρευνας και μοντελοποίησης. Το τρίτο κεφάλαιο περιέχει τη διαδικασία σχεδιασμού κάθε μέρους του αεροσκάφους που πραγματοποιείται με τη βοήθεια του λογισμικού Autodesk Fusion 360. Τον σχεδιασμό ακολουθεί η ανάλυση πεπερασμένων στοιχείων που πραγματοποιείται στο ίδιο λογισμικό ενώ η διαδικασία επιλογής υλικών ολοκληρώνεται με τη βοήθεια του λογισμικού CES Edupack. Μεθόδοι κατασκεύης και κατεργασίας για τα εξαρτήματα του αεροσκάφους αναλύονται στο τέταρτη κεφάλαιο. Οι πιο κατάλληλες μεθόδοι προσδιορίζονται μέσω διερεύνησης της σχετικής επιστημονικής βιβλιογραφίας ενω λαμβάνονται υπόψιν το υλικό, η γεωμετρία και τα ειδικά χαρακτηριστικά κάθε εξαρτήματος. Στο τελευταία κεφάλαιο, οι βέλτιστες επιλογές για τον σχεδιασμό του αεροσκάφους, στις οποίες καταλήξαμε συνοψίζονται.

Institutional Repository - Library & Information Centre - University of Thessaly
03/09/2026 06:00:57 EEST - 216.73.216.156

Contents

Institutional Repository - Library & Information Centre - University of Thessaly
03/09/2026 06:00:57 EEST - 216.73.216.156

Institutional Repository - Library & Information Centre - University of Thessaly
03/09/2026 06:00:57 EEST - 216.73.216.156

LIST OF TABLES

Institutional Repository - Library & Information Centre - University of Thessaly
03/09/2026 06:00:57 EEST - 216.73.216.156

LIST OF FIGURES

Institutional Repository - Library & Information Centre - University of Thessaly
03/09/2026 06:00:57 EEST - 216.73.216.156

Institutional Repository - Library & Information Centre - University of Thessaly
03/09/2026 06:00:57 EEST - 216.73.216.156

Institutional Repository - Library & Information Centre - University of Thessaly
03/09/2026 06:00:57 EEST - 216.73.216.156

LIST OF EQUATIONS

Institutional Repository - Library & Information Centre - University of Thessaly
03/09/2026 06:00:57 EEST - 216.73.216.156

Cha [1]pter 1. Introduction

1.1 Scope

UAV’s in the last two decades have been a topic of continuous research as they have proven to be extremely valuable in many sectors such as agriculture, emergency relief, military operations, environmental monitoring etc. These aerial vehicles are very different based on their application and the availability of commercial drones for intricate missions is limited.

In this diploma thesis the goal set is the mechanical designing and manufacturing of a conceptual drone that would be able to deliver payloads up to 2kg in very high altitudes and extreme heat. The use of this UAV will be to provide goods such as food, water and medicine in communities that reside in such locations that are hard to reach or unreachable after prolonged adverse weather conditions or other environmental emergencies.

The parts of the drone we focus on are the propulsion system and the airframe. The propulsion system should be able to provide the necessary power while storing enough energy to cover a mission where the flight path could consist of a distance of up to 10-15 km in horizontal travelling and several hundred meters to a km in vertical travelling. The airframe is expected to withstand the payload and the heat of this region as well as protect the components of the propulsion and avionics system while being as lightweight as possible. Optimal ways of fabrication and machining of the UAV’s parts are researched and presented.

1.2 Classification of UAVs

The types of small, unmanned aircraft most commonly used today can be narrowed down to the following:

Institutional Repository - Library & Information Centre - University of Thessaly
03/09/2026 06:00:57 EEST - 216.73.216.156

Fixed Wing Aircraft:

The wings of this UAV type are permanently integrated into the airframe (fig. 1.1). The majority of civil aircraft and fighter jets are examples of fixed-wing aircraft. The propulsion system of these aircraft produces forward airspeed, which consequently provides lift to balance the vehicle's weight. Thus, fixed-wing aircraft must keep a specific forward airspeed and cannot take off or land vertically. Compared to traditional helicopters, fixed-wing aircraft feature a simplified structure and can transport heavier payloads over longer distances with lower power consumption, making them fuel efficient. However, a notable downside of fixed-wing aircraft is the requirement for a runway or launcher for takeoff and landing.

Figure 1.1: Typical fixed-wing aircraft. [2]

Single Rotor Blade Helicopter:

In this type of rotorcraft, lift is generated directly through its rotors (fig. 1.2). Unlike fixed-wing aircraft, helicopters do not require a runway or launcher for takeoff and landing, as their lift is not dependent on the airframe's forward velocity. A single rotor helicopter is controlled through four primary inputs: the cyclic, the collective, the anti-torque pedals, and the throttle. The collective is pivotal in adjusting the rotor's angle of attack, thus controlling the helicopter's lift in conjunction with the throttle. The rapid dynamic response of the lift is managed by the collective control, enabling Vertical Take-Off and Landing (VTOL) capabilities. Despite these advantages, single rotor helicopters face certain drawbacks. They typically have shorter endurance times compared to fixed-wing aircraft and feature more complex structures, leading to higher maintenance costs. This complexity contrasts with the simpler design and longer range of fixed-wing aircraft, which can carry heavier payloads more efficiently over extended distances.

Institutional Repository - Library & Information Centre - University of Thessaly
03/09/2026 06:00:57 EEST - 216.73.216.156

Figure 1.2: Typical single rotor blade helicopter. [2]

Multicopter:

A multicopter, also known as a multirotor, is a type of helicopter featuring three or more propellers, enabling Vertical Take-Off and Landing (VTOL). The most common variant is the quadcopter, which is depicted below (fig.1.3). A quadcopter is controlled by regulating the angular speeds of its four propellers. In contrast to single rotor helicopters, rapid lift adjustments in quadcopters are achieved through propeller speed control. The multicopter's multiple-rotor structure inherently cancels out anti-torque moments, enhancing stability. Due to its simple structure, a multicopter is user-friendly, highly reliable, safe and has low maintenance costs. However, these advantages come at the expense of payload capacity and endurance time when using traditional propulsion systems.

Figure 1.3: Typical multicopter, here a quadcopter. [2]

For our mission a multicopter was chosen due to its positive attributes mentioned with the aim is to obliterate its disadvantages (low payload capacity, poor endurance) with an experimental hybrid system that could revolutionize multicopters. [3]

Institutional Repository - Library & Information Centre - University of Thessaly
03/09/2026 06:00:57 EEST - 216.73.216.156

1.3 History of Multicopters

The history of unmanned aerial vehicles (UAVs) dates back to early experiments with vertical flight. In 1907, the Breguet Brothers, guided by Charles Richet, built the Breguet-Richet Gyroplane No. 1 (fig. 1.4), a human-carrying helicopter that briefly lifted off the ground. This attempt is considered one of the earliest in multicopter development.

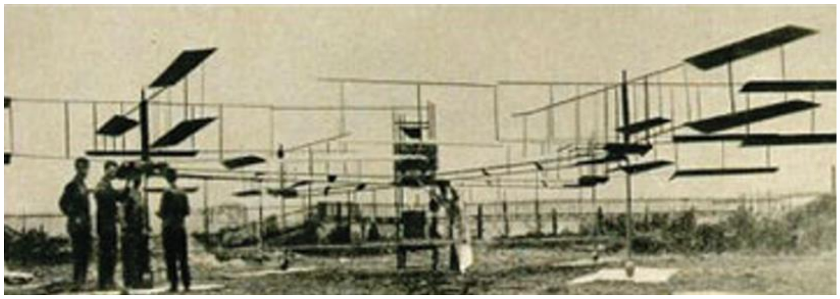

Figure 1.4: The Breguet-Richet Gyroplane No. 1. [3]

Etienne Oemichen also experimented with rotating-wing designs in the 1920s, and his second model, the Oemichen No. 2, set a world record by staying airborne for 14 minutes in 1923. The US Army showed interest in vertical lift machines, hiring George De Bothezat and Ivan Jerome in 1921 to develop a quadcopter. Their design managed to lift off the ground but suffered from poor engine performance and limited altitude, leading to a stall in quadcopter advancements for the next few decades.

In the mid-1950s, Marc Adman Kaplan's Convertawings Model “A” became the first successful quadcopter, capable of hovering and maneuvering. However, it failed to attract interest due to its inability to compete with conventional aircraft in terms of speed, payload, and range. The US Army continued exploring VTOLs (Vertical Take-Off and Landing aircraft) with Curtiss-Wright's VZ-7 in the late 1950s (fig. 1.5), but the project was canceled as conventional helicopters proved more efficient.

Institutional Repository - Library & Information Centre - University of Thessaly
03/09/2026 06:00:57 EEST - 216.73.216.156

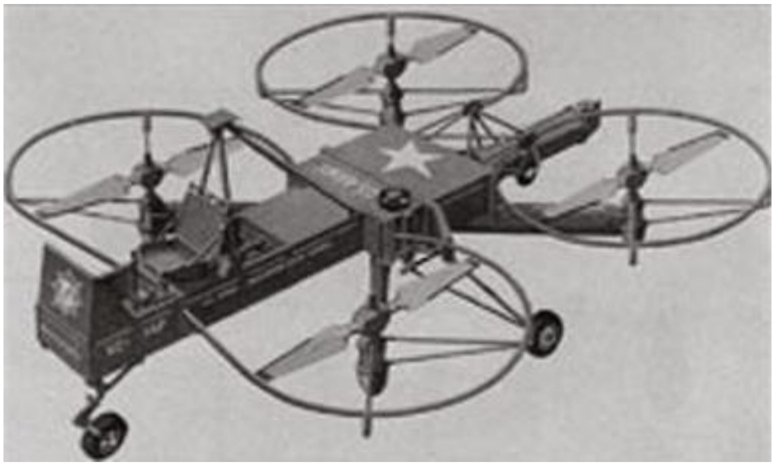

Figure 1.5: The Curtis-Wright's VZ-7. [3]

Multicopters were nearly abandoned until the 1990s when they began to reemerge in the consumer market as RC toys. In Japan, the Keyence Gyrosaucer (fig. 1.6) was introduced, and in the USA, Mike Dammar developed the Roswell Flyer, later marketed by Draganfly. These early consumer quadcopters paved the way for further developments.

Figure 1.6: The Gyro-Saucer 1. [3]

In 2005, Microdrones GmbH was founded, launching the MD4-200 in 2006 and the MD4-1000 in 2010, which achieved commercial success. Around the same time, the MikroKopter autopilot was introduced, enabling semi-autonomous flights. Ascending Technologies GmbH, founded in 2007, designed multicopters for professional and research purposes.

In 2008, Draganflyer released the Draganflyer X6, featuring advanced technology and recognized by Popular Science. Despite high costs and limited consumer appeal, the market continued to evolve. In 2004, Parrot Company initiated the AR. Drone project, which became successful in the toy market upon its release in 2010. The AR. Drone's technology allowed for

Institutional Repository - Library & Information Centre - University of Thessaly
03/09/2026 06:00:57 EEST - 216.73.216.156

easy piloting, indoor hovering, and smartphone control, making it popular for both entertainment and research.

Inspired by AR. Drone's success, DJI released the Phantom quadcopter in 2012 (fig.1.7), which featured GPS and altitude sensors, wind resistance, and payload capacity. It quickly gained popularity in aerial photography, especially with the rise of sports cameras. Enthusiasts shared videos online, further popularizing multicopters.

Figure 1.7: The Phantom by DJI. [3]

In 2012, Chris Anderson, former editor-in-chief of Wired magazine, joined 3D Robotics as CEO, contributing to the development of universal flight code for APM (ArduPilot Mega). The PX4 autopilot platform was announced by ETH Zurich's PX4 team in 2012, followed by the advanced Pixhawk autopilot design in 2013.

In late 2013, Amazon introduced the concept of "PrimeAir," envisioning package delivery via quadcopters within 30 minutes. This idea brought UAVs closer to mass consumer use. By 2015, numerous multicopter models were being designed, marking a significant advancement in the field. This brief history highlights key developments in UAV technology, from early experimental helicopters to modern consumer drones and advanced commercial applications. [3]

Institutional Repository - Library & Information Centre - University of Thessaly
03/09/2026 06:00:57 EEST - 216.73.216.156

1.4 Multicopter Motion Basics

The simplest form of a multirotor is the quadcopter. Generally, an even number of rotors is easier to control and fly due to its symmetric geometry and the less complex one is the one with the least number of rotors which is 4 (a 2-rotor UAV is not considered a multicopter [w]). This is true because in multicopter control theory the inputs used are the angular velocities of each propeller which means the less the rotors the simpler the control model.

According to classical mechanics theory, a force acting on a rigid body can be divided into both linear force and an accompanying rotational force, while a rotational force can be directly translated into movement around the central axis. This means that each propeller can produce a force (thrust) and a moment when rotating. While differentiating the angular speed of all propellers, 3 important moments can be produced. This way the quadcopter can perform maneuvers and move through the air. Propellers #1 and #3 rotate clockwise while #2 and #4 rotate counterclockwise. This way the reaction torque is summed to 0 and the quadcopter is kept in balance (fig. 1.8).

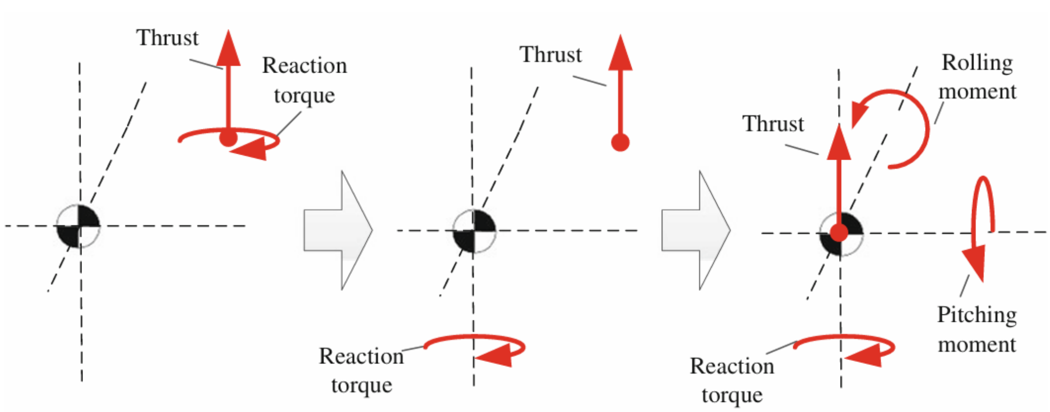

Figure 1.8: Forces, moments and torques on the multicopter's body. [3]

Upward/Downward Motion

To move upwards and downwards, the angular velocities of all propellers should be equal. When the thrust produced is larger than the UAV's weight, it will move up while when the force

Institutional Repository - Library & Information Centre - University of Thessaly
03/09/2026 06:00:57 EEST - 216.73.216.156

is lower than its weight it will descend. If thrust and weight are equal the quadcopter will hover.

Forward/Backward Motion

Decreasing the angular velocities of propellers #1 and #4 while increasing the angular speeds of propellers #2 and #3 by the same amount, will make the quadcopter pitch forward and the thrust will gain a forward component. This will decrease the vertical component of the thrust. To compensate for this phenomenon the angular velocity of all propellers should be sped up by the same percentage. Reversing the roles of propellers #1 and #4 with the roles of #2 and #3 will move the UAV backwards.

Leftward/Rightward Motion

Lowering the angular speeds of propellers #1 and #2 by the same amount as the increase of the speeds of #3 and #4 will create a moment that rolls the UAV to the right. Reversing the procedure will tilt and move the quadcopter to the left. As in the forward/backward motion, due to the decrease of the vertical thrust component an overall increase of each propeller's angular speed needs to take place.

Yaw Motion

To initiate clockwise yaw movement of the quadcopter, a decrease of the angular speeds of propellers #2 and #4 should take place combined with an increase of the angular speeds of propellers #1 and #3 accordingly. Moments in the frontward/backward and leftward/rightward directions will be zero. Based on Newton's Third Law an opposite torque reaction will be created due to the increase of the counterclockwise movement of propellers #1 and #3.

Institutional Repository - Library & Information Centre - University of Thessaly
03/09/2026 06:00:57 EEST - 216.73.216.156

Chapter 2. Propulsion System

The propulsion system of a multicopter, here a quadcopter, includes the propellers, motors, electronic speed controller (ESC) and the power generator of the UAV that can be broadly classified into three types, including fuel, pure electric and hybrid systems such as the one that will be presented here. [4]

Unmanned Aerial Vehicles (UAVs) powered by internal combustion engines rely on a variety of fuels, including hydrogen, gasoline, and methane. These UAVs harness the benefits of conventional fuel propulsion systems, offering significant advantages such as robust payload capacity, extended flight endurance, vast operational range, and swift refueling capabilities, due to the potent power density inherent in fossil fuels. Gas turbine engines are also popular among aircraft propulsion systems due to their significant endurance time and high power to weight ratio. Nevertheless, the effectiveness of internal combustion engines is diminished by their low efficiency resulting from the multi-step energy production process, and concerns regarding fuel consumption in micro air vehicles may lead to stability issues. Due to their low efficiency, increased noise and low fuel economy these types of propulsion systems don't seem appropriate for small/medium size UAVs. Furthermore, as environmental concerns escalate and fossil fuel reserves deplete, the energy dilemma facing aircraft propulsion has been a challenge. Consequently, focus is targeted on purely electric UAVs. [4]

The all-electric propulsion system for UAVs relies solely on electric motors as the power source, offering benefits such as reduced carbon emissions, minimal pollution, cost-effectiveness, and efficient energy utilization. In small UAVs powered by electricity, batteries serve as the primary power source, enhancing the flexibility and simplicity of the propulsion system [5]. Batteries provide a satisfying power density which can withstand the power spikes due to extreme maneuvers of the multicopter during its mission. In addition, the battery system has a good response time in extreme variations of current, compared to other propulsion systems, that is important for external interferences such as strong gusts of wind during flight time. UAVs powered by batteries, particularly those utilizing LiPo batteries, can navigate intricate

Institutional Repository - Library & Information Centre - University of Thessaly
03/09/2026 06:00:57 EEST - 216.73.216.156

routes for up to 90 minutes. Nonetheless, the endurance of battery-powered UAVs is reduced due to the added weight of the battery pack and to increase the energy storage there must be a linear increase of the weight of the battery. Charging time between missions is another issue that makes this type of UAV power system unreliable for delivery and emergency purposes.

Fuel cell technology is currently in development and seems like a promising source of electric power for drones. Several fuel cell technologies are available, including phosphoric acid, solid acid, solid oxide, proton exchange membrane (PEM), and alkaline fuel cells. Among these, PEM fuel cells, direct methanol fuel cells, and solid oxide fuel cells are commonly employed in UAV applications [4]. Hydrogen-powered fuel cells equipped with compressed hydrogen tanks are favored in UAVs for their low operating temperatures and relatively quick response to load fluctuations. Additionally, their high energy density and lightweight nature make them well-suited for various electric vehicle applications. Furthermore, refueling the fuel cell is rapid compared to the considerably longer charging time required for batteries. Yet, experiments have revealed that the overall efficiency of a purely fuel cell-powered UAV lacks efficiency, ranging from 18-20% from hydrogen input to propulsion. Additionally with average dynamic performance and restricted fault-tolerant capabilities, such UAVs do not appear to be optimal. [6]

The propulsion system is the most important part of the multicopter as it is inherently related to the overall performance of the UAV and the ability to complete its mission. This research will look into the utilization of a hybrid fuel cell-battery system as recent research has shown that this combination could be a solution for the short range/endurance and payload carrying inability that defines most battery powered multicopters, especially for medium sized drones (~10kg MTOW) [7]. This combination is the most effective considering energy content/weight ratio when the demanded energy of a mission is more than 4MJ. [7]

Institutional Repository - Library & Information Centre - University of Thessaly
03/09/2026 06:00:57 EEST - 216.73.216.156

2.1) Fuel Cell

Fuel cells represent electrochemical devices that transform the chemical energy derived from a fuel and an oxidizing agent into electrical energy via a series of redox reactions (fig. 2.1). While various types of fuel cells exist, they share a common structure comprising an anode, a cathode, and an electrolyte facilitating the movement of ions, typically protons, between these components. At the anode, a catalyst triggers the ionization of the fuel, resulting in the formation of a positively charged ion and a negatively charged electron. The electrolyte, meticulously engineered, permits the passage of ions while blocking the flow of electrons. These released electrons traverse through a conductor, generating an electric current. Simultaneously, the ions migrate through the electrolyte towards the cathode. Upon reaching the cathode, the ions reunite with the electrons, and together they engage in a reaction with a third substance, often oxygen, culminating in the production of water or carbon dioxide. A typical fuel cell produces a voltage from 0.6 to 0.7 V at a full-rated load. To deliver the desired amount of energy, the fuel cells can be combined in series to yield higher voltage, and in parallel to allow a higher current to be supplied. Such a design is called a *fuel cell stack*. [1]

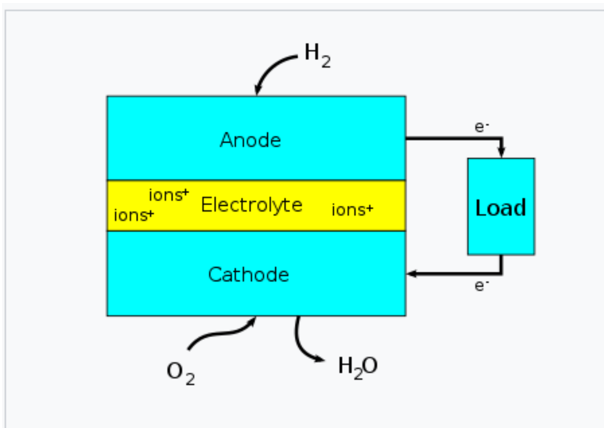

Figure 2.1: Typical Fuel Cell operation. [2]

Fuel cells are primarily categorized based on the type of electrolyte they utilize. This classification plays a pivotal role in defining the electrochemical reactions occurring within the cell, the catalysts necessary, the operational temperature range, the type of fuel utilized, and

Institutional Repository - Library & Information Centre - University of Thessaly
03/09/2026 06:00:57 EEST - 216.73.216.156

additional factors. Consequently, these characteristics influence the suitability of fuel cells for various applications. [8]

2.1.1) Comparison of FC Types

The most studied types of fuel cells to this day are polymer electrolyte membrane, direct methanol, alkaline, phosphoric acid, molten carbonate and solid oxide fuel cells. On the field of UAVs specifically, fuel cell-based propulsion systems most research has been done on PEM fuel cells, followed by Solid Oxide fuel cells and Direct Methanol fuel cells.

Solid Oxide Fuel Cells

Solid oxide fuel cells (SOFCs) employ a rigid, impermeable ceramic compound as an electrolyte to conduct negative oxygen ions from the cathode to the anode (fig. 2.2). This type of fuel cell boasts an efficiency of approximately 60% in converting fuel into electricity. When utilized in systems engineered to harness and utilize the waste heat generated (known as co-generation), the overall fuel utilization efficiency could exceed 85%. Functioning at exceptionally elevated temperatures, typically ranging from 600 to 1,000 °C, SOFCs eliminate the need for costly platinum group metal catalysts, which are presently essential for lower-temperature fuel cells like PEMFCs

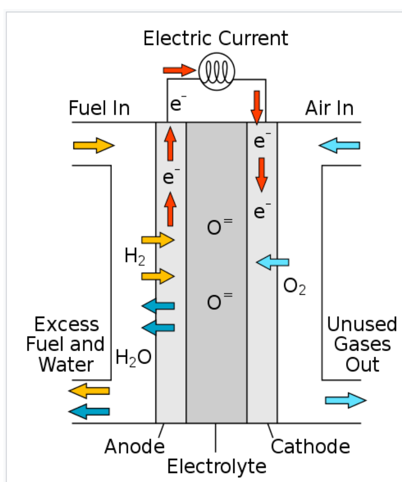

Figure 2.2: Schematic of a SOFC and its power generating process. [2]

Institutional Repository - Library & Information Centre - University of Thessaly
03/09/2026 06:00:57 EEST - 216.73.216.156

The ceramic anode layer requires significant porosity to facilitate fuel flow toward the electrolyte. As a result, granular materials are commonly chosen for anode fabrication. The prevailing choice is a cermet composed of nickel blended with the ceramic material employed for the electrolyte, typically YSZ (yttria-stabilized zirconia), although perovskite materials are increasingly gaining traction. The electrolyte constitutes a compact ceramic layer facilitating the conduction of oxygen ions. Commonly employed electrolyte materials encompass yttria-stabilized zirconia (8YSZ), scandia-stabilized zirconia (9ScSZ), and gadolinium-doped ceria (GDC). The choice of electrolyte material significantly impacts the performance of the cell. The cathode, also known as the air electrode, forms a thin, permeable layer atop the electrolyte, facilitating oxygen reduction. Cathode materials necessitate electrical conductivity at the least. Presently, lanthanum strontium manganite (LSM) stands as the preferred cathode material for industrial applications owing to its compatibility with doped zirconia electrolytes (fig. 2.3). [1] [8]

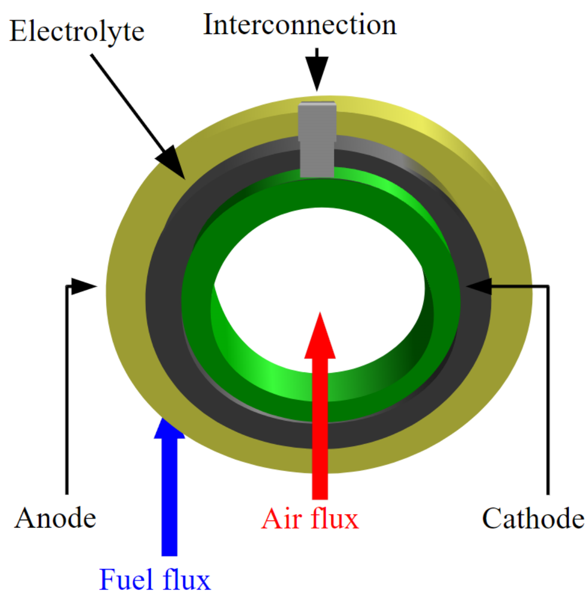

Figure 2.3: Cross-section of a tubular SOFC, showcasing its ceramic layers. [2]

Polymer Electrolyte Membrane Fuel Cells

Polymer electrolyte membrane (PEM) fuel cells, also referred to as proton exchange membrane fuel cells (fig. 2.5), exhibit notable characteristics including high power density and superior weight and volume efficiency in comparison to alternative fuel cell technologies. Operating within the relatively low temperature range of approximately 80°C (176°F), PEM fuel

Institutional Repository - Library & Information Centre - University of Thessaly
03/09/2026 06:00:57 EEST - 216.73.216.156

cells afford rapid start-up capabilities due to reduced warm-up periods, along with diminished wear on system components, thereby enhancing overall durability. PEM fuel cells (PEMFCs) are constructed utilizing membrane electrode assemblies (MEAs), encompassing electrodes, electrolytes, catalysts, and gas diffusion layers. Application of a catalyst, carbon, and electrode ink onto the solid electrolyte, followed by hot pressing of carbon paper on both sides, constitutes the MEA assembly (fig. 2.4), providing protection to the cell interior while functioning as electrodes. The proton-exchange membrane, typically fabricated from materials like perfluorosulfonic acid (PFSA) such as commercially available Nafion and Aquivion, is adept at mitigating gas crossover and short-circuiting within the fuel cell.

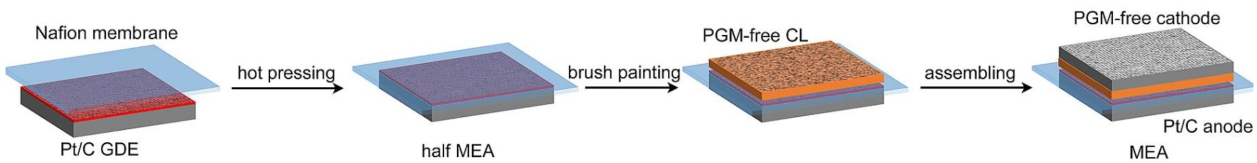

Figure 2.4: Assembly process of the PEM MEA. [2] [8]

Electrodes commonly comprise of carbon support, Pt particles, Nafion ionomer, and/or Teflon binder, each serving distinct functions: electrical conduction, reaction sites, proton conduction pathways, and hydrophobicity enhancement to deter flooding. Facilitating electrochemical reactions at the electrodes necessitates access for protons, electrons, and reactant gases (hydrogen or oxygen) to the catalyst surface, while enabling product water permeation from catalyst to gas outlet. Typically, porous composites of polymer electrolyte binder (ionomer) and catalyst nanoparticles supported on carbon particles realize these properties. Platinum predominantly serves as the catalyst for both anodic and cathodic electrochemical reactions. The Gas Diffusion Layer (GDL) functions to electrically link the catalyst and current collector, requiring porosity, electrical conductivity, and thinness. Balancing reactant accessibility with conductivity and porosity poses a challenge, with an optimal GDL composition comprising approximately one-third Nafion or 15% PTFE. External electrodes, often termed bipolar plates or backplates, play pivotal roles in uniformly distributing fuel and oxygen to catalysts, water removal, and current collection and transmission. [1] [8]

Institutional Repository - Library & Information Centre - University of Thessaly
03/09/2026 06:00:57 EEST - 216.73.216.156

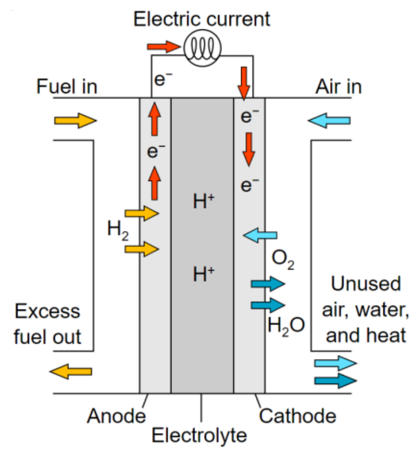

Figure 2.5: Schematic of a PEMFC and its power generating process. [2]

Direct Methanol Fuel Cells

Direct methanol fuel cells (DMFCs) represent a subset of proton-exchange fuel cells that utilize methanol as the primary fuel source. Operating on pure methanol typically diluted with water, DMFCs directly supply this mixture to the fuel cell anode. The operation of the DMFC revolves around methanol oxidation on a catalyst layer, resulting in the production of carbon dioxide. Water undergoes consumption at the anode while being generated at the cathode. Protons (H+) are conveyed across the proton exchange membrane, often composed of Nafion, to the cathode, where they combine with oxygen to yield water. Meanwhile, electrons traverse through an external circuit from the anode to the cathode, supplying power to connected devices. Typically, DMFCs operate within temperatures ranging from 50 to 120 °C (122 to 248 °F), with higher temperatures commonly necessitating pressurization. While DMFCs exhibit greater efficiency at elevated temperatures and pressures, the associated losses within the entire system offset this advantage. Consequently, configurations operating at atmospheric pressure are presently favored. Unlike certain fuel cell systems, DMFCs encounter fewer fuel storage challenges due to methanol's comparatively higher energy density than hydrogen, albeit lower than that of gasoline or diesel fuel. Additionally, methanol's liquid state akin to gasoline facilitates its transportation and integration into existing infrastructures for public supply. [1] [9] [8]

Institutional Repository - Library & Information Centre - University of Thessaly
03/09/2026 06:00:57 EEST - 216.73.216.156

While comparing SOFCs and PEMFCs [10] found that the former needs much less area to provide the same amount of power as the latter with a higher efficiency as well. Even though the larger area of the PEM might compromise the drone's aerodynamic performance and as a result its power consumption, the SOFC's larger weight due to its complex BoP (Balance of Plant) is a bigger issue. The BoP of a SOFC includes the air preheater, prereformer, afterburner, water heat exchanger, anode tail gas oxidizer, power electronics, hydrogen sulfide sensor, fuel tank and fans while the PEMFC BoP consists of the hydrogen tank, cooling system, water management, power electronics, humidifier and pumps [2]. The BoP complexity and payload issues of the SOFC stem from the high temperature needed to activate the solid oxide electrolyte, while this additionally creates the setback of impractically long starting times (up to 1hr). This constitutes SOFC powered UAVs inappropriate for emergency missions. Last but not least, the high operating temperatures could affect the battery's performance and safety in a hybrid fuel cell-battery propulsion system, creating the demand for costly insulating materials and safety measures that could also add up weight-wise [11]. PEMFCs on the other hand, provide a satisfactory operating temperature range, rapid start-up and high energy density making them ideal for long endurance-low maneuverability missions. Also, they are generally low-cost, relatively light and the most mature fuel cell technology while the hydrogen powered PEMFCs specifically earn the advantage of being a purely clean technology when the hydrogen used is acquired through electrolysis [11].

Direct Methanol Fuel Cell (DMFC) stacks, a subset of PEM fuel cells directly fueled by methanol, exhibit approximately half the efficiency (resulting in higher heat losses) and power density of conventional PEM fuel cells. However, they offer higher energy density (yielding greater endurance) and simplicity. Moreover, the storage system for methanol is lighter compared to hydrogen, and the logistics are simpler, potentially leveraging existing fossil fuels distribution networks. Another notable advantage is the ability to derive methanol from biomass sources (e.g., wood distillation), rendering it a renewable fuel option. DMFCs emit only water and CO2, and if the CO2 is distilled, it can be reabsorbed by the biomass used to produce new

Institutional Repository - Library & Information Centre - University of Thessaly
03/09/2026 06:00:57 EEST - 216.73.216.156

methanol, thus completing the cycle. However, the power density of this type of fuel cell is lower than hydrogen powered PEMFCs which makes them inefficient for smaller and medium UAVs as they need relatively much more power for a trip than other vehicles where DMFCs could be more efficient [11]. The missing power could be provided by a battery in a hybrid system but in contrast to hydrogen PEMFCs the battery will have a much larger power supplying duty while operating for the majority of the trip with rare instances where the battery could be recharged by the fuel cell. For hydrogen PEMFC battery hybrid systems the battery acts as a complimentary power supply for specific maneuvers during the mission for a small percentage of the operating time. This means that the battery in the former system should be of high capacity making the propulsion system heavy for a 11kg multicopter.

2.1.2) Selection of Fuel Cell

Having this in mind, the type of fuel cell chosen for our hybrid system is a PEMFC. In [7] a similar PEM fuel cell – battery system is investigated for a 7kg MTOW drone (fig. 2.6). A 500W PEM fuel cell is chosen as the baseline power contributor regarding mild horizontal speeds.

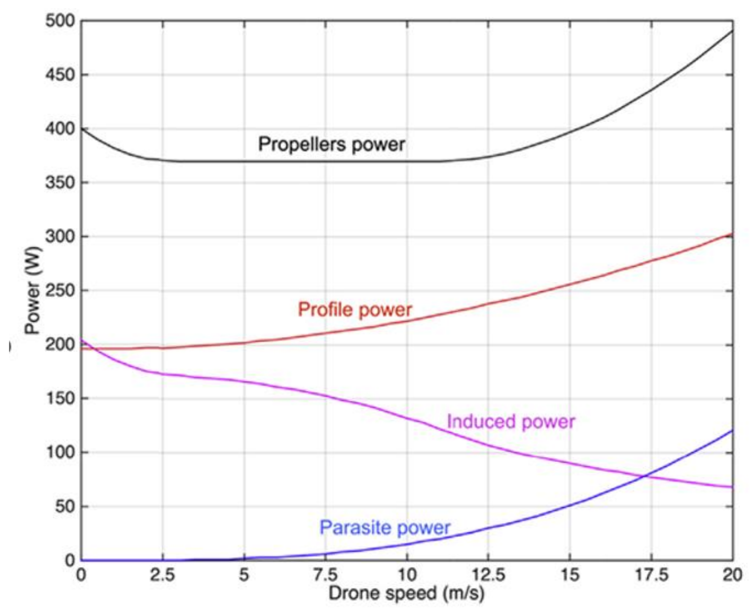

Figure 2.6: Power consumption / horizontal velocity diagram of a 7kg MTOW quadcopter powered by a hybrid FC-Battery system. [7]

Institutional Repository - Library & Information Centre - University of Thessaly
03/09/2026 06:00:57 EEST - 216.73.216.156

The peak power drawn while travelling horizontally reaches approximately 500W – as much as the fuel cell can provide. During vertical flight the desired power exceeds the fuel cells capability and that is where the battery is put to work.

Scaling linearly for our 11kg MTOW quadcopter that will operate in harsh environments (high temperature, high altitude) we assume an 800W rated fuel cell with the ability of 1000W maximum power will be necessary. The model chosen is Aerostack 800 by H3 Dynamics. The specifications of the PEM fuel cell are presented below (table 2.1).

Table 2.1: Specifications of the Aerostack 800 fuel cell. [12]

Stack Design	46 cells
Rated Power	800W
Maximum Power	1000W
Voltage	27-48 V
Current	0-30 A
Weight	1.23 kg
Size	214mm*123mm*130mm
Air Input Temp.	0-40°C
Hydrogen Input Press.	0.6-0.8 bar
Hydrogen Purity	99.998%
Max. Consumption	<8.3 L/min
Start Up Time	20 sec
Suggested Hybrid Battery	7S

The fuel cell will be coupled with a hydrogen tank (F-series F2 by H3 Dynamics) that weighs 1.43 kg and carries 42g of hydrogen in a volume of 2L. The total energy available in the tank is calculated at 1410 Wh which is reduced to 705 Wh while considering a 50% efficiency for the conversion of energy done by the fuel cell. This provides the multicopter with 42 minutes continuous operation at maximum power. [12]

Institutional Repository - Library & Information Centre - University of Thessaly
03/09/2026 06:00:57 EEST - 216.73.216.156

2.2) Battery

An electric battery constitutes an electrical power source comprising one or more electrochemical cells linked to external connections for energizing electrical devices. During power delivery, the battery's positive terminal functions as the cathode, while its negative terminal acts as the anode. Electrons flow from the terminal marked negative through an external electric circuit to the positive terminal. When connected to an external electric load, a redox reaction occurs within the battery, converting high-energy reactants into lower-energy products, with the resultant free-energy difference supplied to the external circuit as electrical energy. Primary batteries, also known as single-use or "disposable" batteries, are utilized once and then discarded due to irreversible changes in electrode materials during discharge. Conversely, secondary batteries, termed rechargeable, can undergo multiple discharge and recharge cycles using an applied electric current, allowing restoration of the original composition of the electrodes through reverse current. [9]

The most common commercial rechargeable types of batteries include Lithium-Ion, Lithium Polymer, Nickel-Metal Hydride, Nickel-Cadmium, Lead-Acid, Lithium-Iron Phosphate. [2]

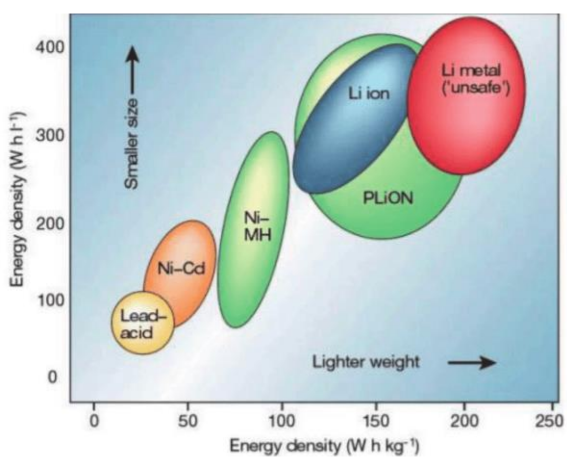

Figure 2.7: Comparison of various battery technologies based on energy, weight and volume. [2]

Institutional Repository - Library & Information Centre - University of Thessaly
03/09/2026 06:00:57 EEST - 216.73.216.156

The advancement in Lithium battery technologies, including enhancements like performance enhancement through doping, modified battery electrodes encapsulated with graphene, and compound-type battery electrolytes, has significantly enhanced both energy storage capacity and power performance when compared to traditional lead-acid or nickel-metal hydride batteries (fig. 2.7). [13]

2.2.1) Comparison of Lithium Based Batteries

Li-ion batteries

All commercial Li-ion cells employ intercalation compounds as active materials, with the negative electrode predominantly being graphite, sometimes incorporating silicon to enhance capacity. The solvent in the electrolyte is typically lithium hexafluorophosphate dissolved in a blend of organic carbonates. Various materials, such as $LiCoO2$, $LiFePO4$, and lithium nickel manganese cobalt oxides, are used for the positive electrode. During discharge, the negative electrode serves as the anode and the positive electrode as the cathode, facilitating the flow of electrons from the anode to the cathode through the external circuit. An oxidation half-reaction at the anode produces positively charged lithium ions and negatively charged electrons, while lithium ions migrate through the electrolyte and electrons travel through the external circuit to the cathode, where they combine with the cathode material in a reduction half-reaction. The electrolyte acts as a conductive medium for lithium ions but does not participate in the electrochemical reaction. Discharging lowers the chemical potential of the cell, transferring energy from the cell to the external circuit. Conversely, during charging, electrons move from the positive electrode to the negative electrode through the external circuit, requiring electrical energy input from the external circuit to store chemical energy in the cell, albeit with some energy loss due to factors like coulombic efficiency being lower than 1. Typically, lithium-ion batteries come encased in stainless steel or aluminum. While the casing is commonly cylindrical, it can also take on button-shaped or rectangular forms, known as prismatic (fig. 2.8). Although

Institutional Repository - Library & Information Centre - University of Thessaly
03/09/2026 06:00:57 EEST - 216.73.216.156

manufacturing the casing incurs significant costs and limits size and shape options, its durability provides robust protection for the battery, guarding against damage. [9] [14]

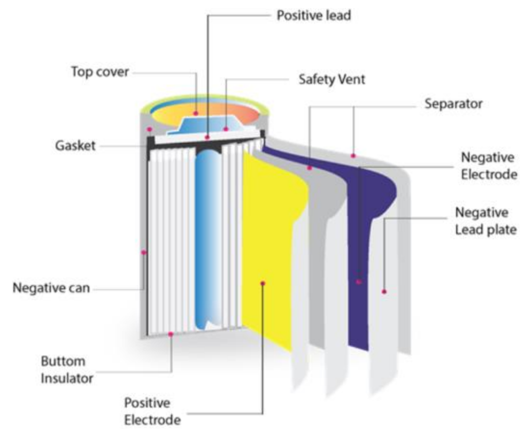

Figure 2.8: Anatomy of a cylindrical Li-ion battery cell. [14]

Lithium-Polymer batteries

Lithium polymer cells represent an advancement over traditional lithium-ion batteries. The key departure lies in their utilization of a solid polymer electrolyte (SPE) instead of a liquid lithium-salt electrolyte, typically lithium hexafluorophosphate (LiPF6), suspended in an organic solvent. These polymers, such as polyethylene glycol (PEG), polyacrylonitrile (PAN), poly(methyl methacrylate) (PMMA), or poly(vinylidene fluoride) (PVdF), facilitate the movement of lithium ions between the positive and negative electrode materials through intercalation and de-intercalation processes, akin to other lithium-ion cells. The separator, a microporous barrier, prevents direct contact between electrodes, allowing only ions to traverse from one side to the other. The voltage of a single LiPo cell hinges on its chemistry, typically ranging from approximately 4.2 V when fully charged to around 2.7–3.0 V when fully discharged. Nominal voltages hover around 3.6 or 3.7 volts, representing an average between the highest and lowest values, particularly for cells incorporating lithium-metal-oxides like LiCoO2. LiPo batteries are enclosed within an aluminum foil "pouch" and are referred to as soft or pouch cells. These pouches are primarily prismatic in shape, making fabrication easier and more cost-effective compared to the stainless steel or aluminum cases used for Li-ion batteries (fig. 2.9). This design flexibility also allows for the creation of batteries with various custom configurations. [14] [9]

Institutional Repository - Library & Information Centre - University of Thessaly
03/09/2026 06:00:57 EEST - 216.73.216.156

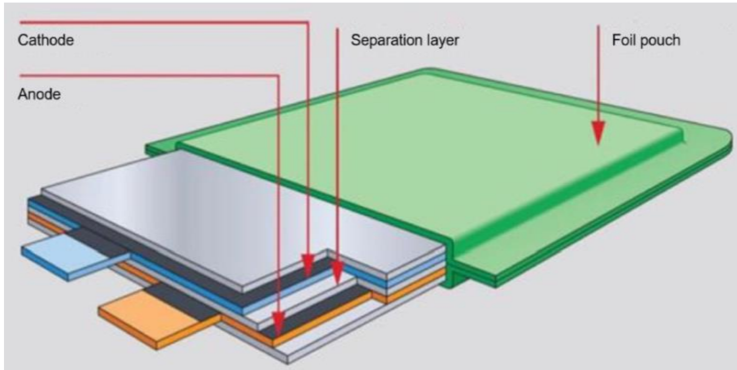

Figure 2.9: Anatomy of a LiPo battery "pouch" cell. [14]

2.2.2) Selection of Battery

LiPo batteries provide higher energy density than standard lithium-ion batteries while also having flexible shaping and sizing helping in the topology problems of the UAV’s fuselage. Generally lighter than other batteries, they boast better specific energy that can be discharged at higher rates making them suitable for applications that require rapid power delivery. Along with a manufacturing process that is simpler and more cost effective than li-ion batteries, LiPo batteries seem the most compatible choice for UAV applications [15]. The battery chosen based on the fuel cell manufacturer recommendation, the energy demand and power demand, is the MaxAmps LiPo 8000mAh 7S 25.9V Battery Pack (table 2.2). [16]

Table 2.2: Specifications of the MaxAmps LiPo 8000 Lite 7S 25.9v. [16]

Capacity	8000 mAh
Nominal Voltage	7S 25.9 V
Maximum Voltage	29.4 V
Minimum Voltage	21 V
Max. continuous discharge	180 A
Max. charge current	40 A
Energy content	207.2 Wh
Size	138mm*50mm*77mm
Weight	1167 g

Institutional Repository - Library & Information Centre - University of Thessaly
03/09/2026 06:00:57 EEST - 216.73.216.156

2.3 Hybrid System Connection

The necessary components for the effective connection of the fuel cell and the battery with the avionics system of the multicopter are a Power Distribution Board (PDB), DC-DC converters, a MOSFET/relay switch and current/voltage sensors. These components will be paired with the fuel cell, battery and electronic speed controllers (ESC) of the propulsion system and the flight controller of the avionics system (fig. 2.10).

Power Distribution Board

The PDB is a circuit board that can distribute power from multiple sources (here a fuel cell and a battery) to all the electrical components of the multicopter but mainly to the electronic speed controllers that can then transfer it to the motors. The inputs of the PDB are the fuel cell power through a DC-DC converter and battery power. The outputs are the ESCs and the flight controller.

DC-DC Converter

The DC-DC converter is an electronic device used to step down the voltage from the power source (here a fuel cell rated at 27-48 V) to the voltage needed by the motors through the ESC and PDB. These "step-down" converters and called buck converters. To select the appropriate converter the current rating should be considered as a high current draw might be needed for the ESCs and motors. Current sensors can be connected between the converter and the PDB to monitor current power drawn from the fuel cell.

Flight Controller

The flight controller is the most important part of the avionics system and works as the "brain" of the multicopter. This device processes inputs from the pilot (autopilot or fully controlled pilot), the sensors (accelerometer, gyroscope) and the GPS to control the ESCs and maintain stable flight. Additionally, the flight controller can monitor current and voltage from the power sources and communicate with the battery switch through Pulse Width Modulation pins

Institutional Repository - Library & Information Centre - University of Thessaly
03/09/2026 06:00:57 EEST - 216.73.216.156

and control it. This way the battery is on or off depending on the power needs of the multicopter. The flight controller is connected to the PDB to receive power for operation, while it is also connected to the ESCs and the battery MOSFET/relay switch through signal pins (PWM pins). This way the controller commands the ESCs to draw the appropriate power from the PDB depending on the speed of the motors while the battery switch is commanded to be on or off based on the current/voltage sensors.

MOSFET/Relay Switch

A Metal Oxide Semiconductor Field Effect Transistor or solid-state relay is an electronic switch. This switch is used to connect or disconnect the battery to the PDB based on the signals provided by the flight controller. The source (input) of the switch connects to the positive terminal of the battery. The drain (output) of the switch connects to the PDB allowing power to flow from the battery to the ESCs and the motors when the switch is on. Finally, the gate of the MOSFET is connected to a PWM pin of the flight controller which controls it.

Current Sensors

This type of sensor monitors the current drawn from both the fuel cell and the battery in order to provide real time power consumption data to the flight controller. The flight controller then can use this information to decide if the battery needs to be activated. Two current sensors will be needed for the multicopter: one between the fuel cell’s DC-DC converter and the PDB and one between the battery and the PDB. The data is sent to the flight controller analog input pins.

Voltage Sensor

This sensor measures the voltage across the battery’s terminals to determine the state of charge (SOC). This is an important task for retaining the battery’s quality and expanding its life by cutting off the power at 15% so it does not over discharge. The sensor is directly connected onto the battery and uses analog input pins to transfer data to the flight controller so it can turn off the MOSFET switch when necessary.

Institutional Repository - Library & Information Centre - University of Thessaly
03/09/2026 06:00:57 EEST - 216.73.216.156

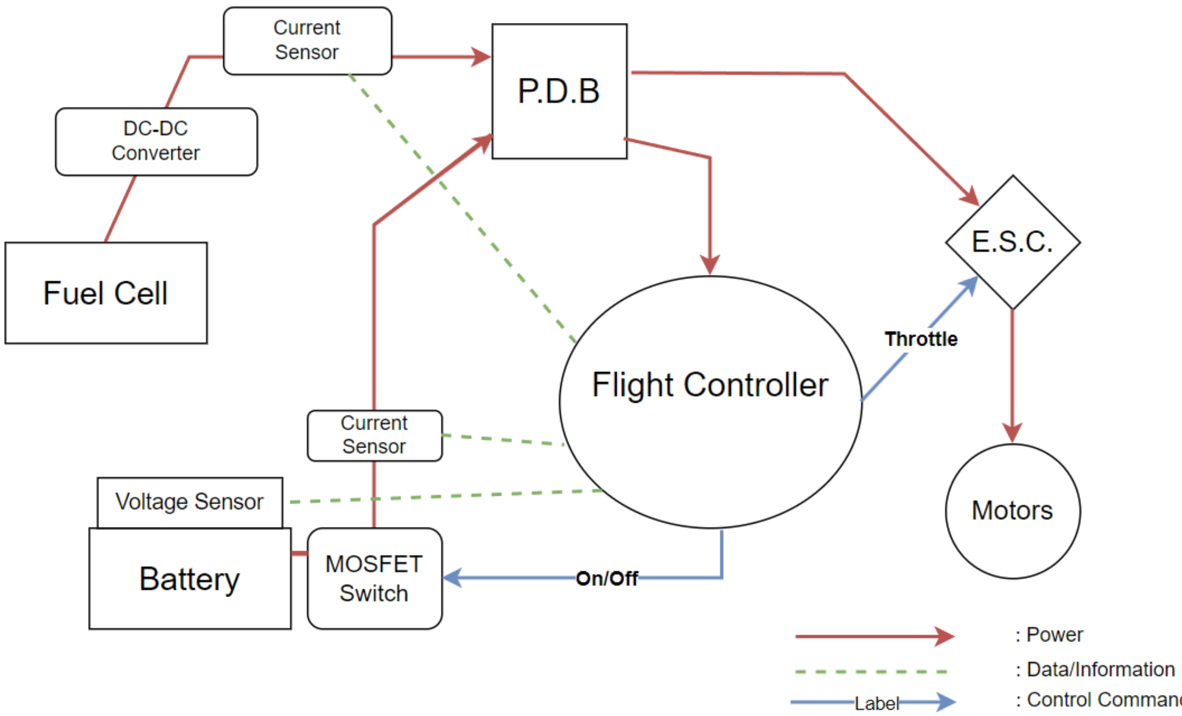

Figure 2.10: Diagram of the propulsion system and avionic system connection.

2.4) Other Propulsion System Components

2.4.1) Propellers

The propellers play a crucial role in generating both thrust and torque to maneuver a multicopter. The efficiency of the motor depends on various factors such as the type, size, speed, and other characteristics of the propeller. Ensuring a good match between the motor and propeller is essential to operate the motor in a highly efficient condition. This ensures that less power is consumed to achieve the same level of thrust, thereby extending the endurance time of the multicopter. Consequently, selecting suitable propellers directly enhances the performance and efficiency of a multicopter [3]. Some important features that need identification are the type of the propeller (four-digit number indicating the diameter and pitch),

Institutional Repository - Library & Information Centre - University of Thessaly
03/09/2026 06:00:57 EEST - 216.73.216.156

chord length, number of blades, airfoil, safe rotation rate, propeller specific thrust and the material (table 2.4). Some of these features will be obtained through modelling and some from empirical work.

Propeller Modelling

Based on Quan's propeller model [3], there are two important parameters that need to be defined to lead us to the propellers parameters; the thrust *T* (N) and torque *M* (Nm) needed for the quadcopter's mission. Their expressions are:

$$T = C_T \rho (\frac{N}{60})^2 D_p^4 \quad (2.1)$$

$$M = C_M \rho (\frac{N}{60})^2 D_p^5 \quad (2.2)$$

The thrust needed for hovering is generally calculated as the weight of the UAV. This means that for an 11kg UAV the thrust for each propeller of a quadcopter should be around 27.5N. When ascending the thrust is conservatively assumed to be approximately double the weight of the aircraft. Choosing 1.8 due to power consideration, means that each propeller must have a maximum of 50N thrust output.

Note that *N* is the propeller speed (rpm), D_p is the propeller diameter (m) and ρ is the air density (kg/m^3) which is dependent on the local altitude h (m) and temperature *T* (^{o}C).

$$\rho = \frac{273 P_a}{101325(273+T)} \rho_0 \quad (2.3)$$

The value of the standard air density @ 273K is ρ_0=1.293(kg/m^3) while the atmospheric pressure is obtained through the equation:

$$P_a = 101325(1 - 0.0065 \frac{h}{273+T})^{5.2561} \quad (2.4)$$

For our UAV's mission the maximum altitude can reach as high as +2000(m) and a maximum temperature of 500^{o}C. The air density for these extreme conditions is calculated as 0.94 (kg/m^3). C_T and C_M are the dimensionless thrust and torque coefficients that have to be calculated next through the equations:

$$C_T = 0.25 \pi^3 \lambda \zeta^2 B_p K_0 \frac{\varepsilon \tan^{-1} \frac{H_p}{\pi D_p} - a_0}{\pi A + K_0} \quad (2.5)$$

$$C_M = \frac{1}{8A} \pi^2 C_d \zeta^2 \lambda B_p^2 \quad (2.6)$$

Institutional Repository - Library & Information Centre - University of Thessaly
03/09/2026 06:00:57 EEST - 216.73.216.156

Where C_d is the drag coefficient, given by the expression:

$$C_d = C_{fd} + \frac{\pi A K_0^2}{e} \frac{\left(\varepsilon \tan^{-1}\frac{H_p}{\pi D_p} - a_0\right)^2}{(\pi A + K_0)^2} \qquad (2.7)$$

The parameters used on the above equations are chosen empirically from Quan's [3] recommendations and validated through the APC website experimental data available and the ECalc online tool (table 2.3). [17]

Table 2.3: Parameter values for Quan's model based on empirical work. [3]

a_0	*zero lift angle of attack*	$-\frac{\pi}{36}$
K_0	*dimensionless parameter*	6.11
$A = \frac{D_p}{c_p}$	*aspect ratio*	8
C_{fd}	*zero lift drag coefficient*	0.015
λ	*correction factor*	0.75
ζ	*correction factor*	0.5
ε	*downwash correction factor*	0.85
e	*Oswald factor*	0.83

1) Diameter (D_p) and Pitch (H_p)

For a payload carrying quadcopter, the general guideline when choosing the appropriate propeller features is to select a larger diameter while keeping a lower pitch. A larger diameter provides the quadcopter with more thrust due to the larger volume of air that is pushed with each rotation, thus decreasing the number of revolutions needed to keep the quadcopter hovering/ascending/travelling alongside the noise and vibrations caused by the motors, which can compromise the structural integrity of the airframe. Lowering the pitch of the propellers might decrease the speed and acceleration of the UAV but offers stability, better balance and

Institutional Repository - Library & Information Centre - University of Thessaly
03/09/2026 06:00:57 EEST - 216.73.216.156

control while carrying a heavy payload. Considering the drone's mission stability and safety are valued higher than rapid delivery. [3] [18]

The maximum thrust needed is 50N per propeller and the air density for our mission is calculated as 0.92 kg/m^3 which is 71% of the air density at standard conditions (1.273 kg/m^3). This means that when using the data available for each propeller in the APC website, the thrust we should be looking at should be significantly higher than the one calculated at sea level for 25℃.

2) Number of Blades (B_p)

Generally, it has been indicated through experiments, that by increasing the number of blades the thrust produced is larger. This means smaller diameter propellers with more blades can do the same work as the larger 2-blade diameter, thus resulting in a more compact UAV that is smaller and probably lighter. On the other hand, it has been shown that more blades can bring down the efficiency of the propeller-motor system [3]. In [19] an experiment was set up to investigate the different effects propellers, motors and UAV arm configurations can have over the efficiency and the thrust produced by the propulsion system.

As can be seen in the graphs below (fig. 2.11), when comparing the 2-blade with the 3-blade propellers on the same motor configurations (puller and pusher) it is clear that the 2-blade propellers hold the edge over the propellers with more blades in terms of efficiency while having a heavier disc load. The average difference in efficiency is calculated at approximately 4%.

Institutional Repository - Library & Information Centre - University of Thessaly
03/09/2026 06:00:57 EEST - 216.73.216.156

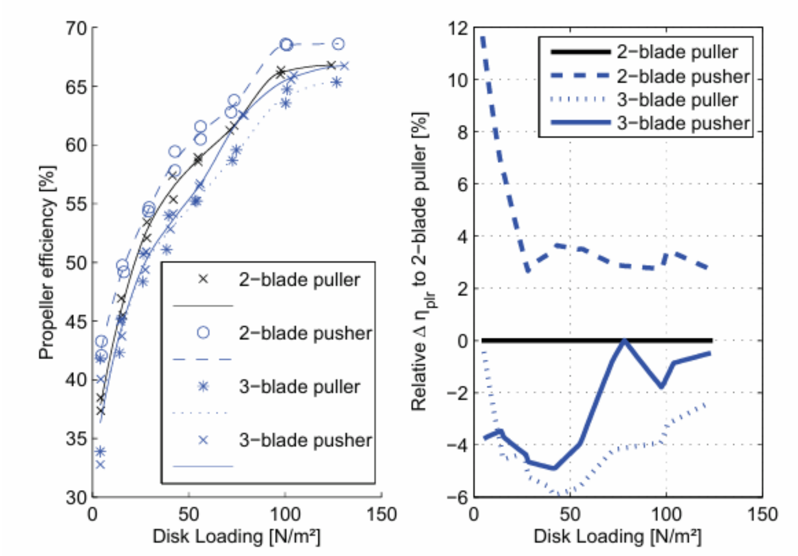

Figure 2.11: Comparison of the 2-blade and 3-blade pusher and puller propeller configuration. [19]

3) Chord Length

The chord length varies along the radius of the propeller and is usually defined by a geometric distribution (e.g. quadratic, linear, elliptical). The nominal chord length is usually measured at 2/3 of the radius of the propeller. For an aspect ratio of 8 as selected based on typical values given in [3] the nominal chord length can be calculated by the propellers diameter.

$$Aspect\ Ratio = \frac{D_p}{C_p} \tag{2.8}$$

4) Material

Typical materials for propellers include aluminum, wood and composites such as GFRP and CFRP. Wood is the cheapest material of the above options. It can provide high strength to weight ratio while resisting fatigue due to high internal friction which also makes it ideal for motor vibration dumping. However, this material's tendency to warp due to humidity and temperature excludes it for our UAV's mission [20]. Aluminum and its alloys are relatively lightweight with high strength to weight ratio and can resist corrosion. Also, this type of material is easily fabricated and processed. On UAV application though, it is not able to handle well the vibrations of the motor which can make the system inefficient and unresponsive. Last but not least, fatigue problems can arise from metal propellers in general when straining them

Institutional Repository - Library & Information Centre - University of Thessaly
03/09/2026 06:00:57 EEST - 216.73.216.156

excessively for long periods (longer trips). Composite materials such as Carbon Fiber Reinforced Plastics and Glass Fiber Reinforced Plastics are seen as recent advances in the aviation industry. What makes these materials so special are features such as high strength to weight ratios (up to 5 times greater than high-strength steels) and high stiffness to weight ratio (up to 8 times greater than structural metals) [21]. Specifically on UAV applications CFRP offers high rigidity decreasing vibrations, higher strength than aluminum with a fraction of the weight and suitability with low KV motors increasing efficiency [3]. On the other hand, CFRP products are costly due to their complexity and difficulty in manufacturing and processing. Finally, this type of composite needs careful design because of its discontinuous nature (matrix-reinforcement) and its unique properties can vary, both with position and direction. [21]

The propellers chosen are the KDE-CF275-DP of KDE Direct.

Table 2.4: Parameters of the selected propellers (KDE-CF275-DP). [22]

D_p x H_p	*27.5' x 8.9'*
B_p	*2*
C_p	*4.23'*
Material	*CFRP*
Weight	*43.2 g/blade*

2.4.2) Motors

The motors utilized in multicopters are predominantly brushless DC motors (BLDC) due to their numerous advantages, including high efficiency, potential for miniaturization, and low manufacturing costs. These motors are responsible for converting electrical energy, stored within the battery, into mechanical energy to drive the propellers [3]. The control circuit generates a Pulse Width Modulated (PWM) signal, which is transmitted to the Electronic Speed Controller (ESC). Within the ESC, this signal is amplified by a driving circuit and directed to the power switch of the inverter [23]. This process controls the motor windings in a specific sequence, creating a

Institutional Repository - Library & Information Centre - University of Thessaly
03/09/2026 06:00:57 EEST - 216.73.216.156

jump-type rotating magnetic field in the air gap of the motor. There is an abundance of BLDC motor types, and the right one must be chosen based on our specific needs.

Rotor Configuration

BLDC motors operate using stationary current-carrying coils and rotating permanent magnets. Two physical configurations of BLDC motors are illustrated: inner-rotor and outer-rotor (fig. 2.12, 2.13). In the inner-rotor configuration, the magnets are centrally located and surrounded by coil windings. Conversely, in the outer-rotor configuration, the coil windings are enclosed by an outer casing composed of permanent magnets. The outer-rotor configuration is preferred for UAV applications due to its requirement for lower energy magnets, reduced copper losses, lower production costs, and greater rotor inertia. [23]

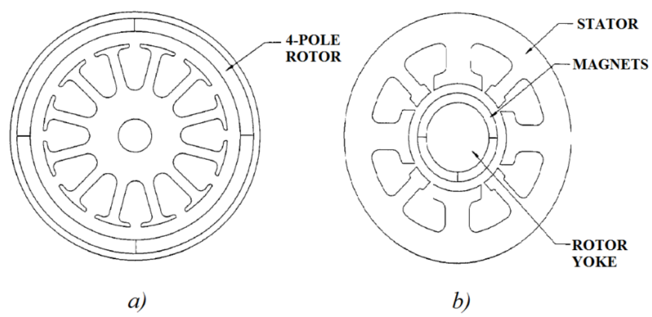

Figure 2.12: The two BLDC motor configurations: a) outer rotor BLDC motor b) inner rotor BLDC motor. [23]

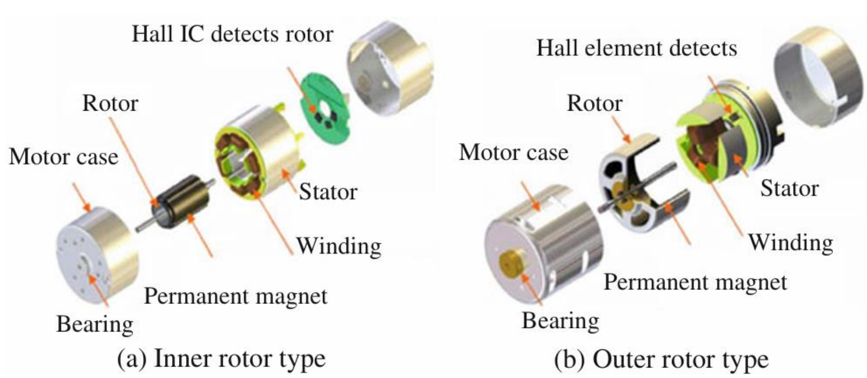

Figure 2.13: Assembly of the components of the two types of BLDC motor configurations. [3]

Institutional Repository - Library & Information Centre - University of Thessaly
03/09/2026 06:00:57 EEST - 216.73.216.156

Winding Configuration

The two most common winding configurations for 3-phase BLDC motors are Wye (Y) and Delta (Δ), each with distinct advantages and disadvantages. Most commercial model aviation BLDC motors utilize the Delta (Δ) winding configuration, which is optimized for high-speed applications. However, Delta (Δ) wound motors exhibit certain drawbacks, including additional ohmic losses compared to the Y configuration and torque ripple due to current circulation within the Delta loop. The Y winding configuration is preferred for lower-speed operations where higher torque production is required making it compatible with the UAV designed here. Y wound motors produce √3 times more torque and 1/√3 times less rotational speed than Delta wound BLDC motors. The relationship between Y and Δ windings can be represented as follows:

$$M_Y = \sqrt{3} M_\Delta \quad (2.9)$$

$$\omega_Y = \frac{1}{\sqrt{2}} \omega_\Delta \quad (2.10)$$

M being torque (Nm) and ω (rad/s) is angular velocity. Other significant parameters that should be taken under consideration (table 2.5) when selecting the correct motor for our application are:

1) *Size*

The size of a motor is typically indicated by its stator dimensions, represented by a four-digit number. The first two digits denote the stator diameter in millimeters, while the last two digits represent the stator height in millimeters. For instance, a motor labeled 2212 has a stator diameter of 22 mm and a stator height of 12 mm. Consequently, a larger first pair of digits corresponds to a wider motor, and a larger second pair indicates a taller motor. Motors with greater width and height generally provide higher power, making them more suitable for large multicopters.

Institutional Repository - Library & Information Centre - University of Thessaly
03/09/2026 06:00:57 EEST - 216.73.216.156

2) *KV Value*

The KV value for brushless DC motors indicates the number of RPM the motor will achieve when 1V (Volt) is applied with no load. For example, a 1000KV motor will have a no-load speed of 1000RPM when 1V is applied. Low KV motors have more windings of thinner wire, allowing them to carry more power, produce higher torque, and drive larger propellers. Conversely, high KV motors generate lower torque and are thus suited for driving smaller propellers for more rpm. This value is very important when matching propellers and motor with the aim of the highest possible efficiency.

3) Maximum Current/Power

The maximum current or power rating of a motor indicates the highest level of current or power the motor can handle safely. For example, a maximum continuous current rating of"30A/30s" means that the motor can operate safely with a continuous current of up to 30A; exceeding this limit for more than 30 seconds may result in motor damage. This definition similarly applies to the maximum continuous power rating.

4) *Resistance*

All motor armatures have some resistance, which, although small, cannot be ignored because the current flowing through this resistance can be very large, sometimes reaching tens of amperes. This resistance generates heat during motor operation, which can lead to overheating and reduced efficiency.

5) Motor Efficiency

$$Electrical\ Power\ (W) = Voltage(V) \times Current(A) \tag{2.11}$$

$$Motor\ Efficiency = \frac{Mechanical\ Power(W)}{Electrical\ Power(W)} \tag{2.12}$$

Motor efficiency is not a standard value but varies with input voltage (throttle) and load (propeller). For a given propeller, increasing the input voltage (and consequently the current) can reduce the motor's efficiency. This reduction occurs because higher current levels

Institutional Repository - Library & Information Centre - University of Thessaly
03/09/2026 06:00:57 EEST - 216.73.216.156

generate more heat due to resistance, along with other losses, thereby decreasing the ratio of effective mechanical power to input power.

6) Overall Specific Thrust

The overall performance of the propulsion system is highly dependent on the compatibility between the motor and the propeller. To evaluate the efficiency of the motor and propeller combination, the overall specific thrust is calculated as follows:

$$Overall\ Specific\ Thrust\left(\frac{g}{W}\right) = \frac{Thrust(g)}{Electrical\ Power(W)} \tag{2.13}$$

The motor chosen is the KDE7208XF-135 of KDE Direct.

Table 2.5: Specifications of the selected motor (KDE7208XF-135). [22]

Size	*7208*
KV Value	*135*
Maximum Current	*45A (180s)*
Resistance	*0.074Ω*
Overall Specific Thrust (avg)	*13.5 g/W*
Weight	*380 g*

2.4.3) ESC

The primary role of Electronic Speed Controllers (ESCs) is to regulate motor speed by interpreting the Pulse Width Modulation (PWM) signal transmitted by autopilots. This signal alone lacks the potency to directly power brushless DC motors. Unlike conventional ESCs, brushless ESCs offer an additional capability: they can function as inverters, converting onboard DC power into three-phase Alternating Current (AC) power suitable for brushless DC motors. Alongside this core function, ESCs often provide auxiliary features like battery and startup protection. ESCs can be categorized into two types: square-wave and sinusoidal-wave drivers.

Institutional Repository - Library & Information Centre - University of Thessaly
03/09/2026 06:00:57 EEST - 216.73.216.156

Square-wave ESCs produce square waveforms, operating their control elements in a binary switch state, which renders them simpler, more cost-effective, and easier to regulate. Conversely, sinusoidal-wave ESCs generate sinusoidal waveforms utilizing Field Oriented Control (FOC). Consequently, sinusoidal drivers exhibit superior performance in terms of operational stability, speed range, efficiency, and minimizing noise and vibrations [3]. To select the appropriate ESC some important parameters (table 2.6), need to be determined.

1) *Maximum continuous/peak current*

The pivotal factor determining the suitability of brushless ESCs is the current, typically denoted in Amperes (A). Each motor necessitates a corresponding ESC to ensure compatibility. Mismatched pairing risks damaging the ESC or even causing motor failure. Specifically, two crucial parameters characterize brushless ESCs: the maximum continuous current and peak current. The former denotes the highest sustained current under normal operation, while the latter indicates the ESC's tolerance for instantaneous peak current. Emphasis should be placed on verifying the maximum continuous current, ensuring it allows for a safety margin (e.g., 20%) to prevent power tube burnout effectively.

2) *Voltage Range*

The voltage range within which the ESC operates effectively is another significant parameter. Typically, specifications for ESCs include indicators such as "5-6S LiPo", signifying compatibility with a voltage range of 5-6 cells of LiPo battery, equating to 18.5–22.2V.

3) *Resistance*

Given that all ESCs inherently possess resistance, the generated heat becomes a notable factor, particularly as currents passing through them can occasionally exceed tens of Amperes. To address heat dissipation concerns, ESCs intended for high current applications are typically engineered with minimized resistance.

Institutional Repository - Library & Information Centre - University of Thessaly
03/09/2026 06:00:57 EEST - 216.73.216.156

4) *Refresh Rate*

The responsiveness of the motor is closely tied to the refresh rate of ESCs. In theory, a higher refresh rate correlates with faster response times. Multicopters, unlike conventional model airplanes, rely on swift adjustments in propeller speed to achieve rapid thrust adjustments. Consequently, the refresh rate of ESCs for multicopters is typically higher. However, to maintain smooth outputs, low-pass filtering is frequently employed on the input or output of ESCs, albeit at the expense of reducing their responsiveness. This adjustment also entails a decrease in control frequency.

5) *Programmability*

Enhancing ESC performance involves adjusting internal parameters, which can be achieved through three methods: programmable cards, computer software accessible via USB, and RC transmitters. These parameters encompass throttle range calibration, low voltage protection, power outage value, current limitation, brake mode, throttle control mode, switch timing setting, starting mode, and PWM mode setting.

6) *Compatibility*

When the ESC and motor are mismatched, the motor may become jammed, posing a risk of mid-air accidents such as a multicopter's fall and crash. In extreme scenarios, like sudden changes in control commands during mode transitions, motors may jam unexpectedly, resulting in high instantaneous currents that are difficult to detect.

The ESC chosen is the F60A MINI 8S 4IN1 ESC by T-MOTOR. [24]

Table 2.6: Specifications of the selected ESC (F60A MINI 8S 4IN1 ESC). [24]

Max current / Peak current	60A / 70A
Voltage range	4S-8S
Resistance	0.75mΩ
Refresh rate	16kHz-96kHz
Weight	14.2 g

Institutional Repository - Library & Information Centre - University of Thessaly
03/09/2026 06:00:57 EEST - 216.73.216.156

2.5) Power Consumption

Accurate power consumption of an intricate machine such as a quadcopter is a very difficult task that many scientists are currently trying to accomplish. A general model that can fit every single UAV is impossible to be created as every single machine has different attributes regarding thrust output, geometry, weight distribution, aerodynamics and environmental operating conditions. Here, the power consumed by the quadcopter during different flight modes will be calculated conservatively using the needed thrust for hovering and ascending, to ensure that the stored energy and the power produced by the hybrid system will be sufficient for the quadcopter's missions.

Using the same methodology as in 2.4.1 where the propellers were modelled, the calculated power for hovering and ascending can be found in the performance charts of the motors and propellers provided by the KDEDirect website (table 2.7) [22]. For a pair of the KDE7208XF-135 and the 27.5"x8.9 DUAL-EDN(KDE) connected to an 8S (30.8V) battery the performance was measured as:

Table 2.7: Motor-Propellers pair performance chart. [22]

Throttle (%)	Amperage (A)	Power Input (W)	Thrust (N)	RPM (rev/min)
25	1.1	38	6.86	1200
37.5	2.9	100	14.71	1740
50	5.7	198	23.54	2180
62.5	10.1	351	34.52	2580
75	15.6	542	45.31	2940
87.5	22.4	779	54.92	3300
100	29.3	1019	67.37	3540

Institutional Repository - Library & Information Centre - University of Thessaly
03/09/2026 06:00:57 EEST - 216.73.216.156

Using the equation for air density (eq. 2.3)

$$\rho = \frac{273P_a}{101325(273+T)}\rho_0$$

where ρ_0 is the air density at standard conditions (1 atm., 25℃) equal to 1.293 kg/m^3 we can calculate the new air density. Here, T denotes the temperature (℃) and P_a is the atmospheric pressure which can be calculated by (2.4):

$$P_a = 101325(1-0.0065\frac{h}{273+T})^{5.2561}$$

where h(m) is the altitude. Based on these equations for different temperatures of and different altitudes/pressures the air density can be calculated. The maximum height the multicopter should be able to reach is around 2000m and the maximum temperature it will operate in is around 50 ℃. These two numbers grow vice versa with the highest temperatures observed near sea level while at the highest altitudes the maximum temperature usually reaches around 30 ℃. To have a clear view of the power demand of the multicopter, 5 different extreme but realistic cases (table 2.8) will be examined to find the local air density (ρ) and relate it to the power input of the motor-propeller pair.

Table 2.8: Different cases regarding altitude and temperature.

Altitude (m)	Temperature (℃)	Pressure	Air Density	ρ/ρ_0
0	45	101314	1.12	0.86
400	41	98033	1.08	0.84
800	38	92727	1.04	0.8
1200	35	88680	1	0.78
1600	32	84453	0.964	0.75

By the expression for the thrust (2.1) produced:

Institutional Repository - Library & Information Centre - University of Thessaly
03/09/2026 06:00:57 EEST - 216.73.216.156

$$T = C_T \rho (\frac{N}{60})^2 D_p^4$$

it can be observed that the air density (ρ) and the rpm of the motor (N) are related to the thrust (T) as follows:

$$T \propto \rho \cdot RPM^2$$

So, for the same thrust for different air densities, we get:

$$\rho_0 \cdot RPM_0^2 = \rho_i \cdot RPM_i^2$$

$$RPM_i = RPM_0 \cdot \sqrt{\frac{\rho_0}{\rho_i}} \quad (2.14)$$

The RPM value in each case is proportional to the power input (P) needed by the motor so for each case the power demand of the multicopter relates to the change in air density:

$$P_i = P_0 \cdot \sqrt{\frac{\rho_0}{\rho_i}} \quad (2.15)$$

For example, for the 5th case where ρ_5=0.75ρ_0 the power related to the power for standard conditions can be calculated as:

$$P_5 = 1.15 \cdot P_0$$

To calculate the power (with the 2kg payload on) for hovering, we use T=mg where m=11kg and g=9.8m/s^2 so the thrust required by all 4 propellers is 107.8N which means each propeller will have to produce 26.9N which. The power in this case can be found in the performance chart. The power for hovering in standard conditions is approximately $P_{0,hov}$= 240 W for each motor.

When ascending the thrust is usually set as 2mg to secure adequate vertical acceleration. For a larger drone as this one we set it as 1.8mg. The thrust for ascending is then calculated as 194N for the whole quadcopter and 48.51N for each motor-propeller pair separately. Using the performance chart, it is observed that in standard conditions the power for ascending is $P_{0,asc}$= 580 W for each motor.

These values can be used to calculate the hovering and ascending power in each case when altitude and temperature information are available. For example, for the most extreme case (5th case, 1600m, 30°C) from the calculations above it easily deduced that for each motor:

Institutional Repository - Library & Information Centre - University of Thessaly
03/09/2026 06:00:57 EEST - 216.73.216.156

$$P_{5,hov} = P_{0,hov} \cdot 1.15 = 276\ W$$

$$P_{5,asc} = P_{0,asc} \cdot 1.15 = 667\ W$$

This proves that using the combination of the fuel cell and the battery, the propulsion system of the multicopter can cope with the power demand in extreme conditions for short trips where speed and high-altitude ascension carrying a 2kg payload is expected.

To conservatively calculate the power demand of a whole mission, a flight path is needed so each segment of hovering, horizontal travelling and ascending can be calculated for the specific conditions the multicopter is facing with or without the payload. For horizontal travelling the power consumed is assumed to be 10% higher than the hovering power as the aerodynamic drag is much smaller than the thrust so the power produced by this force exerted on the quadcopter is much smaller than P_{hov}.

Institutional Repository - Library & Information Centre - University of Thessaly
03/09/2026 06:00:57 EEST - 216.73.216.156

Chapter 3. Airframe Design & Analysis

The airframe structure of a UAV should be engineered to handle limited payloads without causing permanent damage, ensuring safe operation under the UAV'S mission conditions. It should also be capable of supporting the ultimate payload without failure. Once all other requirements are satisfied, the design will look to minimize total weight without compromising durability and aerodynamic efficiency. The dimensions of the multicopter must be well-proportioned, and its structural layout has to be optimal. Finally, the design aims to be visually appealing. Generally, the airframe configuration of a quadcopter includes the arms, the fuselage and the landing gear. In our case a platform for the delivered goods will also be incorporated in the design.

3.1) Design Considerations

3.1.1) Arms

Arm Length

The size of a multicopter is directly linked to the radius of its propeller. For a quadcopter, assuming the angle between two arms is ϑ, this angle would be *360/n*, which equals 90 degrees when *n=4*.

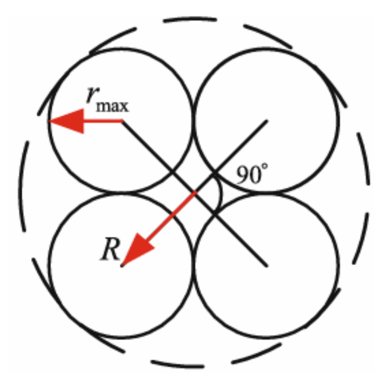

Figure 3.1: The radius from the center of the UAV to the propeller edge can be computed through the propeller's radius. [3]

The minimum radius (fig. 3.1) of the quadcopter can be calculated as:

Institutional Repository - Library & Information Centre - University of Thessaly
03/09/2026 06:00:57 EEST - 216.73.216.156

$$R = r_{max} / \sin(\theta/2) \tag{3.1}$$

For our multicopter the optimal propeller radius was found to be 13.75 inches or 34.93 centimeters (see section 2.4). This means that the minimum possible multicopter radius (measured from the center of the fuselage) is estimated as 19.44 inches or 49.4 centimeters by the equation above. The final value for the arm length of the quadcopter will be given by the minimum radius computed and the size of the fuselage, which depends on the topology of the components mounted onto it.

Arm Cross-Section

Despite extensive research on drone rotor design, the impact of fuselage arms on aerodynamic and aeroacoustic properties has been mostly omitted in drone research. Nevertheless, fuselage arms have a noteworthy effect on aerodynamic drag and noise. When the rotor blade passes over the arm, it creates a high static pressure region on the arm's upper surface. As expected, this interaction reduces the total upward thrust compared to an isolated rotor without the fuselage arm.

Examining the fuselage arms of current commercial UAVs reveals that their cross-sectional shapes usually range from rectangular to circular. Other potentially effective geometries that have been studied include circular with a middle rectangular slit, ellipse, semi-ellipse, and semi-square (fig. 3.2). All of these cross sections are examined in [25] with the help of Computational Fluid Dynamics Software.

Institutional Repository - Library & Information Centre - University of Thessaly
03/09/2026 06:00:57 EEST - 216.73.216.156

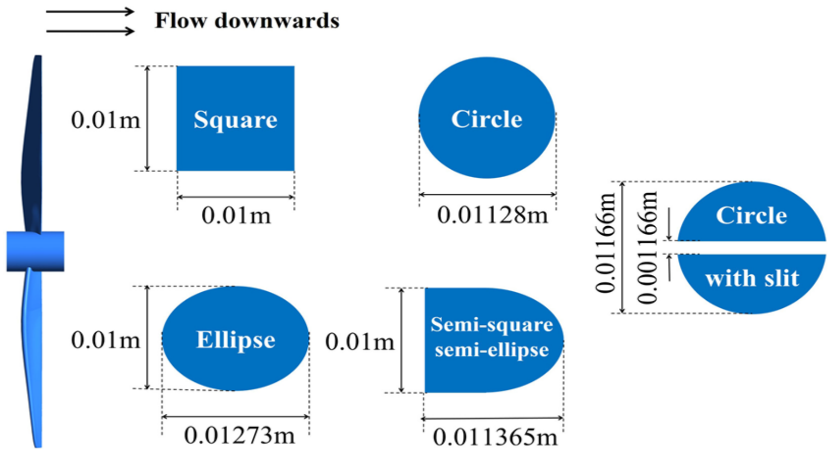

Figure 3.2: Cross-Sectional geometries investigated via CFD software. [23]

The computational region is a cylindrical closed volume that encompasses the rotor-arm model and its potential wake region. In all simulations, the UAV is in a hover state with zero horizontal/vertical speed. The rotor works at speeds of 6000 rpm, 9000 rpm, and 12000 rpm. The flow field around the rotor is analyzed using the three-dimensional compressible flow solver in ANSYS Fluent v15.0.

To assess aerodynamic performance, thrust and transverse forces on all rotor and arm surfaces are measured. Thrust is the key indicator of aerodynamic efficiency, while transverse force suggests potential vibration in the arm's transverse direction. For aeroacoustic performance evaluation, a pressure probe is positioned beneath the rotor-arm model at coordinates [-0.1 m, 0 m, 0.05 m] (fig. 3.3).

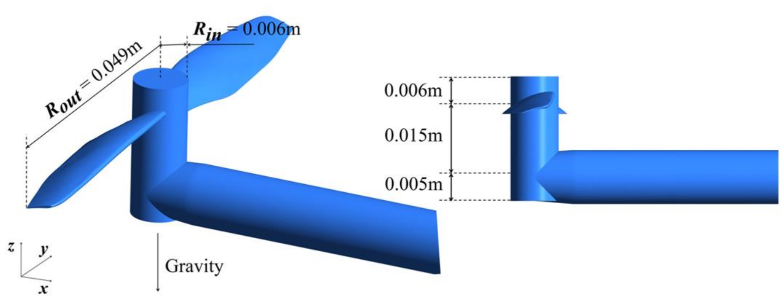

Figure 3.3: Geometry of the rotor-arm model used (here with the circular cross-section). [25]

After running the CFD simulation, it was concluded that the common geometries (square, circular) used for drone arms in commercial and professional applications hold the edge

Institutional Repository - Library & Information Centre - University of Thessaly
03/09/2026 06:00:57 EEST - 216.73.216.156

over the experimental ones (circular with slit, ellipse, semi-ellipse, semi-square). Regarding aerodynamic efficiency, based on the net thrust generated while the arm interferes with the air flow, the square cross section is the best-performing followed by the circular cross section. On the other hand, the circular cross section is the best choice noise-wise, as the sound pressure is minimum when using this type of arm, followed by the square cross-section arm. The results can be viewed below (Table 3.1)

Table 3.1: Thrust and Sound Pressure for different RPM. [25]

Case	Cross-Section	T (N) @ 6000 RPM	T (N) @ 9000 RPM	dB @ 6000 RPM	dB @ 9000 RPM
#0	Isolated rotor	0.2218	0.4897	71.87	79.29
#1	Square	0.1951	0.4564	71.66	76.82
#2	Circle	0.1908	0.4529	69.76	75.30
#3	Circle with slit	0.1902	0.4511	71.51	78.77
#4	Ellipse	0.1855	0.4455	70.66	78.5
#5	Semi square/ellipse	0.1800	0.4355	71.87	79.25

To make the decision between circular and square cross-sectional arms for our drone several factors should be considered besides the two mentioned above (aerodynamics, noise). To begin with, square tubes provide ease of connection with other parts of the UAV such as the fuselage, the motor and the propellers and possibly the landing gear or the cargo platform. In addition, this type of arm is a better structural choice as the highest force is applied on the arm by the propeller producing thrust when the drone is ascending. This force's direction is in the y axis where a squared beam has a better bending behavior in this scenario. A cyclical beam, on the other hand, provides uniform strength which is better suited for other applications. Finally, the manufacturability and cost of each geometry depends on the material (see chapter 4).

Institutional Repository - Library & Information Centre - University of Thessaly
03/09/2026 06:00:57 EEST - 216.73.216.156

3.1.2) Fuselage

The fuselage is the part of the UAV that is responsible for connecting every part of the airframe as well as some of the most important devices of the propulsion system. The fuselage can have many shapes and sizes depending on the nature and mission of the UAV.

Size and Shape

For drones that are used for surveillance and reconnaissance or search and rescue, the fuselage typically has a large, streamlined and aerodynamic shape to optimize flight duration and house cameras, sensors and long-range communication equipment. Multicopters built for photography/videography and racing purposes, it is common to incorporate smaller more compact designs to achieve maneuverability and stability. Agriculture and delivery drones have a larger fuselage to provide stability while carrying multiple payloads. Especially for payload carrying drones the design should also be boxier to maximize internal volume, providing more options.

When designing the fuselage, to determine its size and dimensions the features of the components mounted onto it should be considered. This should be done as everything should fit onto the fuselage without interfering with the propellers or other parts of the airframe and achieve a center of gravity as close to the geometric center as possible. This will make the UAV more stable, maneuverable and fuel efficient. [3]

The propulsion system parts that will be placed on the fuselage are listed below (fig. 3.4, 3.5, 3.6):

Institutional Repository - Library & Information Centre - University of Thessaly
03/09/2026 06:00:57 EEST - 216.73.216.156

1) Fuel Cell: **Size** = 214mm x 123mm x 130mm, **Weight** = 1230g

Figure 3.4: A-800 Aerostack Fuel Cell by H3 Dynamics. [12]

Institutional Repository - Library & Information Centre - University of Thessaly
03/09/2026 06:00:57 EEST - 216.73.216.156

2) Hydrogen Tank: **Size** = Φ 114mm, L 371mm, **Weight** = 1460g

Figure 3.5: F-Series Pressurized Hydrogen Cylinder by H3 Dynamics. [12]

3) LiPo battery: **Size** = 138mm x 50mm x 77, **Weight** = 1167g

Figure 3.6: LiPo 7S 8000mAh by MaxAmps. [16]

Institutional Repository - Library & Information Centre - University of Thessaly
03/09/2026 06:00:57 EEST - 216.73.216.156

Based on the dimensions of the propulsion system components, the fuselage upper plate should be at least 300mm x 300mm length and width wise so the whole system can fit. The camera, landing gear and platform for the delivered goods, will be mounted on the lower fuselage plate. The arms will be attached to both plates, enclosed between the two and secured via bolt-nut configurations. In the gap between the two plates, the avionics system and other electronics will be installed.

3.1.3) Other Components

Landing Gear

The landing gear is a crucial component of a UAV's structure, providing stability during takeoff and landing while maintaining the multicopter's balance. It also ensures that the propellers remain safely elevated above the ground, reducing the impact of ground effect, which occurs when the downwash hits the ground and causes disturbances during takeoff or landing. Additionally, the landing gear absorbs impact energy in the event of a sudden or hard landing, protecting the multicopter from damage. [3]

Mounting Gear

Some components need to be secured in place on the fuselage for the safe and correct function of the UAV but do not have integrated mounting holes in their design. Aiming to make durable, lightweight, functional and easily manufactured mounting gear, parts were designed as a solution to this problem.

Delivery Placing

This component is of great importance in our design as it defines the goal of this multicopter. The placing/shelf should be as large as possible volume-wise, so it can carry a wider variety of goods, from emergency items such as medicine etc., to vital goods such as water, food

Institutional Repository - Library & Information Centre - University of Thessaly
03/09/2026 06:00:57 EEST - 216.73.216.156

etc. It should be able to carry a load of 2kg with ease and be able to secure it as well while keeping the mass carried as close to the geometrical center as possible.

Propulsion System Housing

The housing will be designed with the aim of protecting vital components of the propulsion system from the harsh environment where it will be operating. The main problem is the excessive heat of this region which can damage catastrophically the battery while it also poses a threat to the fuel cell's operation as the limit of temperature in the air used is around 40 degrees Celsius. To achieve acceptable cooling and overall thermal protection, the housing designed should be a lightweight, multilayer construction made of an outer reflective layer, a middle insulating layer and an inner high-emissivity layer while also implementing channels for ventilation and natural convection

3.2) Final Design

The final design of the UAV was realized through Autodesk's Fusion CAD software. The UAV measures at 1190mm diagonally from motor to motor and has a height of 470mm (fig. 3.7, 3.8).

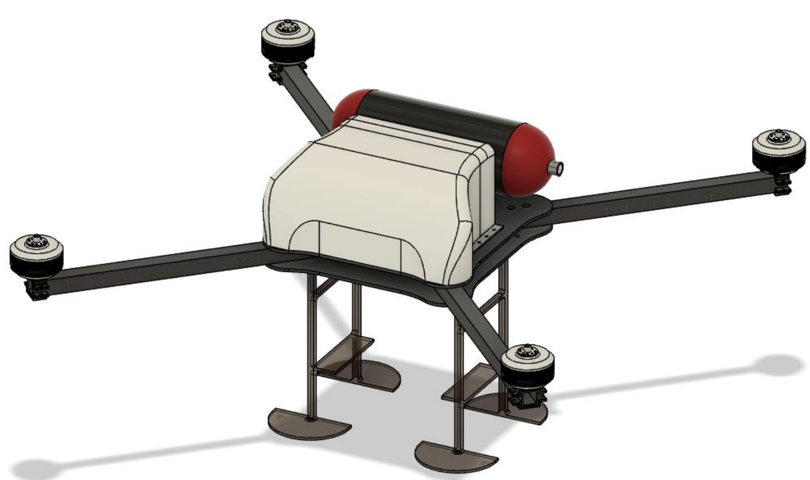

Figure 3.7: UAV final design.

Institutional Repository - Library & Information Centre - University of Thessaly
03/09/2026 06:00:57 EEST - 216.73.216.156

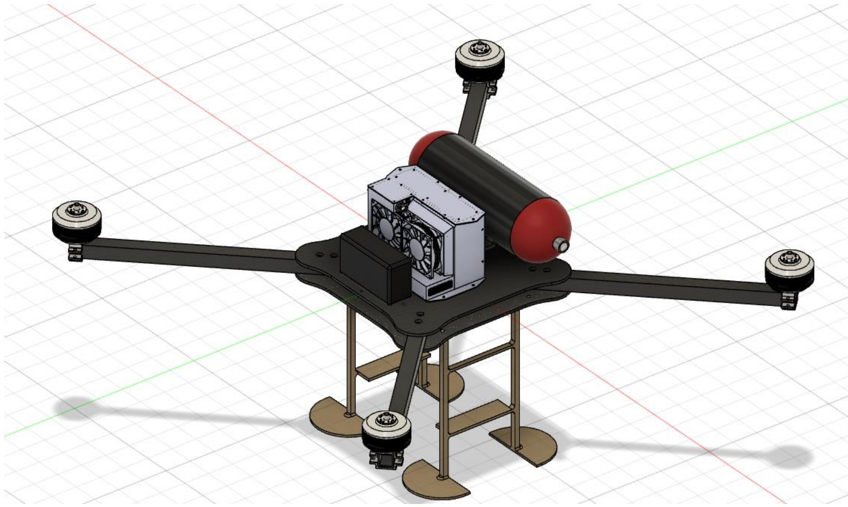

Figure 3.8: UAV without the housing, showing the components inside.

3.2.1) Arms Final Design

Based on the design considerations about the UAV's arms, it was concluded that the best choice would be a square cross section arm of 26mm x 26mm dimensions with a thickness of 2.5 mm (fig. 3.9). The length of the arms was chosen to be 480mm so the propellers of the quadcopter would be clear of the upper fuselage plate and the components mounted on it. Two 10mm holes were integrated in the design near the end of the arm so it can be assembled with the fuselage plates via bolt-nut configuration (fig. 3.10).

Institutional Repository - Library & Information Centre - University of Thessaly
03/09/2026 06:00:57 EEST - 216.73.216.156

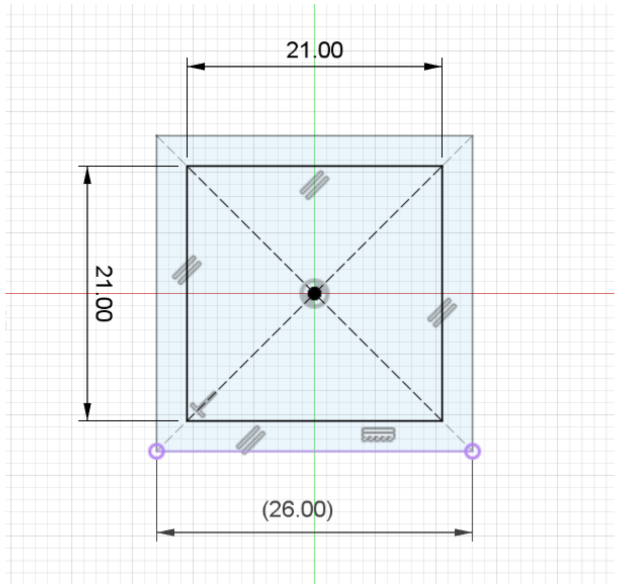

Figure 3.9: Sketch of the cross section of an arm.

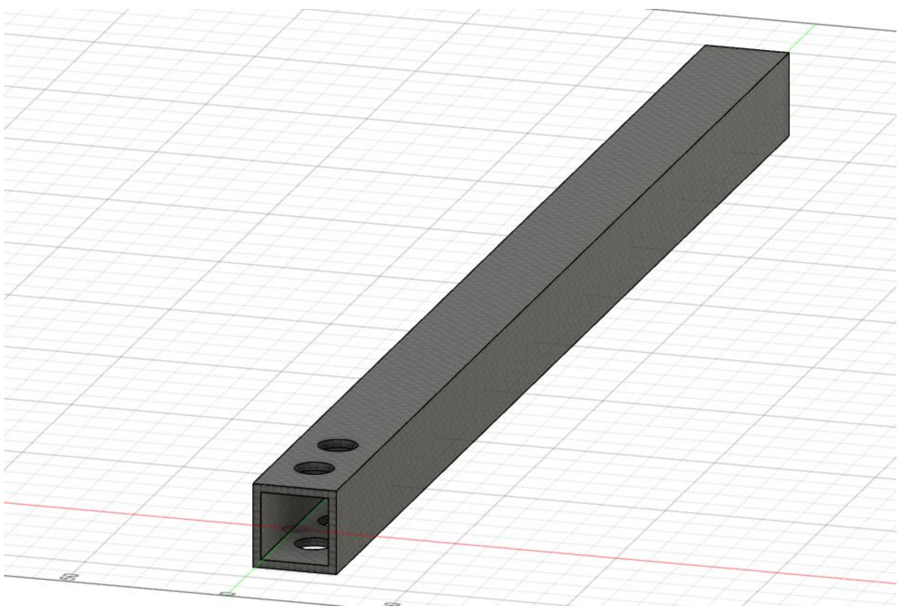
Figure 3.10: 3D design of an arm.

3.2.2) Fuselage Final Design

The fuselage plates designed based on the design considerations are square-like shapes of 320mm x 320mm dimensions with rounded, slightly extruding edges so the arms are better

Institutional Repository - Library & Information Centre - University of Thessaly
03/09/2026 06:00:57 EEST - 216.73.216.156

clamped between the plates. The thickness of each plate is 5mm and each one has holes integrated in their design based on the components that will be attached to it (fig. 3.11). The upper fuselage plate will carry the battery system, the fuel cell system, the hydrogen tank and the housing protecting the fuel cell and the battery. The lower fuselage plate will have the landing gear, the delivery placing, the camera and other avionic system components mounted on it.

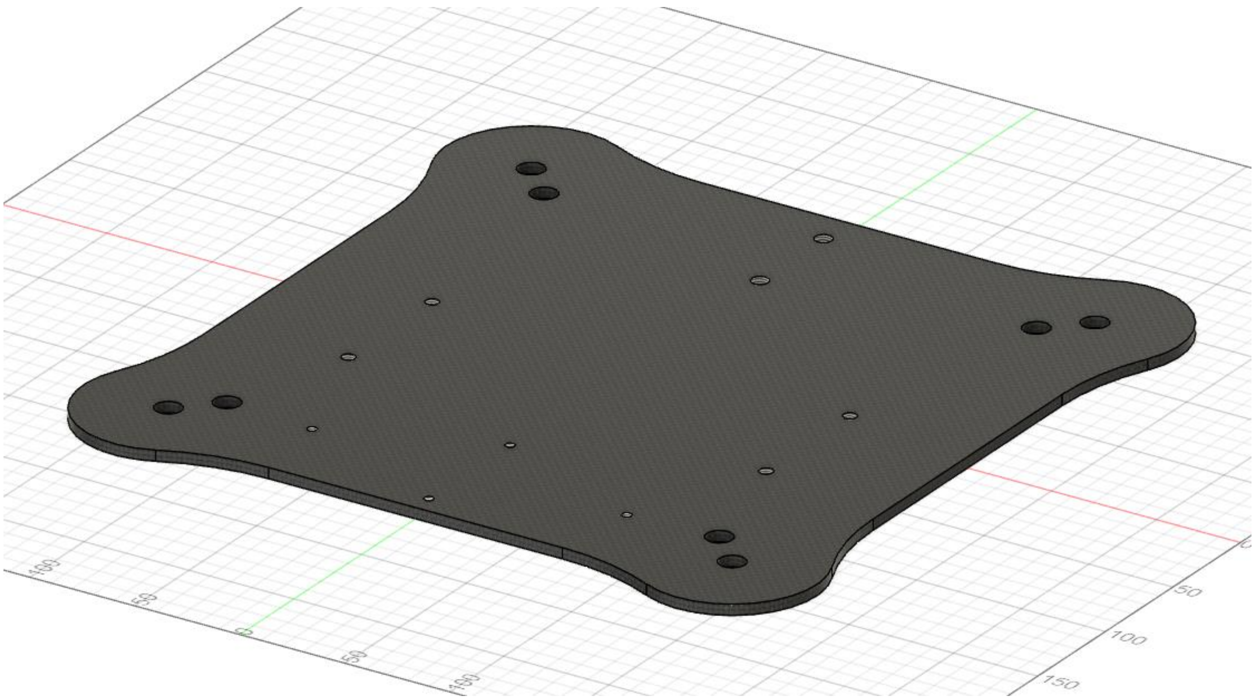

Figure 3.11: 3D design of the upper fuselage plate.

3.2.3) Other Components Final Design

Landing Gear/ Delivery Placing Final Design

The landing gear is composed of two legs attached to two opposing sides of the lower fuselage plate, left and right of the frontward direction of flight. The holes used to attach the legs to the lower fuselage plate are 8mm. The legs are designed to hold the weight of the multicopter vertically on their geometrical axis so buckling can be avoided (fig. 3.12). The surface on the bottom is wide so the landing is more stable and easier. Two shelves are incorporated in the

Institutional Repository - Library & Information Centre - University of Thessaly
03/09/2026 06:00:57 EEST - 216.73.216.156

design so the delivery box can be placed safely underneath the main UAV body. The shelves are designed in a manner that gives a minimum volume of 159mm x 120mm x 222mm and a maximum volume of 320mm x 200mm x 242mm (fig. 3.13).

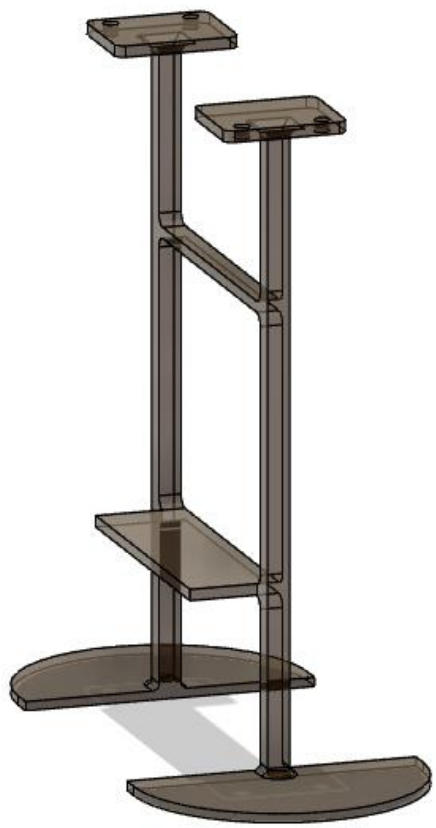

Figure 3.12: Landing Gear with delivery box placing shelves design.

Institutional Repository - Library & Information Centre - University of Thessaly
03/09/2026 06:00:57 EEST - 216.73.216.156

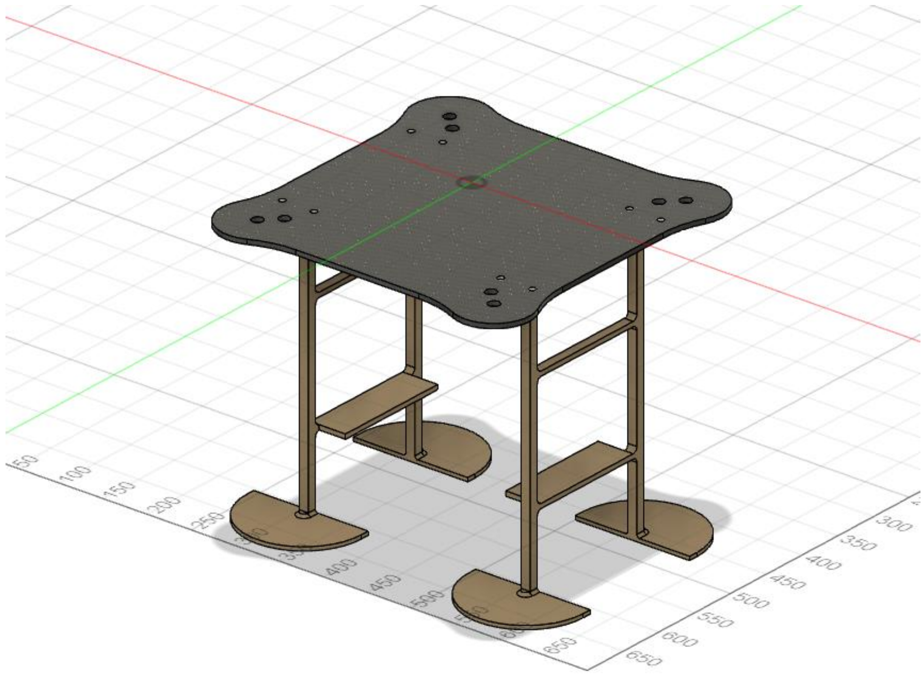

Figure 3.13: Assembly of the lower fuselage plate and the landing gear.

Mountings Final Design

Tank Mounting

The hydrogen tank's mounting is designed to be sturdy and keep the tank steady in the Y axis which is the direction in which the UAV will mostly travel (forward-backward) (fig. 3.14). Zip ties can be used to create a combination that will secure the tank at its place in the other axis (X, Z).

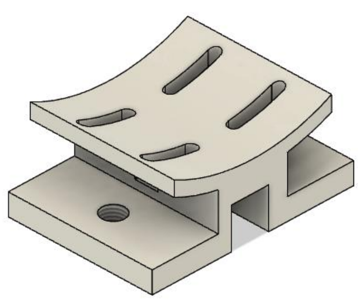

Figure 3.14: Tank mounting.

Institutional Repository - Library & Information Centre - University of Thessaly
03/09/2026 06:00:57 EEST - 216.73.216.156

Motor Mountings

The motor will be held at the end of the arm by an assembly of two mountings – an upper and lower mounting that will be tightened via nut bolt configuration. The two mountings have a similar core design with the difference that the upper mounting has a cylindrical extruding feature where the motor will be attached (fig. 3.15, 3.16). A circular profile was selected for this purpose so the tensile force will be distributed evenly. This would not be the case if the base was cross or square shaped.

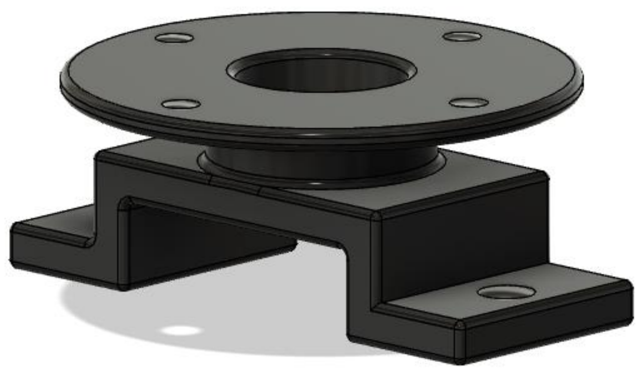

Figure 3.15: Upper motor mounting design.

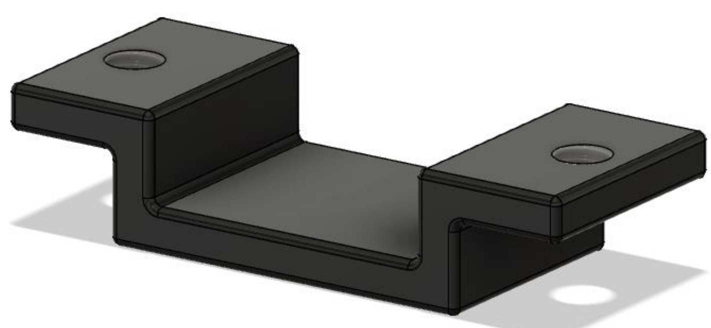

Figure 3.16: Lower motor mounting design.

Institutional Repository - Library & Information Centre - University of Thessaly
03/09/2026 06:00:57 EEST - 216.73.216.156

The holes that are used to assemble the mountings together are 5mm while the ones holding the motor onto the upper mounting are 3.3mm so they match the existing motor threaded holes.

Propulsion System Housing Final Design

The protective housing for the propulsion system components is designed to be compatible with the sketch of the fuselage plate. It has a rounded design on the front, minimizing drag and making it aerodynamical while also featuring slits in the back so sufficient air volume is passed through for the necessities of the fuel cell and the cooling of the components through natural convection (fig. 3.17, 3.18). This component is divided in two parts; the front one is airtight enclosed and additionally insulated to keep the battery cool while the back compartment where the fuel cell is stored is in contact with air. The housing is attached to the fuselage through 6 (3 on each side) 6mm holes.

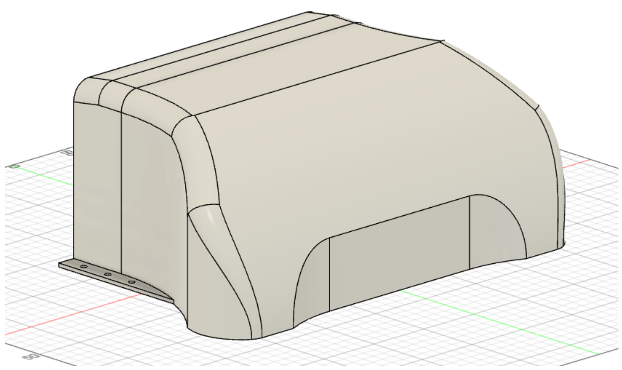

Figure 3.17: Propulsion system housing view (a).

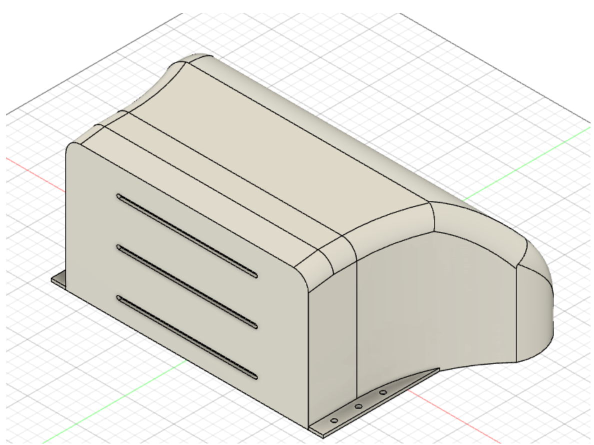

Figure 3.18: Propulsion system housing view (b).

Institutional Repository - Library & Information Centre - University of Thessaly
03/09/2026 06:00:57 EEST - 216.73.216.156

3.3 Materials

Choosing the right material for a machine part or structural component is a critical decision in the design process. While strength and deflection are often the primary considerations, other factors, such as temperature and corrosion, must also be accounted for, especially considering the operating environment of the UAV in question. To identify the most suitable materials, CES EduPack software will be utilized to filter and prioritize options based on the design requirements and the importance of these factors.

3.3.1) Arms and Fuselage Materials

The arms and fuselage plates are the most important structural parts of the UAV as their assembly carries the weight of the UAV during flight. Thus, it is natural that the most important factor is the strength (measured through yield strength) of the material chosen as well as its density due to the large volume of the structural components and the significance of lightweightness in our design (fig. 3.19). Secondary to strength and density, is the material's ability to dissipate energy/damp vibrations which is measured through the mechanical loss coefficient (tan delta) (fig. 3.20). In a multicopter this is very important as the motor-propeller system rotates at high rpm and creates vibrations that could affect the joints of the structure and electronics on the fuselage (accelerometer, gyroscope). Other important factors are the material's response to fatigue, high ambient temperatures and corrosion due to high levels of humidity (fig. 3.21).

Institutional Repository - Library & Information Centre - University of Thessaly
03/09/2026 06:00:57 EEST - 216.73.216.156

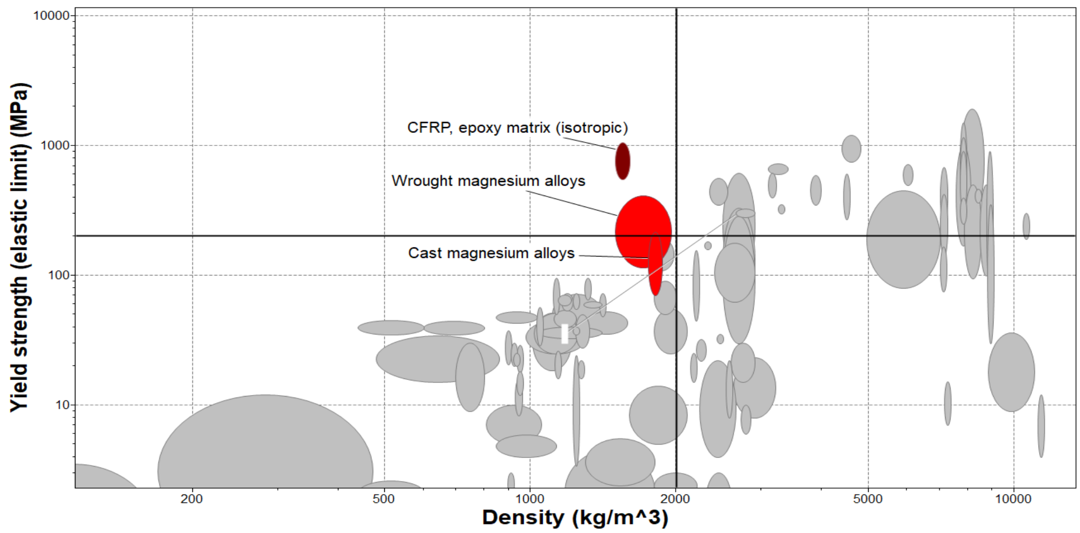

Figure 3.19: Yield Strength vs. Density with limits set at 200 (MPa) and 2000 (kg/m^3) respectively.

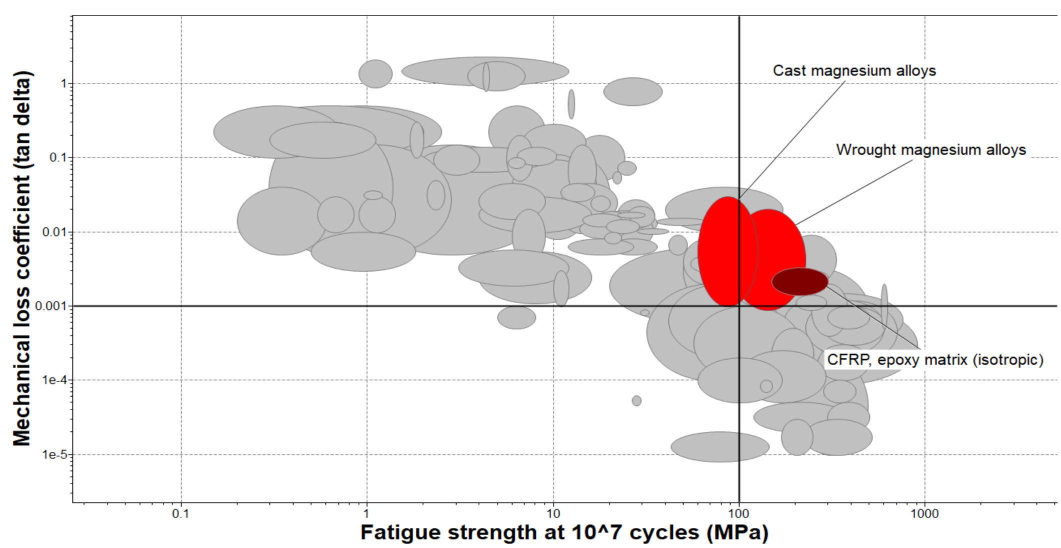

Figure 3.20: Mechanical Loss Coefficient vs. Fatigue Strength with limits at 0.001(tan delta) and 100(MPa) respectively.

Institutional Repository - Library & Information Centre - University of Thessaly
03/09/2026 06:00:57 EEST - 216.73.216.156

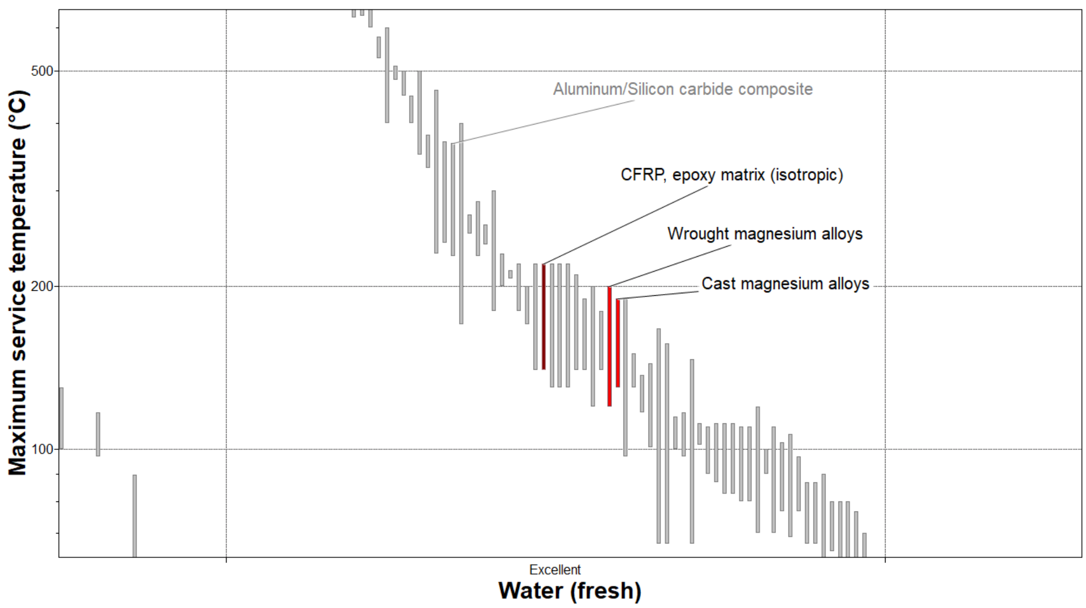

Figure 3.21: Maximum Service Temp. vs. Durability in Fresh Water with limits at 50 (C) and Excellent durability respectively.

The same three materials passed the first three stages in CES Edupack software. Studying the general information pages for cast magnesium alloys and wrought magnesium alloys it is mentioned that these materials are very susceptible to corrosion due to salt water in contrast to fresh water. This fact makes these materials better for indoor use and inappropriate for our design as usage in an open environment could be dangerous. Concluding, CFRP is the material selected for the arms and fuselage plates even though it might be harder to machine.

3.3.2 Other Components' Materials

Landing Gear Materials

As in the fuselage and arms material selection, the first criteria here is the strength and the density of the component as well (fig. 3.22). The material should be strong enough to handle the total weight of the multicopter and the delivery package and also be durable in case of rough landings. In contrast to the arms and fuselage, the design of the landing gear is quite complex, so fabrication and machinability are of great importance. In addition, the ability to dump vibrations

Institutional Repository - Library & Information Centre - University of Thessaly
03/09/2026 06:00:57 EEST - 216.73.216.156

and dissipate energy from abrupt landings will be taken into account (fig. 3.23) [26]. Finally, max. temperature service and corrosion resistance should be in acceptable ranges (fig. 3.24).

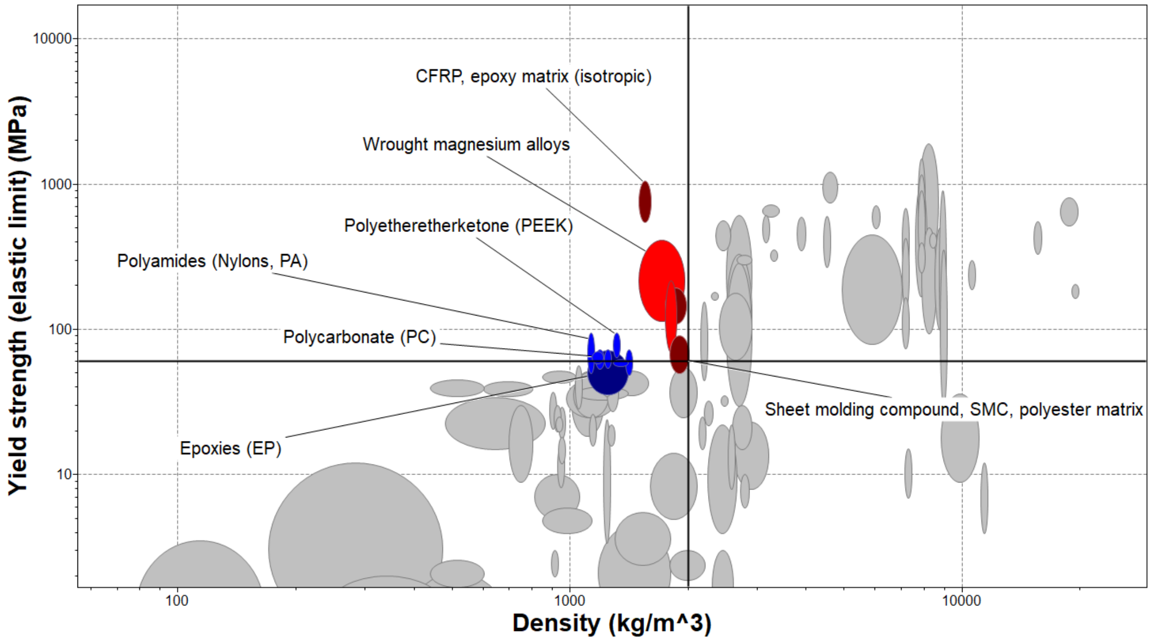

Figure 3.22: Yield Strength vs. Density with limits set at 60 (MPa) and 2000 (kg/m^3) respectively.

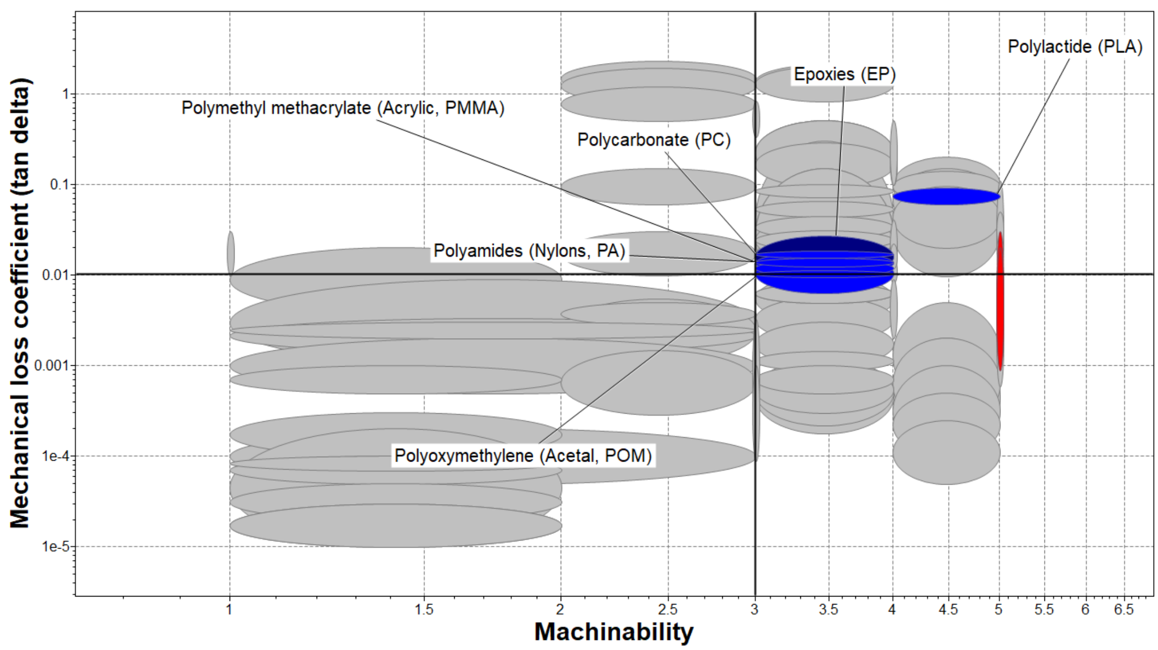

Figure 3.23: Mechanical Loss Coefficient vs. Machinability with limits set at 0.01 (tan delta) and 3 respectively.

Institutional Repository - Library & Information Centre - University of Thessaly
03/09/2026 06:00:57 EEST - 216.73.216.156

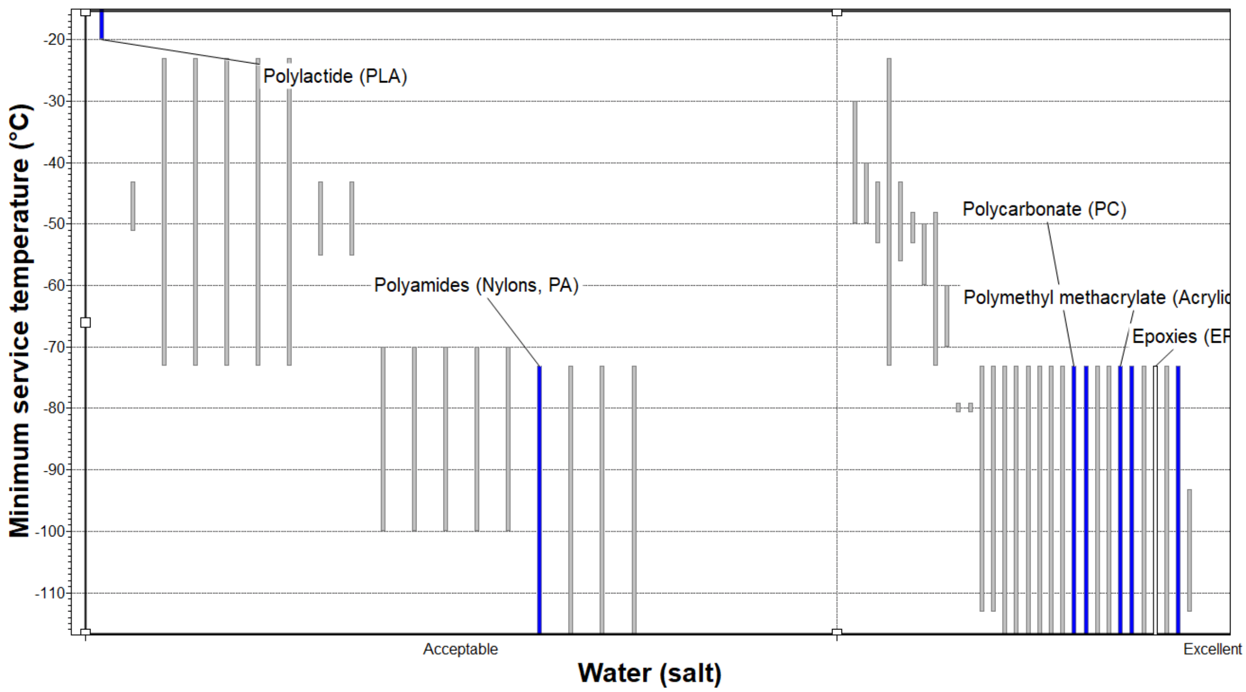

Figure 3.24: Maximum Service Temperature vs Durability in Salt Water(box limits).

After three stages in the CES Edupack software, many materials from the family of polymers have passed through (fig. 3.25). Examining again the most important factors (strength and density) knowing that most polymers pass the limits set on other stages, some materials such as PEEK and Polycarbonate plastic stand out. Researching the general information provided by the software for these materials, PC is finally selected as it is slightly lighter (1200kg/m^3) and 50 times cheaper (2.5$/kg) than PEEK even though it has a 10% lower yield strength (65MPa).

Institutional Repository - Library & Information Centre - University of Thessaly
03/09/2026 06:00:57 EEST - 216.73.216.156

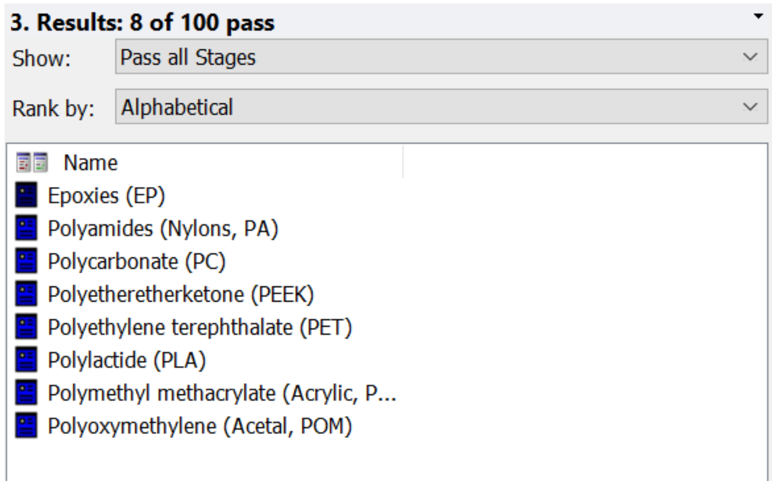

Figure 3.25: List of materials that passed all of the stages.

Mountings Materials

For the mountings, as in the components examined above, strength, lightweightness, dumping ability, fabrication, machinability and durability to thermal loads and corrosion are the significant factors that will help with material selection. Especially for the motor mountings, the design and role of these components are very close to the landing gear in terms of expected durability and design complexity. This is why for the tank mounting and the motor mountings, the same material as the landing gear will be used (Polycarbonate).

Propulsion System Housing Materials

The propulsion system protective housing is a multipurpose component that should be insulating the propulsion system, protecting it from UV radiation and other environmental effects. The main attributes of this material are low thermal conductivity, good durability at UV radiation, low density, high strength and easy fabrication (preferably moldability) as the design of the housing is complex (fig. 3.26, 3.27, 3.28).

Institutional Repository - Library & Information Centre - University of Thessaly
03/09/2026 06:00:57 EEST - 216.73.216.156

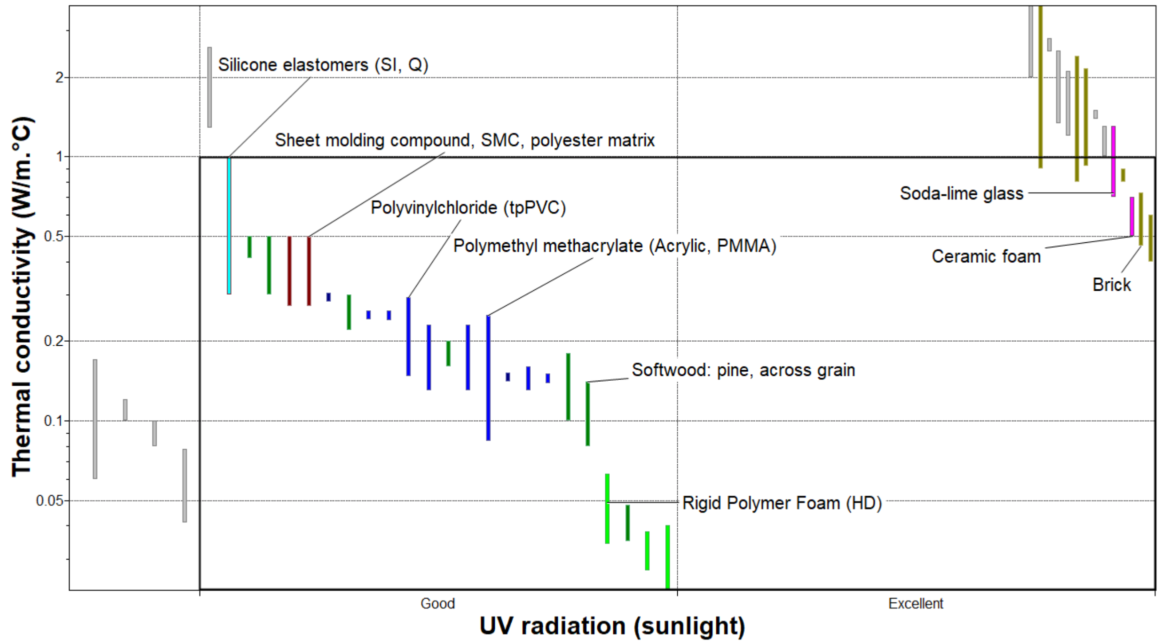

Figure 3.26: Thermal Conductivity vs. UV Radiation Durability (box limits).

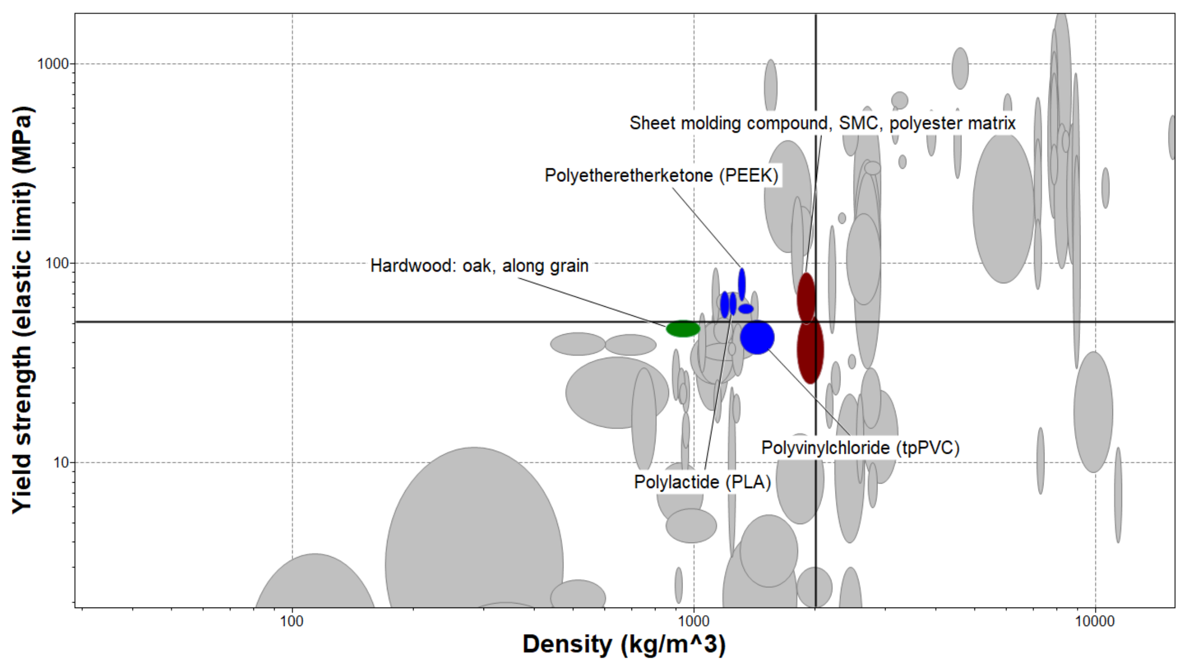

Figure 3.27: Yield Strength vs. Density with limits at 50 (MPa) 2000 (kg/m^3).

Institutional Repository - Library & Information Centre - University of Thessaly
03/09/2026 06:00:57 EEST - 216.73.216.156

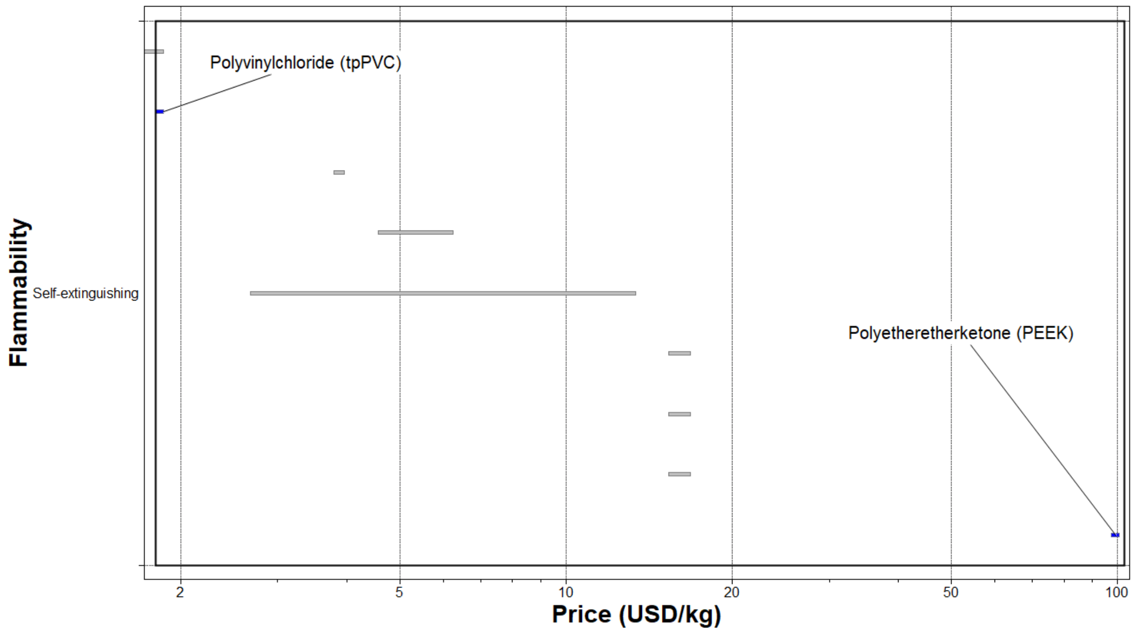

Figure 3.28: Flammability vs Price (box selection)).

By examining the materials that passed the two stages Polyvinylchloride (tpPVC) seems as the best choice as it is nonflammable, durable to UV radiation and corrosion, cheap and sturdier than the other candidates making it a great fit as the main layer of the housing.

Housing Coating

When a paint or coating is applied onto a solid the most important factor to promote adhesion on the solid is the ability of the paint/coating to “wet-out” the surface. For this phenomenon to occur, the surface tension of the liquid should be lower than the surface tension (also called surface energy) of the solid. When the contact angle of the liquid and the solid is smaller than 90 degrees the liquid tends to spread and “wet” the solid surface while if that is not the case, the liquid tends to “bead” upon the surface (fig. 3.29). [26]

Institutional Repository - Library & Information Centre - University of Thessaly
03/09/2026 06:00:57 EEST - 216.73.216.156

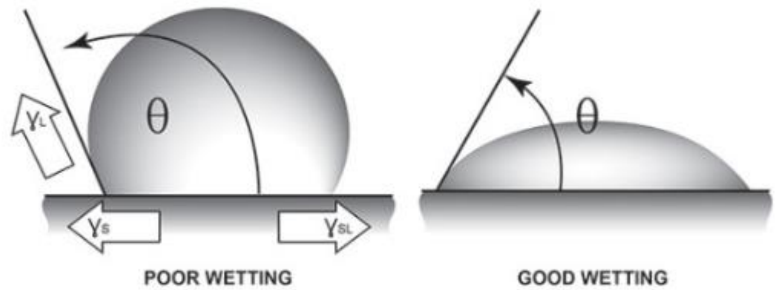

Figure 3.29: Good and bad "wetting" based on contact angle. [26]

The surface tension (γ) can be measured through units called dynes or dynes/cm. For a painting or coating to be able to spread on a surface the difference between the two in dynes should be at least 10 dynes. Polymers such as PVC (used for the housing) have a very low surface tension of approximately 40-45 dynes/cm making it very difficult for liquid to wet efficiently their surface. This number can be increased to the region of 50+ dynes/cm by a variety of treatments of the surface, with the most simple and inexpensive being surface roughening. Some of the lower surface tensions can be found in acrylic coatings. These coatings made of polymer are a good match for the PVC housing but with a surface tension of 40 dynes/cm, they cannot wet the housing's surface efficiently. To achieve good adhesion, primers and tie coats can be used as a "bridge" to promote adhesion of the paint onto the solid by dropping the surface energy of the acrylic coating as low as 30-35 dynes/cm. This way an acrylic coating mixed with aluminum can be used onto the housing to protect it from UV radiation as acrylics can handle sunlight very well and the aluminum flakes dispersed into the mix are great for reflecting most of this radiation. [26]

Housing Insulation

To achieve better insulation for the battery compartment so the battery operates as efficiently as possible, and its degradation is slow, fiberglass will be attached on the inside of the housing. This material is made of molten glass that is then spun into fibers (fig. 3.30). Higher density fiberglass has a lower thermal conductivity but is harder and more difficult to shape which would be problematic for a complex shape such as the housings battery compartment. Typical low-density fiberglass has a thermal conductivity coefficient of 0.05 W/mK at maximum. [8] [27]

Institutional Repository - Library & Information Centre - University of Thessaly
03/09/2026 06:00:57 EEST - 216.73.216.156

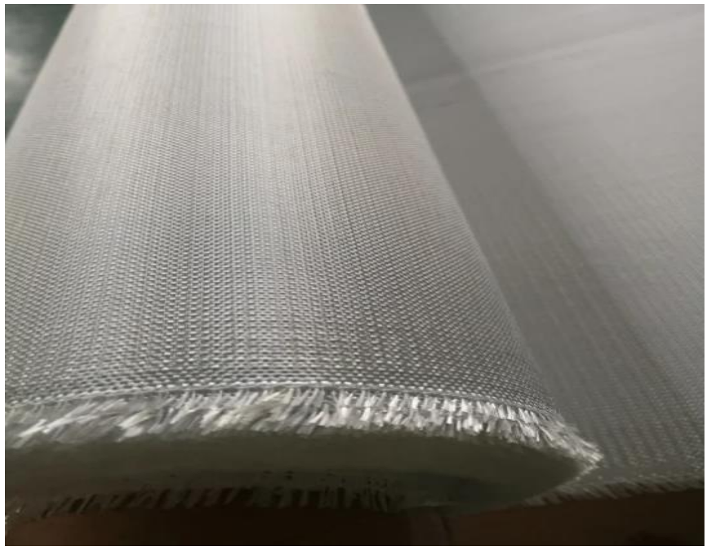

Figure 3.30: 4mm thickness 3D fiberglass woven fabric. [28]

3.4 Impermanent Joints

CFRP Parts Joining

Mechanical joining of composites has been an issue due to the problems arising from the generation of holes on the fiber reinforced plastic. Depending on the method of cutting/drilling, failure mechanisms can begin because of the rupture of composite fibers, the concentration of stresses around the holes or the high probability of micro-cracks that may cause structural instability. Besides these issues bolting can still be an acceptable method when proper design rules are followed. [27]

Based on experimental investigation presented on [27], for near isotropic lay-ups in graphite/epoxy composites, tensile/compressive failure probability can be minimized when the ratio between bolt diameter *D* and laminate width *W* is lower than 0.25 ($D/W <0.25$). In addition, it was observed that smaller washers combined with low bolt preload show higher offset bearing strength. Finally, the use of inserted threads in the composites hole using epoxy could be a solution for delamination and fiber rupturing.

Institutional Repository - Library & Information Centre - University of Thessaly
03/09/2026 06:00:57 EEST - 216.73.216.156

The bolts chosen are pan head black oxide stainless steel for better load distribution on the surface of the CFRP parts coupled with nylon insert stainless steel black oxide hex lock nuts to provide vibration resistance. Additionally split lock stainless steel black oxide washers with black rubber gaskets will complete the configuration to provide security, vibration dumping and protection from friction. Finally, stainless steel black oxide helix coils will be inserted in the holes and secured with epoxy resin (fig. 3.31, 3.32, 3.33, 3.34, 3.35).


Figure 3.31: Pan Head Black Oxide Stainless Steel Bolt. [29]

Figure 3.32: Nylon insert stainless steel black oxide hex lock nuts. [29]


Figure 3.33: Split lock stainless steel black oxide washers. [29]

Figure 3.34: Black rubber gaskets. [29]

Institutional Repository - Library & Information Centre - University of Thessaly
03/09/2026 06:00:57 EEST - 216.73.216.156

Figure 3.35: Stainless steel black oxide inserted helical coils. [29]

Polymer Parts Joining

[29]In the same context as composites, polymers are difficult to machine and thread creation could create problems such as cracks. This is why inserted threads secured with adhesives or molded in the original design during fabrication of the parts are a good choice for this specific design as some of the polymer parts used (motor mountings, landing gear) require high load bearing connections. Additionally, the bolts, nuts and washers used should be made of plastic (nylon) and rubber gaskets should be used as well (fig. 3.36, 3.37, 3.38).

Figure 3.36: Nylon black pan head bolts. [29]

Figure 3.37: Nylon black hex nuts. [29]

Institutional Repository - Library & Information Centre - University of Thessaly
03/09/2026 06:00:57 EEST - 216.73.216.156

Figure 3.38: Nylon washers. [29]

Based on [21] [30] the dimensions of the parts of the bolt nut configurations (in composites and in polymers) should be in relation to the nominal diameter (*D*) of the bolt. The nut height (*h*) should be approximately the same as *D,* engaging fully with the threads along the length of the bolt's diameter. The outer diameter of the washer should be equal to 2*D while the inner diameter should be slightly larger than D. Its thickness must measure at $1/10^{th}$ of the diameter of the bolt.

3.5 Analysis of the UAV

While analysis of simple mechanical components such as beams, bars etc. can be done by basic methods of mechanics, familiar to an engineer, real complicated components like the ones designed for this project can be analyzed only by approximations that are less effective. This is why in this age of advanced digital computation, numerical techniques are utilized in engineering applications. The most popular method is Finite Element Analysis (FEA) which happens to work effectively with Computer Aided Design (CAD) software. The capabilities of FEA cover a wide spectrum of applications like static, dynamic, linear and non-linear stress-deflection analysis, vibrations, buckling and heat transfer.

Institutional Repository - Library & Information Centre - University of Thessaly
03/09/2026 06:00:57 EEST - 216.73.216.156

3.5.1) The Finite Element Analysis Method

The initial stage of any numerical method involves discretization. In this step, the medium under consideration is partitioned into several smaller subregions and nodes. Following this, integral formulations are applied to develop a system of algebraic equations. Additionally, an approximate continuous function is assumed to represent the solution within each subregion. The overall solution is then obtained by combining these individual solutions, ensuring continuity across the boundaries between the subregions.

The Finite Element Analysis method is generally divided into three phases:
Preprocessing Phase: The domain under analysis is broken down into finite elements, dividing the problem into individual elements and nodes. Shape functions are used to model the physical behavior of each element, while a continuous function is assumed to describe the solution within each element. The required equations are formulated for each element. These elements are then combined to construct the entire problem, leading to the formation of the global stiffness matrix. Finally, initial conditions, boundary conditions, and loading are applied to complete the analysis.
Solution Phase: A set of linear or nonlinear equations are solved simultaneously to obtain nodal results, such as displacement values at different nodes in a structural problem or temperature values at different in a heat transfer problem.
Postprocessing Phase: Gather crucial information. Key aspects of the problem, such as the values of principal stresses, heat fluxes, and other significant factors, require further investigation.

Structural Analysis Using FEA

The basic element used for 3D FEA analysis is the four-node tetrahedral element. For characterization of the general state of stress at a point, 6 independent stress components are needed:

$$[\sigma^T] = [\sigma_{xx} \quad \sigma_{yy} \quad \sigma_{zz} \quad \tau_{xy} \quad \tau_{yz} \quad \tau_{zx}]$$

where σ represents normal stress components and τ represents shear stress components. The displacement vector that calculates the difference occurring in the position of a point within a body when the body is loaded is written as:

$$\vec{\delta} = u(x, y, z)\vec{i} + v(x, y, z)\vec{j} + w(x, y, z)\vec{k}$$

Institutional Repository - Library & Information Centre - University of Thessaly
03/09/2026 06:00:57 EEST - 216.73.216.156

The state of strain is represented by six independent components as shown below:

$$[\varepsilon] = [\varepsilon_{xx} \quad \varepsilon_{yy} \quad \varepsilon_{zz} \quad \gamma_{xy} \quad \gamma_{yz} \quad \gamma_{zx}]$$

where the ε components represent normal strain and γ components represent shear strain. Strain and displacement are correlated by the relations:

$$\varepsilon_x = \frac{\partial u}{\partial x}, \quad \varepsilon_y = \frac{\partial u}{\partial y}, \quad \varepsilon_z = \frac{\partial u}{\partial z}$$

$$\gamma_{xy} = \frac{\partial u}{\partial y} + \frac{\partial v}{\partial x}, \quad \gamma_{yz} = \frac{\partial v}{\partial z} + \frac{\partial w}{\partial y}, \quad \gamma_{zx} = \frac{\partial w}{\partial x} + \frac{\partial u}{\partial z}$$

Stress and strain are correlated by the expression:

$$[\sigma] = [D][\varepsilon]$$

where the stress and strain matrix are analyzed above, while the matrix for the constitutive matrix is written as:

$$[D] = \frac{E}{(1+\nu)(1-2\nu)} \begin{bmatrix} 1-\nu & \nu & \nu & 0 & 0 & 0 \\ \nu & 1-\nu & \nu & 0 & 0 & 0 \\ \nu & \nu & 1-\nu & 0 & 0 & 0 \\ 0 & 0 & 0 & \frac{1-2\nu}{2} & 0 & 0 \\ 0 & 0 & 0 & 0 & \frac{1-2\nu}{2} & 0 \\ 0 & 0 & 0 & 0 & 0 & \frac{1-2\nu}{2} \end{bmatrix}$$

Selecting a tetrahedral element (fig. 3.39) will give us 3 degrees of freedom per node leading to 12 degrees of freedom per element.

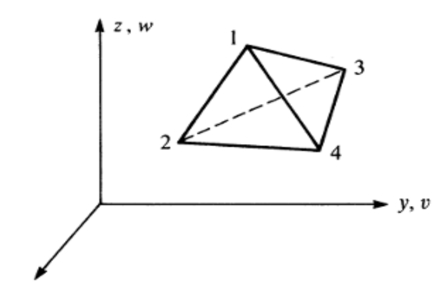

Figure 3.39: Tetrahedral element. [30]

This way the unknown nodal displacements will now be expressed as:

Institutional Repository - Library & Information Centre - University of Thessaly
03/09/2026 06:00:57 EEST - 216.73.216.156

$$[d] = \begin{bmatrix} u_1 \\ v_1 \\ w_1 \\ . \\ . \\ u_4 \\ v_4 \\ w_4 \end{bmatrix}$$

To obtain a compatible displacement field *u, v, w* must be linear along the edges as only the corner nodes exist on each edge. The linear displacement functions are selected as:

$$u(x, y, z) = a_1 + a_2 x + a_3 y + a_4 z$$

$$v(x, y, z) = a_5 + a_6 x + a_7 y + a_8 z$$

$$w(x, y, z) = a_{9+} a_{10} x + a_{11} y + a_{12} z$$

The a_i terms can be written in relation to the known nodal coordinates $(x_1, y_1, z_1, ..., z_4)$ and the unknown nodal displacement $(u_1, v_1, w_1, ..., u_4)$.

$$u(x, y, z) = \frac{1}{6V} \sum_{i=1}^{4} (\alpha_i + \beta_i x + \gamma_i y + \delta_i z) u_i$$

Where *6V* can be calculated by the determinant:

$$\begin{vmatrix} 1 & x_1 & y_1 & z_1 \\ 1 & x_2 & y_2 & z_2 \\ 1 & x_3 & y_3 & z_3 \\ 1 & x_4 & y_4 & z_4 \end{vmatrix}$$

and it represents the volume of the tetrahedron.

For the values of α_ι, β_ι, γ_ι and δ_ι the known coordinates are used:

$$\alpha_1 = \begin{vmatrix} x_2 & y_2 & z_2 \\ x_3 & y_3 & z_3 \\ x_4 & y_4 & z_4 \end{vmatrix}, \quad \beta_1 = -\begin{vmatrix} 1 & y_2 & z_2 \\ 1 & y_3 & z_3 \\ 1 & y_4 & z_4 \end{vmatrix}$$

$$\gamma_1 = \begin{vmatrix} 1 & x_2 & z_2 \\ 1 & x_3 & z_3 \\ 1 & x_4 & z_4 \end{vmatrix}, \quad \delta_1 = -\begin{vmatrix} 1 & x_2 & y_2 \\ 1 & x_3 & y_3 \\ 1 & x_4 & y_4 \end{vmatrix}$$

The rest of the values are calculated using the same pattern and alternating the +/- signs. This procedure is then done in the same way for *v(x, y, z)* and *w(x, y, z)*.

Institutional Repository - Library & Information Centre - University of Thessaly
03/09/2026 06:00:57 EEST - 216.73.216.156

The displacement relation for *u* can be written similarly in expanded form in terms of the shape functions and unknown nodal displacements as:

$$\begin{bmatrix} u \\ v \\ w \end{bmatrix} = \begin{bmatrix} N_1 & 0 & 0 & N_2 & 0 & 0 & N_3 & 0 & 0 & N_4 & 0 & 0 \\ 0 & N_1 & 0 & 0 & N_2 & 0 & 0 & N_3 & 0 & 0 & N_4 & 0 \\ 0 & 0 & N_1 & 0 & 0 & N_2 & 0 & 0 & N_3 & 0 & 0 & N_4 \end{bmatrix} \begin{bmatrix} u_1 \\ v_1 \\ w_1 \\ . \\ u_4 \\ v_4 \\ w_4 \end{bmatrix}$$

where the equations for the shape functions are:

$$N_i = \frac{\alpha_i + \beta_i x + \gamma_i y + \delta_i z}{6V}$$

The elemental strain equations that were related to displacement in the 3 dimensional space can now be written related to the shape functions as:

$$[\varepsilon] = [B][d]$$

where:

$$[B] = [B_1 \quad B_2 \quad B_3 \quad B_4]$$

and for each submatrix the expression used is:

$$[B_i] = \begin{bmatrix} N_{i,x} & 0 & 0 \\ 0 & N_{i,y} & 0 \\ 0 & 0 & N_{i,z} \\ N_{i,y} & N_{i,x} & 0 \\ 0 & N_{i,z} & N_{i,y} \\ N_{i,z} & 0 & N_{i,x} \end{bmatrix}$$

Where the shape functions can be found after solving the determinants for α, β, γ, δ.

Solving for the equations for strain and having the constitutive matrix the equation is complete:

$$[\sigma] = [D][\varepsilon]$$

For the element stiffness matrix, we use the expression:

$$[k] = \iiint [B]^T [D][B] dV$$

but both [B] and [D] matrices are constant for the simple tetrahedral element so it can be simplified to:

$$[k] = [B]^T [D][B] V$$

Institutional Repository - Library & Information Centre - University of Thessaly
03/09/2026 06:00:57 EEST - 216.73.216.156

with V being the volume of the element. This matrix is of order 12 x 12.

Finally, the element body force is given by:

$$[f_b] = \iiint [N]^T [X] dV$$

where N is given by the 3x12 matrix and $[X] = \begin{bmatrix} X_b \\ Y_b \\ Z_b \end{bmatrix}$ which gives a 12 x 1 matrix,

while the surface forces are expressed:

$$[f_s] = \iint [N]^T [T] \mathrm{dS}$$

This way the software can perform the cumbersome equations and find the solutions to the fundamental equilibrium equation:

$$[F] = [K][u]$$

[30]

3.5.2) Structural Analysis Using FEA Software

Analysis Setup

This analysis' goal is to study the UAV's stress/strain response to the loading occurring in two cases: while hovering and while resting on the landing gear. For the structural simulation, Autodesk's Fusion software will be used. To simulate these events, simplification of the overall assembly needs to be done. Hence, nonstructural components are omitted from the analysis, leaving the fuselage plates, arms, landing gear and motor mounts.

To simulate hovering, the force (110N = the UAV's total weight) from the thrust produced is applied on the threads of each lower motor mount which will then transport this force to the bottom of the arm's edge. Gravity is turned on for the simulated components while the weight of the missing components is simulated as a force applied on the upper fuselage plate. Finally, the maximum carried payload (20N) is applied on the shelves of the landing gear (fig. 3.40, 3.41, 3.42).

Institutional Repository - Library & Information Centre - University of Thessaly
03/09/2026 06:00:57 EEST - 216.73.216.156

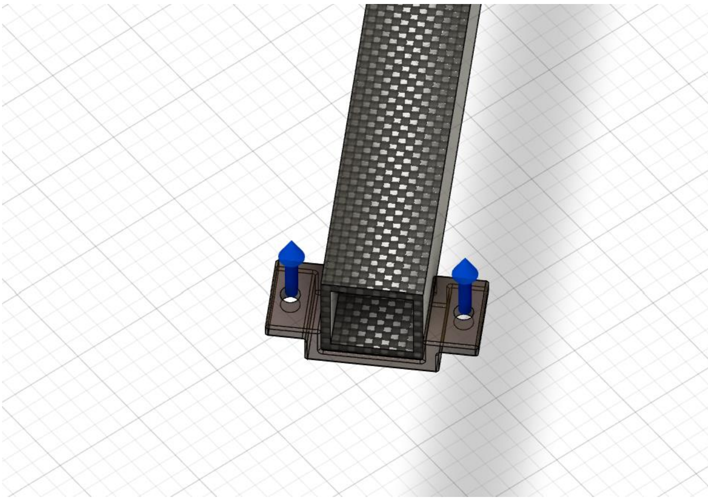

Figure 3.40: Hovering - Thrust force applied onto the lower mounting threads.

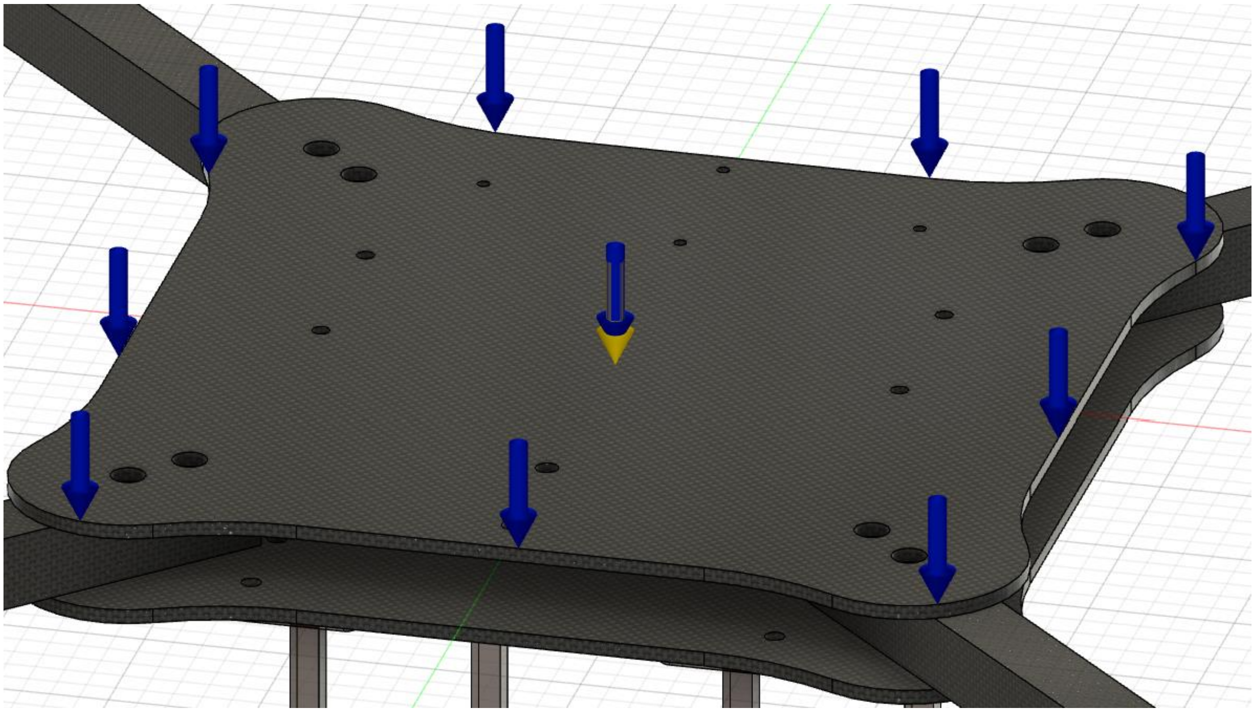

Figure 3.41: Hovering - Weight of the components applied onto the upper fuselage plate.

Institutional Repository - Library & Information Centre - University of Thessaly
03/09/2026 06:00:57 EEST - 216.73.216.156

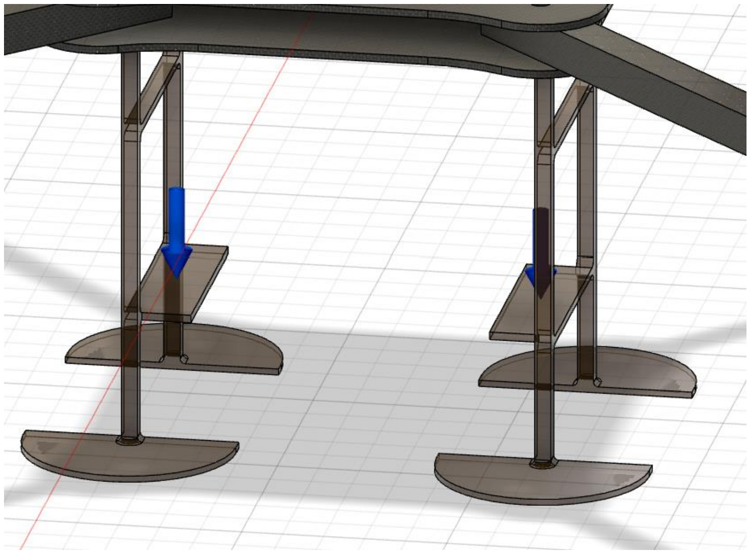

Figure 3.42: Hovering - Delivery payload applied on the landing gear shelves.

To simulate the UAV resting on its landing gear, gravity for the simulated components will be turned on, a force of 5N will be applied on the edges to simulate the weight of the motor/propeller/mountings configuration, 20N will be applied on the shelves of the landing gear and the weight of the missing components (approx. 60N) will be applied onto the upper fuselage plate (fig. 3.43). Finally, for the bottom of the landing gear, fixed structural constraints will be used. (fig. 3.44)

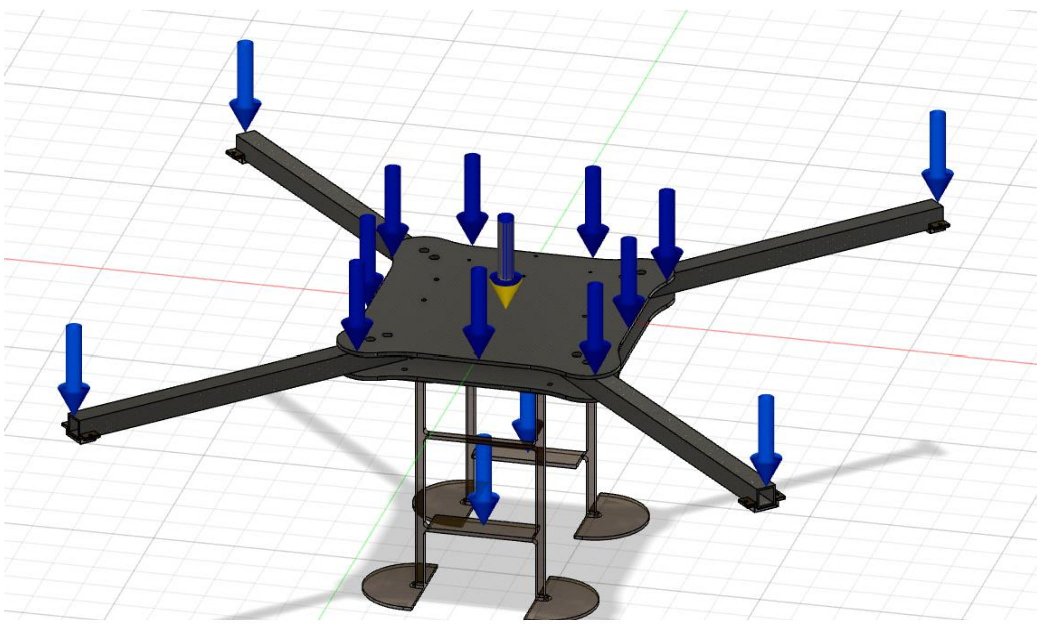

Figure 3.43: Resting – Loads simulating the weight are applied.

Institutional Repository - Library & Information Centre - University of Thessaly
03/09/2026 06:00:57 EEST - 216.73.216.156

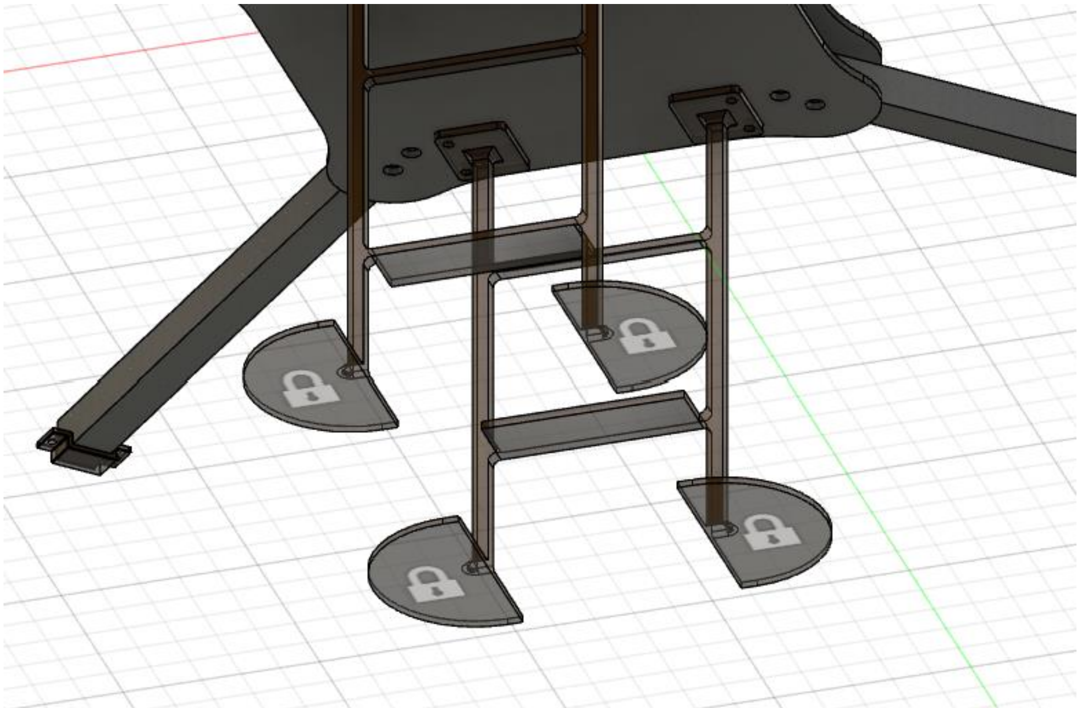

Figure 3.44: Fixed structural constraints applied on the bottom of the landing gear.

Model Mesh

The meshing of the model for both structural simulations will be the same. The element sizes are adaptive to the model size at 3% on average (fig. 3.45). In addition, the elements are sized based on each specific part as sizes of components vary. The element order is parabolic, including curved mesh element so the meshing adapts better to curved faces/edges of parts. The maximum turn on angle curves is set to 55 degrees and the maximum aspect ratio (largest edge/smallest edge of an element) is set to 5. The adaptive mesh refinement setting is set to "high", so a better meshing is done around critical points like holes, sharp edges and contact points and more accurate results are yielded. The maximum number of mesh refinements is set to 6 with a results convergence tolerance of 5%.

Institutional Repository - Library & Information Centre - University of Thessaly
03/09/2026 06:00:57 EEST - 216.73.216.156

Figure 3.45: Meshed model.

Results

For the hovering UAV analysis case, the results show that the assembly is full proof with a safety factor of 15. The maximum Von Mises stress (equivalent stress) is located at the contact edge between the arms and upper fuselage plate, measured at 14.633 MPa (fig. 3.46), way lower than the yield stress of CFRP. The maximum strain is located at the lower motor mounts (around the hole) and on the sides of the delivery shelves of the landing gear, measured at 0.002 (fig. 3.47).

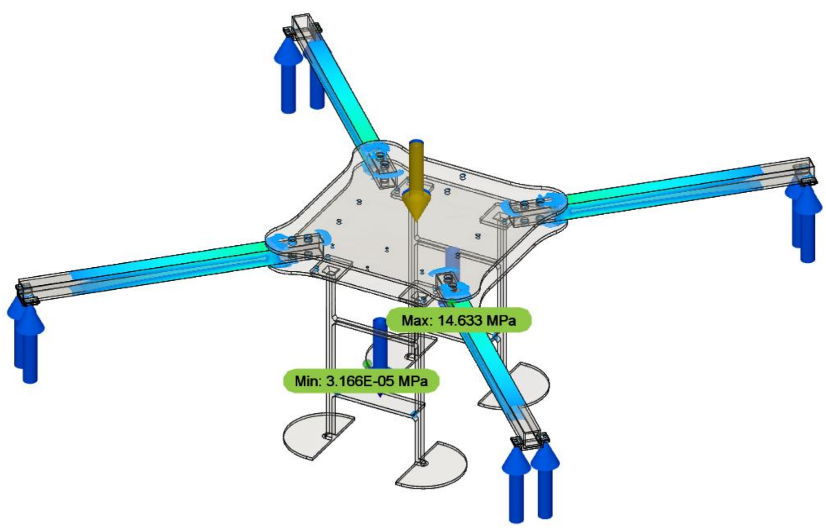

Figure 3.46: Hovering - Maximum and minimum stresses.

Institutional Repository - Library & Information Centre - University of Thessaly
03/09/2026 06:00:57 EEST - 216.73.216.156

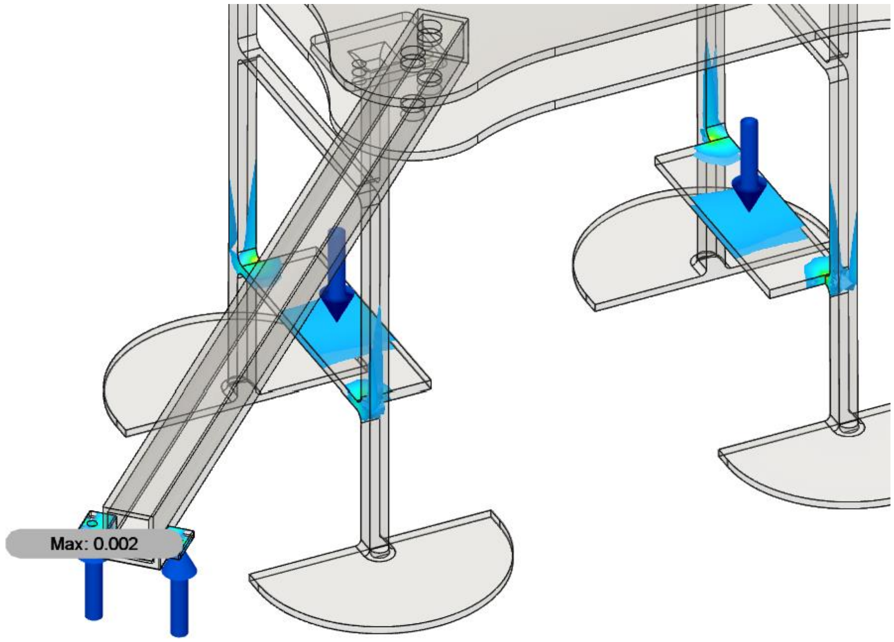

Figure 3.47: Hovering - Maximum strains.

For the resting UAV analysis case, the results show that the construction is safe with a minimum safety factor of 10.8 on a point of the landing gear shown below. The maximum Von Mises stress (equivalent stress) at that point is measured at 5.692 MPa significantly lower than the yield strength of PC plastic (fig. 3.48). As expected, the maximum strain is measured at the same point at 0.004 (fig. 3.49).

Institutional Repository - Library & Information Centre - University of Thessaly
03/09/2026 06:00:57 EEST - 216.73.216.156

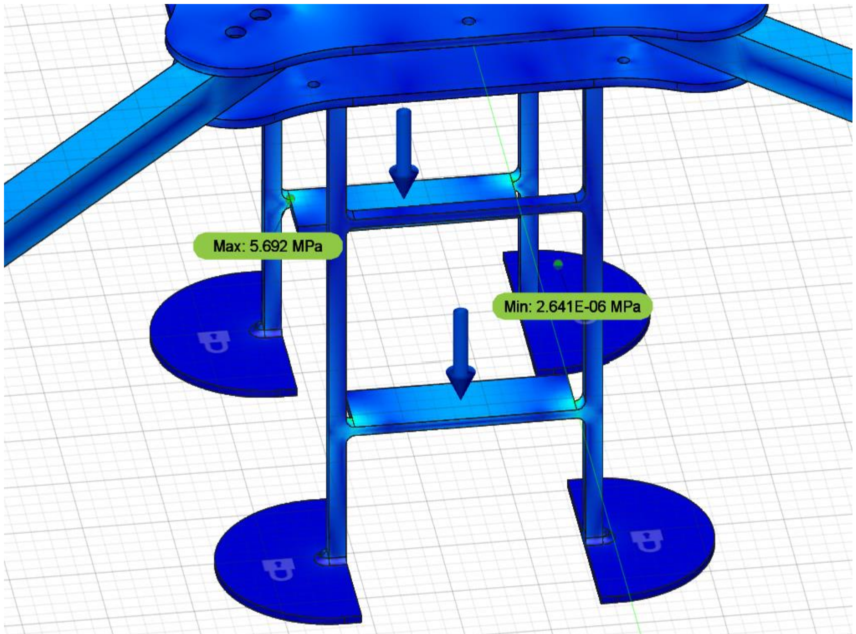

Figure 3.48: Resting - Maximum and minimum stresses.

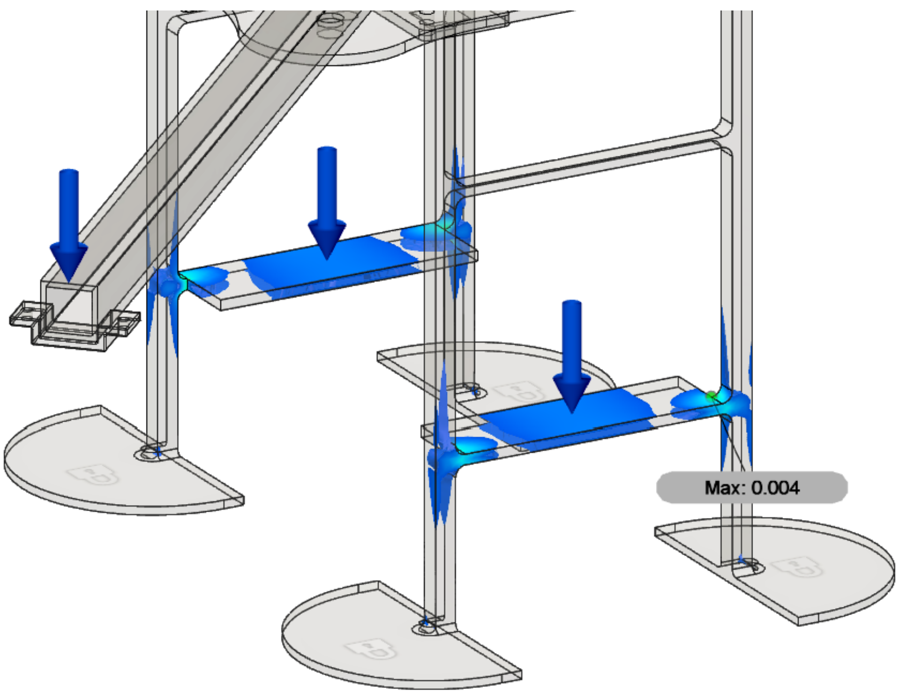

Figure 3.49: Resting - Maximum strains.

Institutional Repository - Library & Information Centre - University of Thessaly
03/09/2026 06:00:57 EEST - 216.73.216.156

Chapter 4. Fabrication and Machining of UAV Parts

4.1) Carbon Fiber Reinforced Plastics

Composite materials have been a very useful tool for engineers over the years in the process of solving complex design problems due to their ability to be custom-designed and fabricated based on the needs of each application accordingly. One such material is CFRP as it has been replacing traditional metals and metal alloys since its commercialization in the 1960s. Some of the reasons behind this trend is that CFRP materials boast low density, enhanced strength, increased rigidity, and a variety of manufacturing methods. It excels in resisting corrosion, offers superior fatigue performance, and ensures a longer service life. Overall, it provides a lightweight yet strong structure with flexible design options, allows for part integration, and supports multifunctional capabilities. Based on these attributes the CFRP industry is set to reach 32 billion $ in the global market by 2025.

The CFRP composite consists of two parts: a polymer matrix, either a thermoplastic (Polyamide, Polyetheretherketone, Polyphenylene Sulfide etc.) or a thermoset (Epoxy resins, Polyester resins, Polyvinyl resins etc.) and carbon fiber as reinforcement. Among these two parts, exists a three-dimensional interphase region with its specific characteristics (fig. 4.1) . [31]

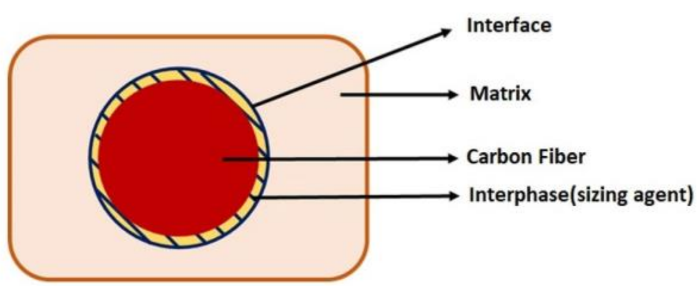

Figure 4.1: Zoomed cross-section of a CFRP part. [31] [32]

4.1.1) Carbon Fibers

Carbon fibers are typically of 5-10 μm diameter and consist of approximately 95-99% carbon. The nanostructure of carbon fibers is a network of hexagonal graphene layers that experience negligible interaction between them. When treated in high temperatures these structures are distorted while the core is in turbostatic form which is the basic structural unit of

Institutional Repository - Library & Information Centre - University of Thessaly
03/09/2026 06:00:57 EEST - 216.73.216.156

CF. In this turbostatic structure, the previously parallel layers are now arranged in a crumbled or folded way. The CF does not have a totally homogenous consistency but rather it can be synoptically described as a mix of amorphous and graphitic carbon.

The first materials used to create carbon fibers were cotton and bamboo in the late 1800s while synthetic rayon was used in the 1950s. PAN, the most widespread material that is still the most dominant precursor to carbon fiber today, was first used in the 1960s showing promising mechanical properties while being more viable economically. Many other materials were tested through the years, but none came close to the combination of properties PAN provides. [32]

While the processing for creation of CF differs from precursor to precursor, the basic stages are similar. These stages include oxidation, carbonization and finally graphitization (fig. 4.2).

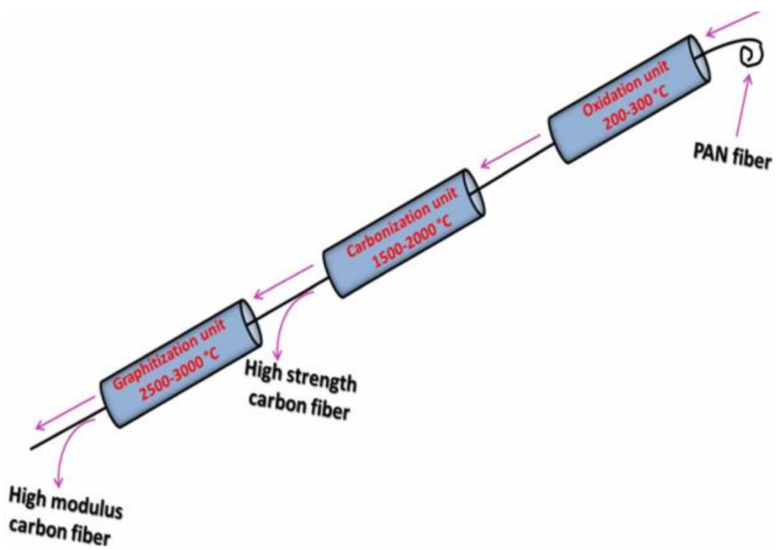

Figure 4.2: Stages of CF manufacturing using PAN-based fiber. [32]

During each stage, based on the precursor used the structures of the carbon fibers and the properties we get vary.

Institutional Repository - Library & Information Centre - University of Thessaly
03/09/2026 06:00:57 EEST - 216.73.216.156

When designing CFRP parts there are many parameters to be considered beforehand, so the composite constructed has the mechanical properties expected for the application in which they are going to be used. As listed in [31] these parameters are:

- Type of fibers: Continuous fibers and chopped fibers can be used is CFRP. The former provides better mechanical properties due to homogeneity and higher FVF values as well as fiber orientation control but is harder to process and manufacture.
- The value of fiber volume fraction (FVF) which is linearly correlated to the mechanical properties of the composite. This value is based on the way of manufacturing. For continuous carbon fiber composites, a value of at least 50% is expected.
- Length of the fiber: For continuous carbon fiber composites, the length of the fibers is at least the same length as the width, or the length of the part manufactured.
- Stacking and orientation of the fibers. The layer stacking determines the strength and stiffness in each axis. When using unidirectional stacking, only one axis has the exceptional mechanical properties provided by CFRP materials, while bidirectional stacking gives the designed part an isotropic behavior when loaded.
  The orientation angle of the carbon fibers is related to the mode of loading. At 0 degrees the part behaves better for axial loading, for 45 degrees the part gains excellent shear strength and at 90 degrees the part can withstand larger bending loads (fig. 4.3, 4.4).[4.1]

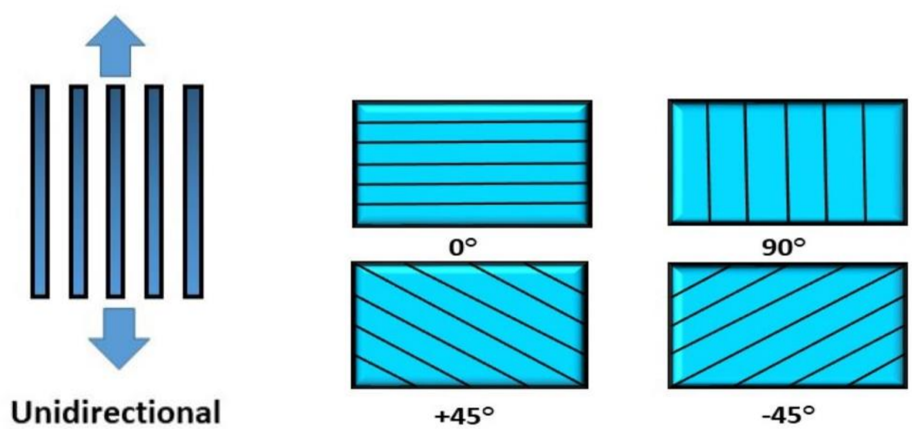

Figure 4.3: Stacking variations for unidirectional orientation of fibers. [31]

Institutional Repository - Library & Information Centre - University of Thessaly
03/09/2026 06:00:57 EEST - 216.73.216.156

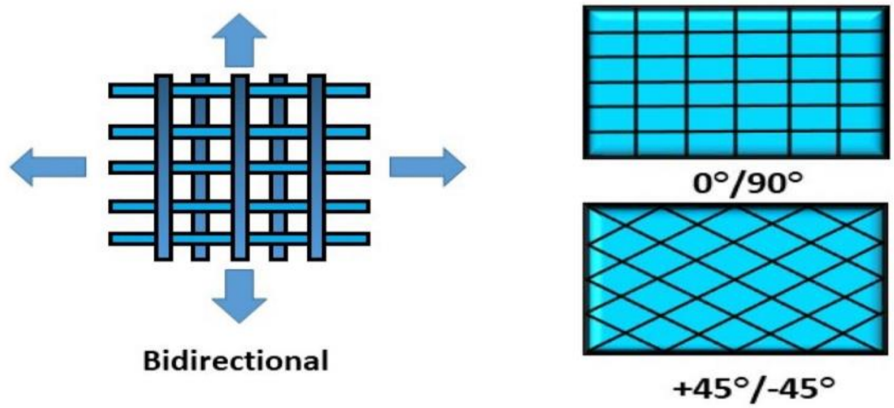

Figure 4.4: Stacking variations for bidirectional orientation of fibers. [31]

4.1.2) Polymer Matrices

As mentioned above the matrices used in CFRP composites are thermosetting (63% of CFRP market) and thermoplastic (37% of CFRP market). The selection of the matrix is a vital part of the composite design as it determines the manufacturing, processing and properties of the composite that are needed on each application. [32]

Thermoplastic & Thermosetting Matrices

Thermoplastic resins are made of lengthy polymers that do not cross-link with each other. While curing, these resins do not undergo chemical changes which means they can be recycled many times. The most common manufacturing methods for thermoplastic matrix CFRP are injection molding, rotational molding, extrusion, vacuum forming, and compression molding which is done by applying high temperatures on the thermoplastic granules. This type of composite has a better impact strength and toughness. On the other hand, the ductility of thermoplastic-using CFRP creates problems on the machining of parts of this material (cutting tool wear, material delamination, high temperatures). Finally, thermoplastic resins have higher viscosity than thermosets, which makes it more difficult to thoroughly impregnate carbon fibers, resulting in voids and reduced composite performance. [33]

Institutional Repository - Library & Information Centre - University of Thessaly
03/09/2026 06:00:57 EEST - 216.73.216.156

Thermosetting resins are polymers that come in liquid form and cannot be reused in the way thermoplastics do as their structure cannot be reversed after curing. Instead of curing in low temperatures like thermoplastics, thermosets need irradiation (UV lights, infrared lights or electron beams), chemical reactions of heat application. In addition, they are easier to process and laminate due to lower pressures and temperatures needed combined with better wetting of the carbon fibers. The most common manufacturing methods for thermosetting matrix CFRP are hand lay-up, vacuum bagging, resin transfer molding, autoclave molding and filament winding. Finally, this type of CFRP is much easier to machine as the matrix makes it more brittle and it is easier to predict chip formation and produce tight tolerances. Overall thermosetting matrices are more suitable for the CFRP parts designed for the UAV. [33]

The most widespread commercial thermosetting resins used in fiber reinforced plastics are polyester resins, vinyl ester resins and epoxy resins, each having unique properties (table 4.1) and processing stages.

Polyester resins are unsaturated polymers created through the reaction between dibasic organic acids and polyhydric alcohols. They present moderate strength and stiffness compared to other FRP matrices and have a lower service temperature. On the other hand, they are characterized by adequate resistance to ultra-violet radiation and moisture for prolonged periods of time. These properties combined with their low cost make these resins the most popular in the composite world. The adhesion of polyester resins to carbon fibers is moderate while glass fibers are better suited for this type of matrix. Processing times are short as curing is done exothermically with the proper curing agents, while the shrinkage during this stage can create internal stress and structural instability.

Vinyl ester is a resin synthesized by esterifying an epoxy resin with an unsaturated monocarboxylic acid. This resin merges the beneficial properties of both epoxy and polyester resins for a bigger price than that of PE resins. These resins are stronger than polyester resins and can handle large straining. In addition, VE resins have high service temperature and moisture resistivity. Due to their high reactivity, VE resins have very low curing times when the appropriate

Institutional Repository - Library & Information Centre - University of Thessaly
03/09/2026 06:00:57 EEST - 216.73.216.156

curing agent is used. The problem with VE resins is their low viscosity compared to other thermosetting resins which makes the wetting of the CF and overall bonding of fibers and matrix very problematic making VE CFRP unreliable for high load applications.

Epoxy resins are thermosetting polymers formed through the reaction of epichlorohydrin with bisphenol-A or other polyols, resulting in a highly cross-linked structure that provides excellent mechanical properties and chemical resistance. These resins have the highest strength, stiffness and impact strength of their commercial counterparts making it the most used in industries like aerospace and automotive and sporting goods as they combine excellent strength to weight ratio. The durability shown in UV radiation and moisture is great making it suitable for open environment applications. The epoxy resin has high viscosity and its adhesion to CF is very effective while the shrinkage during curing is low, avoiding internal stresses. Curing and processing epoxy resins is time consuming and needs precision making it the most expensive of other thermosetting resins. [33]

Table 4.1: Properties of the most used thermosetting resins. [34]

Properties	**Polyester**	**Vinyl Ester**	**Epoxy**
Density	1.2	1.1	1.25
T_g (°C)	60	100	80-150
Modulus of elasticity (GPa)	3.3	3.5	5
Tensile strength (MPa)	55	75	75
Strain limit in tension(%)	1.8	2.2	2.5
Shear strength (MPa)	50	65	80
Shear strain limit (%)	3.8	3.7	5

Institutional Repository - Library & Information Centre - University of Thessaly
03/09/2026 06:00:57 EEST - 216.73.216.156

4.2 CFRP Parts Manufacturing Methods

The manufacturing processes of CFRP have evolved since the beginning of its commercial success and now there is a variety of methods implemented based on the carbon fiber used, the type of polymer matrix and the geometry of the parts. To navigate through the selection of the appropriate method for each specific part/application a diagram was created (fig. 4.5). In this diagram the most popular methods are ranked by the quality of manufacturing, laboring expenses (specialized skills), tooling costs (equipment, initial investment), productivity (short cycle times), size potential (small batches/mass production), geometry flexibility and property flexibility.

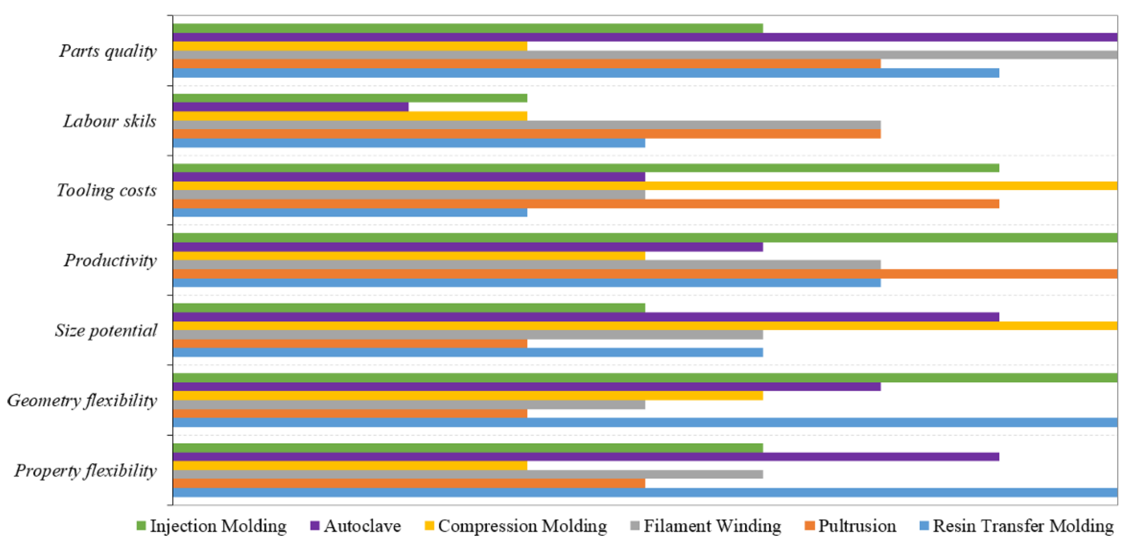

Figure 4.5: Comparison of CFRP manufacturing methods. [35]

4.2.1 Fuselage Plates Manufacturing

Through short research it was easily concluded that for a part like the fuselage plates, the ideal method of fabrication would be one of the many molding methods, due to its geometry. Consulting the diagram, it is shown that resin transfer molding (RTM) is a good choice for this

Institutional Repository - Library & Information Centre - University of Thessaly
03/09/2026 06:00:57 EEST - 216.73.216.156

specific application as it provides final products of very good quality, has low tooling costs while it is the most flexible method property-wise and geometry-wise.

Resin Transfer Molding (RTM)

RTM is a simple widespread method for FRP composites construction, also called liquid molding. This close-mold technique combines high quality products with low equipment costs and low labor intensity. There are five main stages in RTM manufacturing: creating a preform of the reinforcement, securing the preform in the mold, pouring the thermoset liquid through injection, curing the part (depends on the resin used) and demolding of the final part (fig. 4.6).

In our case instead of a preform, woven carbon fiber cloth, with 0°/90° angle, that is cut in the shape of the fuselage plate can be used. The mold plates can be designed with the help of CAD and created by materials such as aluminum or steel using traditional methods. These plates are then heated and closed via clamping to avoid resin leaking []. Afterwards the resin used and a catalyst to speed up curing are premixed in a special pumping vessel and the mixture is injected to the mold by moderate pressure (3.5 – 7 bar). This stage should include many ports for injections, so the pressure is applied equally, and the resin is dispersed on the whole of the precut fiber cloth stacks and wets them effectively minimizing void space on the interphase of CF-thermoset matrix. [35]

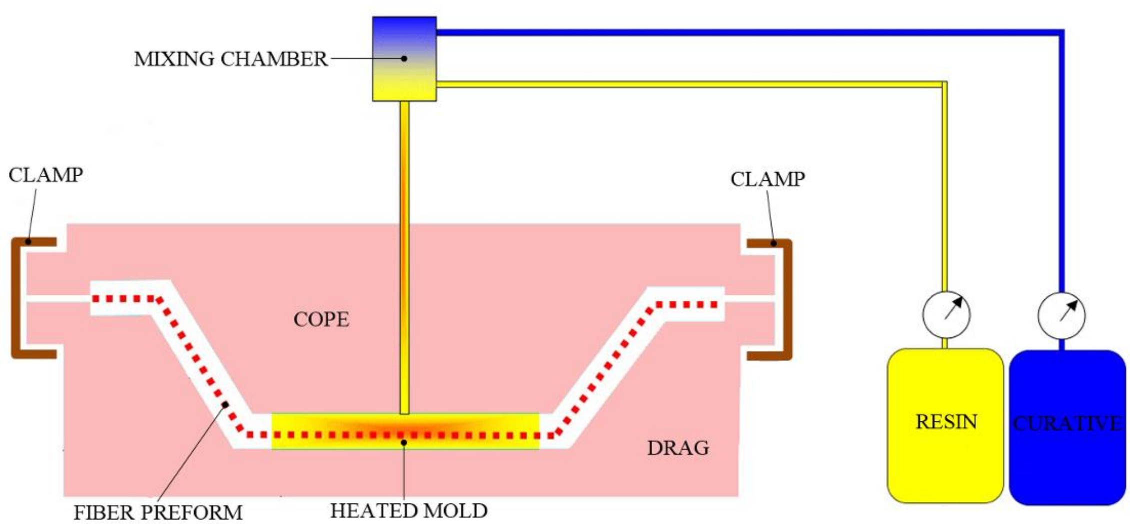

Figure 4.6: Illustration showing the RTM process. [35]

Institutional Repository - Library & Information Centre - University of Thessaly
03/09/2026 06:00:57 EEST - 216.73.216.156

To reduce the internal voids to a greater extent and help the total resin impregnation vacuum assistance can be used to assist with the flowing of the curing agent–resin mixture. This procedure is also known to be effective for parts that are designed to have a large FVF value (up to 70%). VARTM is similar to RTM with the difference that instead of an upper mold tool, a vacuum bag (VB) is used. The VB applies vacuum to forward the flow of the resin through the whole mold. The stacks of woven CF are oriented as desired and held together by a binder onto the bottom mold tool while a deformable top mold tool is placed and vacuum sealed. The thermosetting resin is then injected into the mold and distributed with the help of suction created by the vacuum (fig. 4.2). The part is then cured at room temperature while post-curing is sometimes applied. [35]

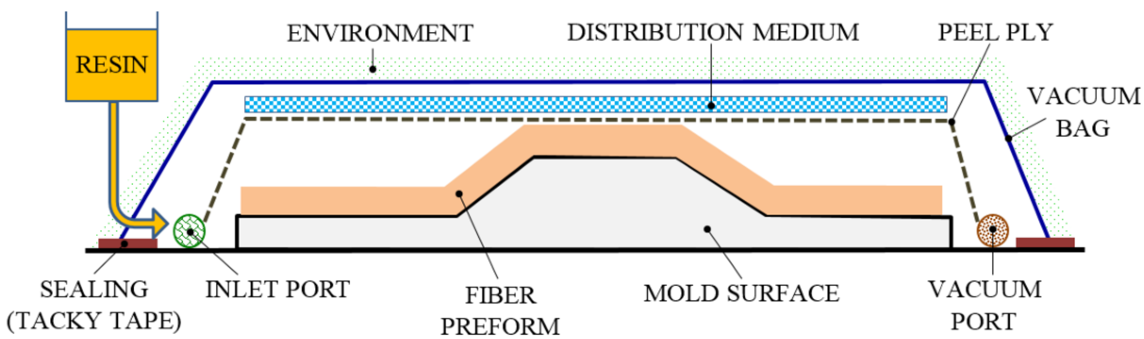

Figure 4.7: Illustration showing the VARTM process. [35]

4.2.2 Arms Manufacturing

The geometry of the arms of the UAV makes manufacturing more complex and narrows down the available fabrication methods. Of the popular methods mentioned above, pultrusion could be an option that would be able to create this specific geometry, but the increased tooling costs and labor skills needed exclude it. In addition, in pultrusion the fibers can only be stacked unidirectionally with no ability to manipulate the orientation angle making it impossible to create square hollow rods with 0°/90° degree stacking.

Institutional Repository - Library & Information Centre - University of Thessaly
03/09/2026 06:00:57 EEST - 216.73.216.156

Hand Lay-Up

The most compatible and simple method to create this part is hand lay-up/wrap-up assisted by very careful curing. A mandrel in the shape of the inside of the rod is made from a metal that behaves differently in temperature changes so the CFRP can be easily extracted after curing. This mandrel (usually aluminum alloy) is wrapped around by a woven CF fabric (0°/90° orientation) which is the same length as the rod. For every wrap epoxy resin is applied on the virgin surfaces through rollers and brushes and moderately compressed. The aluminum rod is wrapped as many times is needed to reach the demanded thickness of the part. Pre heating the aluminum to a temperature of around 60°C helps resin impregnate the fibers and wet the CF. After wrapping is finished the part is cured in an oven at 90° C for about 100-120 minutes.

Parts created through this method have a low to moderate quality based on the experience of the technician and the ability to follow curing instructions carefully. However, the properties acquired by the proper stacking and orientation of the fibers equal the loss of quality due to the poorer wetting occurring in hand lay-up compared to other methods such as pultrusion.

4.2.3 CFRP Parts Properties

To calculate the properties of the parts produced using the CFRP methods mentioned above the rule of mixtures can be used. This equation can describe approximately the influence of the properties of the fibers and the matrix of a composite material.

$$P_{CFRP} = P_{CF}V_{CF} + P_M V_M \qquad (4.1)$$

where P denotes the mechanical properties, we want to calculate of each component used in the composite. V is the volume fraction that each component takes up of the total volume (1) of the composite.

Institutional Repository - Library & Information Centre - University of Thessaly
03/09/2026 06:00:57 EEST - 216.73.216.156

The fiber material for the parts discussed above could be woven fabric bidirectional with 0°/90° orientation as it can be applied both in the hand lay-up method and in resin transfer molding. This commercially available material has its properties provided by the manufacturer and in combination with the properties of the epoxy resins given in section 4.1.2 the properties of each part can be calculated (table 4.3).

Table 4.2: Properties of CF Fabric (Plain-Weave). [36]

Density (kg/m^3)	1.7
Modulus of Elasticity (GPa)	231
Tensile Strength (GPa)	3.65
Tensile strain to failure (%)	1.5

Assuming the RTM method achieves a FVF of 60 % while the hand lay-up (wrapping) method can reach approximately 40 % in fiber volume content the properties of the parts using this type of CF and epoxy resin can be calculated conservatively through the rule of mixtures.

Table 4.3: Properties of the CFRP Parts.

UAV Part	Arms	Fuselage
Manufacturing Method	Hand Lay-Up	RTM
FVF (%)	40%	60%
Density	1.43	1.52
Modulus of Elasticity (GPa)	95.4	140.6
Tensile Strength (GPa)	1.505	2.22
Tensile Strain to Failure (%)	2.1	1.9

Institutional Repository - Library & Information Centre - University of Thessaly
03/09/2026 06:00:57 EEST - 216.73.216.156

4.3 CFRP Machining

Generally, machinability of composites should be approached differently than traditional materials as they are characterized by heterogeneity and anisotropy. For example, when drilling (in the case of the UAV) the material encountered by the drill is different in each part of the cutting tool (can be either the epoxy resin matrix, the carbon fibers or the interphase) creating problems for the final product and the cutting tool. In addition, it is observed that the orientation of the fibers is an important parameter during machining as every CFRP product, based on the orientation of the CF plys has different cutting forces produced. Some of the failures attributed to hole creation in CFRP parts are:

- Fiber pull-out: this occurs when fibers are pulled out from the matrix without breaking, usually due to weak bonding between the fiber and the matrix.
- Swelling: the matrix expands due to moisture absorption or heat, causing dimensional changes and weakening fiber-matrix bonds.
- Matrix cracking: cracks form in the resin matrix due to machining stresses or heat, compromising the composite structure.
- Delamination: layers of the composite separate or peel apart, typically due to interlaminar shear stresses or improper cutting forces during machining (fig. 4.8) . [37]

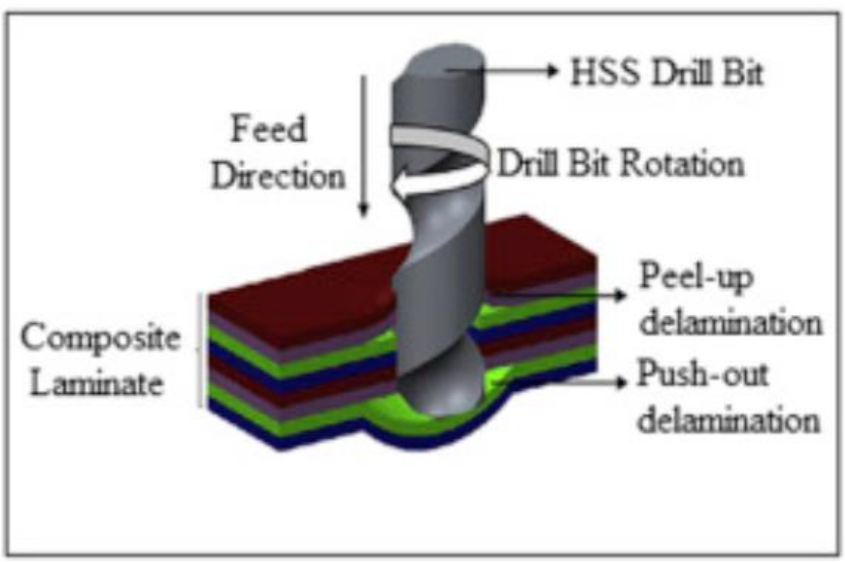

Figure 4.8: Delamination failure emerging during drilling. [37]

Institutional Repository - Library & Information Centre - University of Thessaly
03/09/2026 06:00:57 EEST - 216.73.216.156

Conventional Machining Methods

Extensive research on conventional drilling for hole formation on CFRP parts concluded similar results on the parameters that could reduce the damage of the hole surface. The most notable observation was that the compressive force produced during drilling could be minimized when the cutting speed was increased, and the feed rate (advancement of the drill for every revolution) was lowered. Gaitonde et al. found that minimizing point angle (the angle formed at the tip of the drill bit) in combination with the above could effectively limit delamination on the hole surface. The type of drill bit seems to have an effect on the damage of the parts during machining as well. Grilo et. al found that the use of SPUR, R950 and R415 drill bits tend to obliterate the presentation of delamination (most common failure). More specifically, the most effective of the drill bits was the SPUR drill bit. Finaly, Ekici and Isik after experimenting with bits that had a different number of cutting edges found that the least damage was done by drilling in very high cutting speeds with very low feed rate, a point angle of 60° and a drill bit with two cutting edges. [37]

Unconventional Machining Methods

For fiber reinforced plastics, some of the few unconventional methods that are typically used are:

- water jet machining (WJM): In this method, a high-pressure stream of water, often reaching up to 4000 bar, is used to cut through softer materials such as rubber and plastics. The water acts as a cutting tool, eroding the material along the cutting path without generating heat, making it suitable for materials that could be damaged by high temperatures.
- Abrasive water jet machining (AWJM): AWJM is similar to standard water jet cutting but incorporates abrasive particles like garnet or aluminum oxide into the water stream. This abrasive mix enables the machine to cut through tougher materials such as metals, ceramics, and composites. It allows for intricate cuts without the heat-affected zones that are common with thermal cutting methods, preserving the material's properties (fig. 4.9).

Institutional Repository - Library & Information Centre - University of Thessaly
03/09/2026 06:00:57 EEST - 216.73.216.156

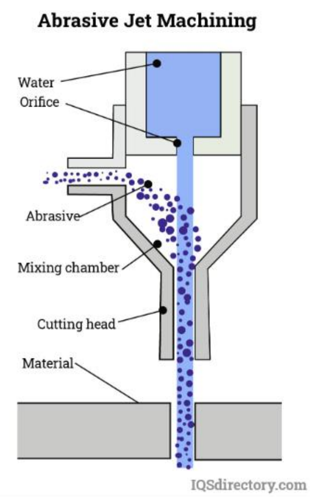

Figure 4.9: Illustration of AWJM machining method. This method is very similar to WJM. [38]

- Laser jet machining (LJM): This technique uses a concentrated laser beam to cut, melt, or vaporize material, making it ideal for precise cutting of metals, plastics, ceramics, and composites. The laser's precision and speed are major advantages, but it does produce heat, which can alter the properties of the material near the cut area (fig. 4.10).
  [2]

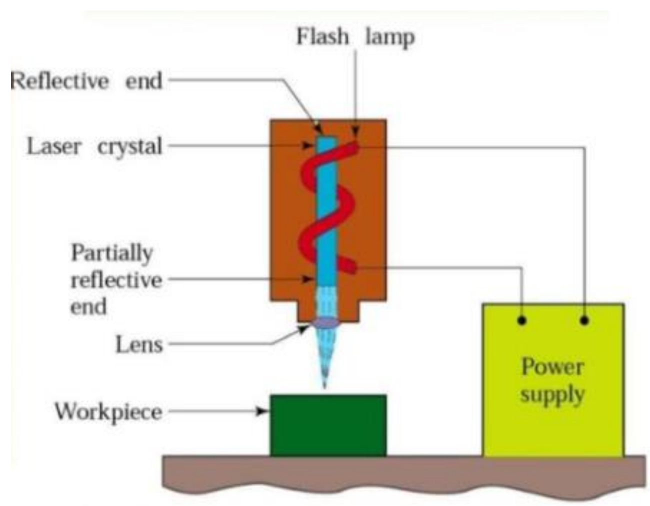

Figure 4.10: Illustration of the LJM method. [39]

For WJM and AWJM, it was observed that to avoid delamination on the holes created, low water pressure should be used in combination with low mass flow rate and small standoff distance. Also, the type of abrasive used can have an effect on the delamination factor. One of

Institutional Repository - Library & Information Centre - University of Thessaly
03/09/2026 06:00:57 EEST - 216.73.216.156

the safest options is fine grit garnet abrasives due to their sharp edges, high hardness and moderate erosion characteristics. [37]

Laser cutting is a complex procedure when applied on a composite and many factors should be considered for minimizing damage on the machined part. The different materials used in a composite such as CFRP vary in thermal conductivity thus the generated heat affected zone (HAZ) cannot be calculated precisely. Simulation using the eigenvalue and isotherm method were used to predict thermal conductivity in non-principal directions and concluded that the HAZ produced is smaller when grooving is done in parallel to the fiber orientation [40]. To obtain a narrower kerf (more precise cutting) and a limited HAZ the Multi-Passes scan technique (repeatedly passing the laser over the same area multiple times with lower power settings) can be used with an increased time between two consecutive scans. [37]

4.4 Polymer Parts Manufacturing Methods

4.4.1 Polycarbonate

Polycarbonates are polymers that include carbonate groups in their chemical structure. These polymers are mainly produced by the monomer bisphenol A (BPA) when it reacts with phosgene ($COCl_2$). High strength to weight ratio, good impact resistance and high temperature resistance make polycarbonates a popular plastic in engineering applications. [2]

For polycarbonates, the most popular manufacturing methods are molding techniques used in the manufacturing process of most polymers. The complicated designs of the UAV parts made of polycarbonate (landing gear, upper and lower motor mounts) could be created by specific molding methods such as Injection Molding and Compression Molding. Novel methods such as Fused Deposition Modeling (3D Printing) can also be utilized for such intricate parts.

Institutional Repository - Library & Information Centre - University of Thessaly
03/09/2026 06:00:57 EEST - 216.73.216.156

- **Injection Molding**: This process is divided into two parts: Firstly, the melt is generated followed by the mixing and pressurization of the flow which take place in the injection unit of the molding machine. Afterwards shaping and structuring of the part is done in the mold cavity. For the polymer to be injected in the mold cavity, pressure must be applied to the melt by the forward force of a piston pushed by the screwdriver. The mold is assembled by two components, one static and one free to move so the mold can be opened and closed during different parts of the molding cycle. The molds should be held at a temperature below T_g (=147℃ for polycarbonate). The molten material exits the nozzle of the injection unit and flows through the sprue, runner, and gate into the mold cavity (fig. 4.11). Each of these components within the mold has specific functions that influence the molding process. [41]

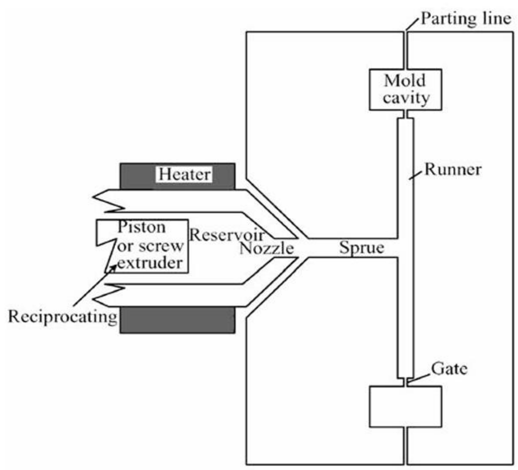

Figure 4.11: The injection molding technique. [41]

- **Compression Molding:** For this molding procedure, a thermoplastic resembling the desired part is fitted in a mold cavity that is preheated. Afterwards, the top part of the mold starts closing and pressure is applied, further increasing the temperature, forcing it to reach the mold temperature and allow the polymer to flow and fill the mold cavity completely. During this process, the polymer undergoes cross linking (polymerization). At the end, the mold is opened, and the encapsulated final part is ejected. This method is less precise than injection molding and needs careful evaluation of the volume of the preform so the best possible tolerances are yielded.
  The whole procedure consists of 3 discrete parts timewise as shown below. In the first part the plunger force is increased rapidly until t_f where the polymer is assumed to be molten. For the next part the molten polymer flows through the whole of the mold cavity until t_c where the filling is finished and compression starts and curing reactions take place (fig. 4.12). [41]

Institutional Repository - Library & Information Centre - University of Thessaly
03/09/2026 06:00:57 EEST - 216.73.216.156

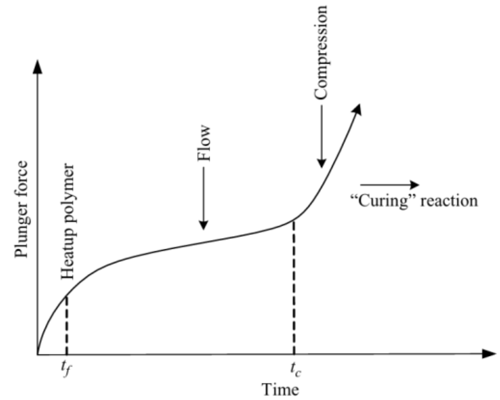

Figure 4.12: Molding plunger force-time elapsed diagram. [41]

- **Fused Deposition Modelling (3D Printing):** FDM is a material extrusion based process that belongs in the family of Additive Manufacturing methods. This method uses thermoplastic polymers such as PLS (Polylactic acid), ABS (Acrylonitrile butadiene styrene) and PC (Polycarbonate). Filaments of the chosen material are stored on rollers that can feed them directly to the extrusion head. The head can move in the X and Y axis while the platform onto which the part is built moves on the Z axis. Usually, two material filaments are used for this method: the built material and a supporting material (fig. 4.13).

  The whole process is divided into 3 parts: pre-processing, production and post-processing. During pre-processing, the part is designed using CAD software and then stored as an STL file. The designer can then choose the printing parameters (slicing parameters, building orientation, temperature of machine, material deposition speed etc.) Afterwards the slicing of the design is done with an appropriate software and the path of the head is determined and stored as the G-code.

  During production of the part, the head moves along the path dictated by the G-code and deposits the material that has come to a semi-liquid phase due to the machines temperature. The table of the printer moves down after every layer (slice) is deposited and the part is completed.

  For the post processing chemical or mechanical methods are used to optimize the surface quality of the part. The chemical methods include painting, coating and heating. The mechanical methods that can be used to produce better surfaces are sanding, abrasive, vibratory, barrel finishing etc. These methods ultimately enhance the mechanical properties of the part besides its surface. [42]

Institutional Repository - Library & Information Centre - University of Thessaly
03/09/2026 06:00:57 EEST - 216.73.216.156

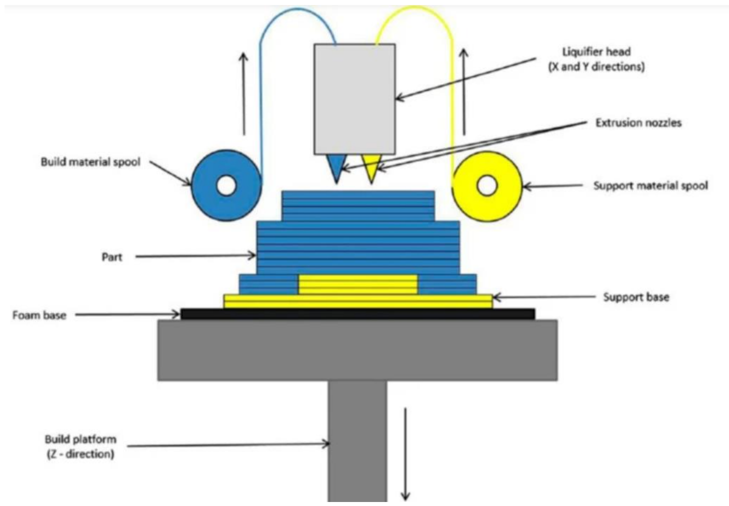

Figure 4.13: The FDM method. [42]

4.4.2 Polyvinyl Chloride (PVC)

Polyvinyl chloride is made through the polymerization of vinyl chloride monomers. This synthetic polymer is the third most-used polymer in the world due to its wide spectrum of applications. In its rigid form this material can be used for pipes, windows, doors, packaging and bank cards.

As other polymers, PVC parts can be created through a variety of methods with the most popular being molding techniques. Specifically for rigid PVC parts the suitable molding methods consist of injection molding, compression molding and blow molding. The former two were analyzed above for polycarbonate parts while the latter is analyzed below.

- **Blow Molding :** This method is frequently used for the creation of hollow parts and could be a good fit for the housing of the propulsion system component as this part has a thin tray-like geometry. For the traditional blow molding technique called extrusion, firstly the forming of a molten tube takes place. This tube is called the parison. To extrude the parison a rotating screw extruder, an accumulator head with a piston-driven extrusion or a reciprocating screw can be utilized. The parison can be extruded through one or more dies. As the parison is extruded inside the two mold halves, air is provided inside through injection. The parison is blown like a balloon and takes the form of the mold (fig. 4.14). The molten PVC rapidly solidifies after contacting the low temperature molds and is ejected. [41]

Institutional Repository - Library & Information Centre - University of Thessaly
03/09/2026 06:00:57 EEST - 216.73.216.156

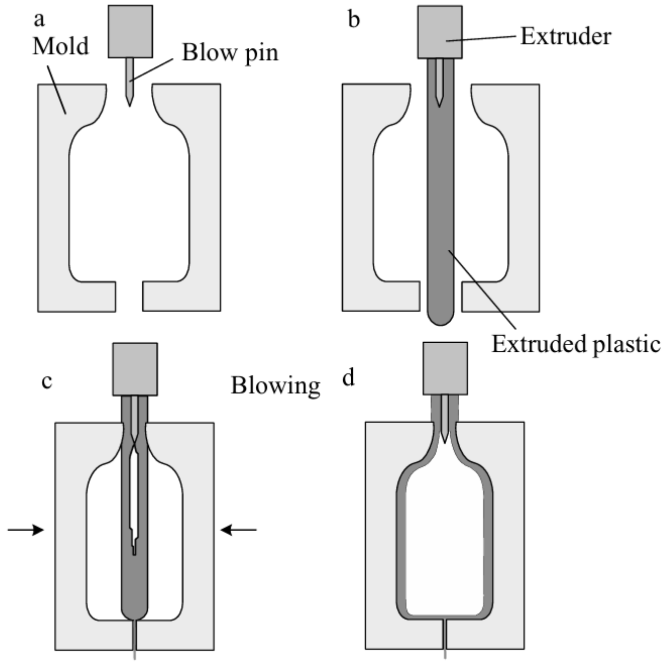

Figure 4.14: Steps of the extrusion blow molding technique. [41]

4.4.3 Polymer Parts Properties

The properties of the polymers used in this project do not deviate when fabricated through traditional molding methods such as the ones mentioned above. For the PC parts, which are the only structural polymer parts in the UAV their properties are listed below (table 4.4).

Table 4.4: Polycarbonate & PVC properties. [43]

Polymer	Polycarbonate	Polyvinyl Chloride
Density (kg/m^3)	1.2	1.39
Modulus of elasticity (GPa)	2.38	2.7
Tensile strength (MPa)	65.5	50
Tensile strain (%)	80	20-50
Tg (℃)	120	80

Institutional Repository - Library & Information Centre - University of Thessaly
03/09/2026 06:00:57 EEST - 216.73.216.156

In [44] a series of experiments was conducted to compare the structural properties of FDM manufactured PC parts in different temperatures and through different stacking orientations. The results showed that when these parts were put under multi-directional stresses, the modulus was decreased at approximately 45% while the ultimate tensile strengths decrease ranged from 30% to 60%. This means that the FDM method could be more suitable for the PVC part as it does not play a role structurally for the UAV and has a complicated geometry that is easier to manufacture through additive manufacturing. On the other hand, the PC parts are of vital importance for the structural integrity of the UAV so a molding method should be selected for the fabrication.

Institutional Repository - Library & Information Centre - University of Thessaly
03/09/2026 06:00:57 EEST - 216.73.216.156

Chapter 5. Conclusion

Based on the goals set in section 1.1, decisions were taken based on scientific literature, software analysis and modelling to construct a lightweight (9kg net weight) UAV with a propulsion system consisting of an 800W rated/1000W max. PEM fuel cell system coupled with a 7S LiPo battery with a capacity of 8000mAh. The rest of the propulsion system components chosen to meet the criteria set, were 27.5' x 8.9' dual blade CF propellers, a 7208 135kV motor and a 60A 4S-8S ESC. The UAV loaded with the 2kg payload can travel horizontally consuming approximately 960W which is less than the maximum power of the fuel cell. Based on the payload, the atmospheric conditions, the battery capacity and the hydrogen mass in the tank, the power/energy sufficiency for a specific flight path can be determined using the equations in section 2.5

The design of each part of the UAV was realized with the aim to make it structurally viable, aerodynamic and as light as possible. The materials were determined with the use of CES Edupack software and were CFRP for the arms and fuselage, while PC was used for mountings and the landing gear. For the housing of the propulsion system PVC was selected. The appropriate joints for polymer and composite materials were picked based on literature and a FEM analysis was conducted using the software Autodesk Fusion 360.

For the manufacturing of the fuselage and the arms (CFRP parts) the methods more suitable were found to be resin transfer molding and hand lay-up (wrapping) respectively. For the polymer parts traditional molding techniques and the FDM method were studied. For the polycarbonate parts it was found that traditional molding methods should be applied as better properties are yielded while for the PVC part, FDM can be used as the housing is not a structural element of the drone. For the machining of CFRP parts, conventional and non-conventional methods were studied. To minimize the damage on the composite, specific cutting parameters should be set for each different possible machining method.

Institutional Repository - Library & Information Centre - University of Thessaly
03/09/2026 06:00:57 EEST - 216.73.216.156

References

[1] R. O'Hayre and S.-W. Cha, Fuel Cell Fundamentals, John Wiley & sons, 2016.

[2] "Wikipedia," [Online]. Available: https://www.wikipedia.org.

[3] Q. Quan, Introduction to Multicopter Design and Control, Springer, 2017.

[4] B. Zhang, " Overview of Propulsion Systems for Unmanned Aerial Vehicles," *Energies,* 2022.

[5] D. Joshi, D. Dipankar and M. Muyeen, "Comprehensive Review on Electric Propulsion System Unmanned Aerial Vehicles," *Frontiers in Energy Research,* 2022.

[6] L. Xu, Yigeng Huangfu, RuiMa, Renyou Xie, Dongdong Zhao, Yongheng Yang and Yupeng Wang, "A Comprehensive Review on Fuel Cell UAV Key Technologies: Propulsion System, Management Strategy, and Design Procedure," *IEEE TRANSACTIONS ON TRANSPORTATION ELECTRIFICATION,* 2022.

[7] F. Ustolin and R. Taccani, " Fuel cells for airborne usage: Energy storage comparison," *International Journal of Hydrogen Energy,* vol. 43, 2018.

[8] D. o. Energy, "ENERGY.GOV," [Online]. Available: https://www.energy.gov.

[9] J. Besenhard and C. Daniel, Handbook of battery materials, John Wiley & sons, 2011.

[10] J. Wang, Rui Jia, Jing Liang, Chen She and Yi-Peng Xu, " Evaluation ofasmalldroneperformanceusingfuelcellandbattery;," *Energy Reports ,* vol. 7, 2021.

[11] Ó. González-Espasandín, Teresa J. Leo and Emilio Navarro-Arévalo, "Fuel Cells: A Real Option for Unmanned Aerial," *The Scientific World Journal,* 2014.

[12] "H3 Dynamics," 2024. [Online]. Available: https://www.h3dynamics.com.

Institutional Repository - Library & Information Centre - University of Thessaly
03/09/2026 06:00:57 EEST - 216.73.216.156

[13] C. Xiao, Bin Wang, Dan Zhao and Chaohui Wang, "Comprehensive investigation on Lithium batteries for electric and hybrid-electric unmanned aerial vehicle applications," *Thermal Science and Engineering Progress ,* vol. 38, 2023.

[14] "Battery Power Tips," 2021. [Online]. Available: https://www.batterypowertips.com/difference-between-lithium-ion-lithium-polymer-batteries-faq/.

[15] "Makezine," [Online]. Available: https://makezine.com.

[16] "MaxAmps," [Online]. Available: https://maxamps.com/products/lipo-8000-7s-25-9v-battery-pack.

[17] "ECalc," [Online]. Available: https://www.ecalc.ch.

[18] M. Simmons, Model Aircraft Aerodynamics, Special Interest Model Books, 2015.

[19] B. Theys, G. Dimitriadis, P. Hendrick and J. De Schutter, "Influence of propeller configuration on propulsion system efficiency of multi-rotor Unmanned Aerial Vehicles," in *International Conference on Unmanned Aircraft Systems*, 2016.

[20] B. Rutkay and J. Laliberte, " Design and manufacture of propellers for small unmanned aerial vehicles," *NRC Research Press,* 2014.

[21] R. Budynas and K. Nisbett, Shigley's Mechanical Engineering Design, McGraw Hill Educatiom, 2015.

[22] "KDE Direct," [Online]. Available: https://www.kdedirect.com.

[23] D. L. Gabriel, Johan Meyer and Francois du Plessis, "Brushless DC Motor Characterisation and Selection for a Fixed Wing UAV," in *IEEE Africon* , Livingstone, 2011.

[24] "T-Motor," [Online]. Available: https://store.tmotor.com.

[25] L. Jizhou, L. Ming, Y. Kaimin and G. Lei, " Influence of fuselage arm cross-section on the aerodynamic and aeroacoustic performance of quadcopter

Institutional Repository - Library & Information Centre - University of Thessaly
03/09/2026 06:00:57 EEST - 216.73.216.156

unmanned aerial vehicles: A numerical investigation," *International Journal of Micro Air Vehicles,* 2023.

[26] "Just Paint," 2014. [Online]. Available: https://justpaint.org/acrylics-on-plastics/.

[27] S. A. Nassar and Xianjie Yang, "Fastening and Joining of Composite Materials," in *Annual Conference on Experimental and Applied Mechanics*, 2013.

[28] [Online]. Available: https://tzjiahe.en.made-in-china.com/product/ZOQmpTuYOGhv/China-High-Strength-4mm-Thickness-3D-Fiberglass-Woven-Fabric-Supplier.html.

[29] "Amazon," [Online]. Available: www.amazon.com.

[30] D. Logan, A First Course in The Finite Element Method, Thomson, 2007.

[31] A. Sayam, Masudur Rahman, Md. Sakibur Rahman, Shamima Akter Smriti, Faisal Ahmed, Fogla Rabbi, Mohammad Hossain and Omar Faruque, "A review on carbon fiber-reinforced hierarchical composites: mechanical performance, manufacturing process, structural applications and allied challenges," *Carbon Letters,* vol. 32, 2022.

[32] T. K. Das, Prosenjit Ghosh and Narayan Ch. Das, "Preparation, development, outcomes, and application versatility of carbon fiber-based polymer composites: a review," *Advanced Composites and Hybrid Materials,* 2019.

[33] F.-L. Jin, Seul-Yi Lee and Soo-Jin Park, "Polymer matrices for carbon fiber-reinforced polymer composites," *Carbon Letters,* vol. 14, 2013.

[34] L. Ascione, Jean-François Caron, Patrice Godonou and Liesbeth Tromp, "PROSPECT FOR NEW GUIDANCE IN THE DESIGN OF FRP Support to the implementation, harmonization and further development of the Eurocodes," European CommissionJoint Research Centre, 2016.

Institutional Repository - Library & Information Centre - University of Thessaly
03/09/2026 06:00:57 EEST - 216.73.216.156

[35] D. K. Rajak, Pratiksha H. Wagh and Emanoil Linul, " Manufacturing Technologies of Carbon/Glass Fiber-Reinforced Polymer Composites and Their Properties: A Review," *Polymers,* 2021.

[36] "ACP Composites," [Online]. Available: https://acpcomposites.com.

[37] M. A. Karatas and Hasan G€ okkaya, "A review on machinability of carbon fiber reinforced polymer (CFRP) and glass fiber reinforced polymer (GFRP) composite materials," *Defence Technology,* 2018.

[38] "IQS Directory," [Online]. Available: https://www.iqsdirectory.com/articles/water-jet-cutting.html.

[39] "GO Seeko," [Online]. Available: https://www.goseeko.com/reader/notes/jharkhand-university-of-technology-jharkhand/engineering/mechanical-engineering/second-year/sem-2/manufacturing-process-i/unit-7-laser-beam-machining.

[40] D. Kumar and K.K. Singh, "An approach towards damage free machining of CFRP and GFRP composite material: a review," *Advanced Composite Materials,* vol. 24, 2014.

[41] Z. Tadmor and C. G. Gogos, Principles Of Polymer Processing, John Wiley & Sons, 2006.

[42] K. Rajan, Mahendran Samykano, Kumaran Kadirgama, Wan Sharuzi Wan Harun and Md. Mustafizur Rahman, "Fused deposition modeling: process, materials, parameters, properties, and applications," *The International Journal of Advanced Manufacturing Technology,* 2022.

[43] B. Freeland, "A Review of Polylactic Acid as a Replacement Material for Single-Use Laboratory Components," *Materials,* vol. 15, no. 9, 2022.

[44] W. C. Smith and Richard W. Dean, "Structural characteristics of fused deposition modeling polycarbonate material," *Polymer Testing,* vol. 32, no. 8, 2013.

Institutional Repository - Library & Information Centre - University of Thessaly
03/09/2026 06:00:57 EEST - 216.73.216.156

Institutional Repository - Library & Information Centre - University of Thessaly
03/09/2026 06:00:57 EEST - 216.73.216.156